ERRATA

Page	
Notices	The statement: "DDC release to OTS is authorized", should be deleted.
DD 1473	The statement: "DDC release to OTS is authorized", should be deleted from block 10.

DEVELOPMENT OF SUBSONIC BASE PRESSURE
PREDICTION METHODS

TECHNICAL REPORT AFFDL-TR-65-157

VOLUME I

AUGUST 1965

AF FLIGHT DYNAMICS LABORATORY
RESEARCH AND TECHNOLOGY DIVISION
AIR FORCE SYSTEMS COMMAND
WRIGHT PATTERSON AIR FORCE BASE, OHIO

PROJECT NO. 1366, TASK NO. 136613

(PREPARED UNDER CONTRACT NO. AF 33(615)-1615 BY THE AERODYNAMICS GROUP, CONVAIR DIVISION, GENERAL DYNAMICS CORPORATION IN SAN DIEGO, CALIFORNIA. J. E. BUTSKO, W. V. CARTER AND W. HERMAN, AUTHORS).

NOTICES

When Government drawings, specifications, or other data are used for any purpose other than in connection with a definitely related Government procurement operation, the United States Government thereby incurs no responsibility nor any obligation whatsoever; and the fact that the Government may have formulated, furnished, or in any way supplied the said drawings, specifications, or other data, is not to be regarded by implication or otherwise as in any manner licensing the holder or any other person or corporation, or conveying any rights or permission to manufacture, use, or sell any patented invention that may in any way be related thereto.

Qualified users may obtain copies of this report from DDC. Foreign announcement and dissemination of this report is not authorized. ~~DDC release to OTS is authorized.~~

Copies of this report should not be returned to the Research and Technology Division unless return is required by security considerations, contractual obligations, or notice on a specific document.

AF-WP-O-FEB 65 1500

FOREWORD

This report presents the results of an analytic/experimental program for the development of subsonic base pressure prediction methods conducted by the Convair Division of General Dynamics Corporation, San Diego, California. The effort was conducted under contract AF33(615)-1615 Project No. 1366, Air Force Task 136613 under the direction of Mr. G. M. Gilbert and Lt. L. W. Rogers, USAF of the Air Force Flight Dynamics Laboratory, Research and Technology Division, located at Wright-Patterson Air Force Base, Ohio.

The authors wish to express their appreciation to Mr. Tor Strand, Dr. W. H. Shutts of San Diego State College and Dr. J. M. Bowyer, Jr. of Kansas State University for their consultation.

The manuscript was released by the authors 28 October 1965 for publication as an RTD Technical Report.

This technical report has been reviewed and is approved.

Alfred C. Draper

A. C. DRAPER
Asst for R&T
Flight Mechanics Division
Air Force Flight Dynamics Laboratory

ABSTRACT

A combined analytic-experimental investigation of the subsonic base pressure phenomenon, especially as applied to blunt bodies typical of hypersonic flight vehicles, has resulted in the development of a generalized method to predict base pressure in three-dimensional flow at subsonic speeds. A mathematical description of the fluid mechanics of steady two-dimensional subsonic base flow has been developed. Wind tunnel testing of two-dimensional and three-dimensional blunt based configurations have been conducted to verify the two-dimensional analytic solution and to obtain empirical relations which extend the analysis to three-dimensional base flow. The prediction method which has been developed accounts for the independent effects of boundary layer thickness at separation, base flow angularity and base planform effects. The technique also predicts the effects of base asymmetry and the interaction of large blunt-based fins.

Volume II contains the results of the experimental investigation. Volume II discusses the methods and scope of the experimental program as well as presenting tabulated, plotted and photographic data obtained.

TABLE OF CONTENTS

	Page
INTRODUCTION	1
1/ ANALYTICAL PROGRAM	
1.1 Review of Research on Subsonic Base Flow	2
1.2 Development of Two-Dimensional Analytic Solution	8
1.2.1 Definition of Theoretical Flow Model	12
1.2.2 Solution of Two-Dimensional Steady Base Flow	14
1.2.2.1 Analysis of Two-Dimensional Turbulent Base Flow	15
1.2.2.2 Free-Streamline Analysis of Shear Layer Geometry	17
2/ EXPERIMENTAL PROGRAM	
2.1 Summary of Wind Tunnel Program	26
2.2 Correlation of Wake Flow Properties	39
2.2.1 Two-Dimensional Wakes	39
2.2.2 Three-Dimensional Wakes	44
3/ DEVELOPMENT OF GENERAL PREDICTION TECHNIQUE	
3.1 Development of Empirical Factors to Account for Three-Dimensional Effects	54
3.2 Description of General Prediction Digital Program	66
3.3 Correlation of Experimental Data with General Prediction Technique	66
3.4 Effect of Trailing Edge Sweep	70
4/ CONCLUSIONS	71
5/ RECOMMENDATIONS	72
6/ REFERENCES	73
7/ BIBLIOGRAPHY	
Survey of Literature on Subsonic Base Flow	76
APPENDIX I - Derivation of Equations for Viscous Mixing Solution	90
APPENDIX II - Derivation of Equations for Inviscid Free-Streamline	100
APPENDIX III- Documentation of Generalized Prediction Digital Program	137

ILLUSTRATIONS

FIGURE NO.		PAGE
1	Correlation of Base Pressure Data Based on Skin Friction Coefficient.	4
2	Correlation of Base Pressure Data Based on Vehicle Geometry Parameters.	6
3	Correlation of Base Pressure Data Based on Vehicle Geometry Parameters, Including Effective Base Angle.	7
4	Correlation of Base Pressure Coefficients Based on Vehicle Geometry, Including Effective Base Angle.	9
5	Effects of Sting-Support Interference on Base Pressure.	10
6	Correlation of Base Pressure Data Obtained in Smoke Wind Tunnel.	11
7	Flow Model of Von Karman; Two-Dimensional Unsteady Flow.	13
8	Flow Model of Chapman; Steady Two-Dimensional Flow.	13
9	Free-Streamline Base Flow Model.	19
10	Base Geometries Analyzed Using Free-Streamline Theory.	20
11	Example of Predicted Geometry of Free-Shear Layer.	24
12	Diagram of Digital Computer Program for Two-Dimensional Analytic Solution.	25
13	Two-Dimensional Models.	27
14	Two-Dimensional Configuration - Transition Grit and Splitter Plate Location.	28
15	Three-Dimensional Body - M_1.	29
16	Three-Dimensional Wing - W_3.	30
17	Three-Dimensional 4 Inch Wing - W_4.	31

ILLUSTRATION (cont'd)

FIGURE NO.		PAGE
18	Three-Dimensional Body with Boattail and Fin Configurations.	32
19	Typical Force and Moment Data - 3-D Body.	37
20	Typical Visualization of Flow Past a 2-D Model with Zero Base Angle.	38
21	Velocity Fluctuations in the Wake of a Two-Dimensional Configuration with Zero Base Angle.	40
22	Correlation of Non-Dimensional Wake Periodicity of Two-Dimensional Isolated Blunt Bases in Subsonic Flow.	41
23	Velocity Fluctuations in the Wake of a Two-Dimensional Configuration with Horizontal Splitter Plate.	42
24	Effect of Horizontal Splitter Plate on Centerline Static Pressure Behind Two-Dimensional Blunt Base Configurations in Subsonic Flow.	43
25	Total Pressure Contours in the Wakes of Configurations with and without Horizontal Splitter Plates.	45
26	Velocity Fluctuations in the Wake of an Axisymmetric Configuration.	46
27	Velocity Fluctuations in the Wake of a Thick Delta Wing Configuration (W_3).	47
28	Velocity Fluctuations in the Wake of a Thick Delta Wing Configuration (W_4).	48
29	Comparison of Static Pressure Distributions in the Wakes on Axisymmetric Configuration (M_1) and a Two-Dimensional Configuration with Horizontal Splitter Plate (T_{10} + P).	49
30	Spanwise Variation of Static Pressure in the Wake of a Thick Delta Wing Configuration.	51
31	Comparison of Total Pressure Contours in the Wakes of an Axisymmetric Configuration (M_1) and a Two-Dimensional Configuration with Horizontal Splitter-Plate (T_{10} + P).	52

ILLUSTRATIONS (cont'd)

FIGURE NO.		PAGE
32	Spanwise Variation of Total Pressure Contours in the Wake of a Thick Delta Wing Configuration.	53
33	Predicted Effect of Boundary Layer Thickness on Base Pressure for Steady Two-Dimensional Flow and Comparison with Experiment.	56
34	Viscous Effects of Base Angle and Boundary Layer Thickness on Base Pressure for Steady Two-Dimensional Flow.	57
35	Effect of Base Angle on Limiting Base Pressure for Two-Dimensional Steady Flow.	59
36	Effect of Base Angle on Limiting Base Pressure for Axisymmetric Configurations.	60
37	Method for Determination of Geometrical Parameters for Symmetrical Three-Dimensional Base Configurations.	61
38	Effect of Base Planform on Limiting Base Pressure for Symmetrical Three-Dimensional Configurations.	64
39	Method for Determination of Geometrical Parameters for Configurations Made up of Combinations of Base Regions.	67
40	Method for Determination of Geometrical Parameters for Configurations having Unsymmetrical Boattailing	68
41	Correlation of Experimental Data with Prediction.	69
42	Viscous Separation Flow Model.	91
43	Equivalent Mixing Layer Flow Model.	91
44	Free-Streamline Mapping Planes $\theta_1 = 0$.	101
45	Free-Streamline Mapping Planes $\theta_1 > 0$.	118
46	Free-Streamline Mapping Planes $\theta_1 < 0$.	132
47	Flow Diagram for Generalized Prediction Computer Program.	138

ILLUSTRATIONS (cont'd)

FIGURE NO.		PAGE
48	Generalized Prediction Digital Computer Program Input Format	153
49	Generalized Prediction Digital Computer Program Sample Output-Option 1	155
50	Generalized Prediction Digital Computer Program Sample Output-Option 2	156

TABLES

TABLE NO.		PAGE
I	Average Base Pressures - 2-D Configurations (Convair Tests)	33
II	Average Base Pressures - 3-D Configurations (Cal Tech Test	34
III	Generalized Prediction Digital Computer Program Listing	139
IV	Input Nomenclature for Generalized Prediction Digital Computer Program	154

SYMBOLS

q_∞	free-stream dynamic pressure ~ psf
C_{D_b}	base drag coefficient ~ $\frac{D_b}{q_\infty S_B}$
C_f	skin friction coefficient
S_W	surface wetted area ~ ft^2
S_B	base area ~ ft^2
D_B	base drag ~ lb.
C_{P_b}	base pressure coefficient ~ $\frac{P_b - P_\infty}{q_\infty}$
P_b	base pressure ~ psfa
P_∞	free stream static pressure ~ psfa
Ⓟ	perimeter of base-ft
L	vehicle overall length ~ ft
h_b	base height ~ ft
b_b	base width ~ ft
δ	effective base angle ~ degrees
P_r	static reattachment pressure ~ psf
N	reattachment parameter ~ $\frac{P_r - P_b}{P_t - P_b}$
θ_1	base angle ~ radians
θ_2	fence angle ~ radians
k, k_1, k_2	arbitrary constants
q	bleed rate ~ lb/sec
M_∞	free stream Mach number
$C_{P_{b_{lim}}}$	limiting base pressure coefficient
C_Z	normal force coefficient ~ $\frac{\text{normal force}}{q_\infty S_{ref}}$
C_X	axial force coefficient ~ $\frac{\text{axial force}}{q_\infty S_{ref}}$
C_m	pitching moment coefficient ~ $\frac{\text{pitching moment}}{q_\infty S_{ref} \text{ (M.A.C.)}}$
H	total head ~ psf
δ^{**}	boundary layer momentum thickness ~ ft
X	development length ~ ft

LIST OF SYMBOLS (cont'd)

U_∞	free stream velocity ~ fps
ν	kinematic viscosity ~ $ft^2 \cdot sec^{-1}$
h_{max}	maximum semi-thickness ~ ft
θ_{eff}	effective base angle ~ radians
M.A.C.	mean aerodynamic chord ft
h	base semi-height ~ ft
h_{eff}	effective base semi-height ~ ft
l_{eff}	mean approach length ~ ft
u^2	square of instaneous velocity in X-direction ~ $(fps)^2$

INTRODUCTION

The current design and development of hypersonic cruise vehicles, lifting re-entry vehicles and recoverable boosters has given new impetus to subsonic aerodynamic research. Vehicles of these types, designed for hypersonic flight and characterized by blunt trailing edges and bases, require a subsonic flight capability in order to execute landing manuevers. Prediction of the subsonic aerodynamic characteristics of this class of vehicles has become a critical problem area. Since base drag constitutes the major portion of the total subsonic drag of a blunt based vehicle, investigation of subsonic base flow is currently receiving more than the academic attention it once held.

The present study was conducted to develop a prediction technique to accurately predict the base pressure for a vehicle of the class described above. The development of a general prediction technique was approached by the use of a study program which involved the following tasks:

1. Analytic investigation of the fluid mechanics of subsonic base flow and mathematical description of an idealized flow model.

2. Experimental verification of the analytic predictions and experimental investigations to extend the theory to the prediction of base pressures behind complex, as well as simple, configurations.

The following paragraphs present the results of the analytic and experimental tasks and describe the development of a generalized prediction technique.

1/ ANALYTICAL PROGRAM

1.1 REVIEW OF RESEARCH ON SUBSONIC BASE FLOW

1.1.1 HISTORICAL REVIEW. Research on base flow phenomenon originates from the work of Prandtl and others who investigated the discrepancy between classical potential solutions and the observed viscous separation from the rear of bluff bodies in low velocity flow. Identification of the considerable drag penalty associated with base separation resulted in the logical design practice; bluff shapes were to be avoided in subsonic aerodynamic and hydrodynamic design. Although the problem subsequently received only academic interest, several investigations are noteworthy. Von Karman first hypothesized a mathematical description of the periodic shedding of vortices which characterize flow over two-dimensional bluff bodies at Reynolds numbers above 50. The work of Fage and his associates contributed a considerable amount of experimental data on bluff body flow that to this date have not been fully exploited (references 1, 2 and 3). More recently, the investigations of Roshko (reference 4 and 5) have yielded a semi-empirical method for predicting the drag of two-dimensional bodies with periodic wakes in low velocity flow.

based on what?

The advent of research on projectiles and later, missiles and space vehicles, gave new impetus to research on the fluid dynamics of base flow. Emphasis has been placed almost excusively on the supersonic flow regime and considerable research, both theoretical and experimental, has been conducted to investigate the mechanics of supersonic base flow. The analyses and investigations of Chapman et al (references 6 and 7) and Korst el al (references 8 and 9) established the ground work for analytic methods by which the properties in the separation behind a vehicle in supersonic flight can be predicted.

The majority of the effort on subsonic base flow research during the past decade has been concerned with the acquisition of experimental base pressure and base drag data of specific configurations. Section G of the bibliography is a survey of current experimental investigations. Several empirical investigations, such as those of references 10, 11 and 12, have used this type of experimental data to identify the parameters which influence base pressure level. The following section reviews two existing empirical methods.

1.1.2 REVIEW AND EXTENSION OF CURRENT EMPIRICAL INVESTIGATIONS. Several empirical investigations have attempted to identify the significant parameters which influence the subsonic base pressure characteristics of blunt bodies (for instance, references 13 and 14).

These investigations have indicated that the magnitude of the pressure in the separated region formed at the base is determined by the combined effects of two distinct fluid dynamic actions. The exchange of momentum in viscous mixing layer which bounds the separated base flow region and the inviscid external flow field acts to reduce the pressure in the separated region to below ambient. The static pressures associated with the inviscid flow field surrounding the base region influence the base pressure by interaction with the viscous mixing process. The pressure within the separated cavity depends, therefore, on the extent of the viscous mixing process, which is related to the condition of the boundary layer approaching the base, on the extent or size of the mixing region in relation to the base region, and on the static pressures in the external flow which are related to the shape of the forebody ahead of the base.

Hoerner, (reference 10), was able to correlate base drag of axisymmetric bodies by the expression:

$$C_{D_B} = .029/\sqrt{C_{f_B}} \qquad (1)$$

where $C_{f_B} = C_f \dfrac{S_W}{S_B}$

and

C_f = skin friction coefficient

S_W = wetted surface area

S_B = base area

A similar correlation using these parameters was made during the present investigation using the data of reference 15. The empirical relationship

$$C_{D_B} = .055/\sqrt{C_{f_B}} \qquad (2)$$

yiels excellent agreement with the experimental base pressures of the four elliptical cones tested. Reference 16 contains experimental subsonic base pressure data for a large number of hypersonic configurations for which the wetted surface areas and base areas have been tabulated. These data were correlated using a value of C_f of .0040 as suggested in reference 12 and are shown in Figure 1. Good agreement with the empirical relation developed for elliptical cones is shown, especially for configurations with symmetrical base geometries tending to elliptical or diamond sections. These bodies are characterized by body geometries which maintain the flow ahead of the base essentially parallel to the free-stream, allowing the data to be correlated satisfactorily using a parameter which represents only the viscous phenomenon. However, the interrelationship between skin friction, boundary layer thickness, and base pressure, suggests that boundary layer thickness is a more logical parameter than skin friction coefficient.

The investigation reported in reference 12 included the development of an empirical method for predicting subsonic base pressures of hypervelocity

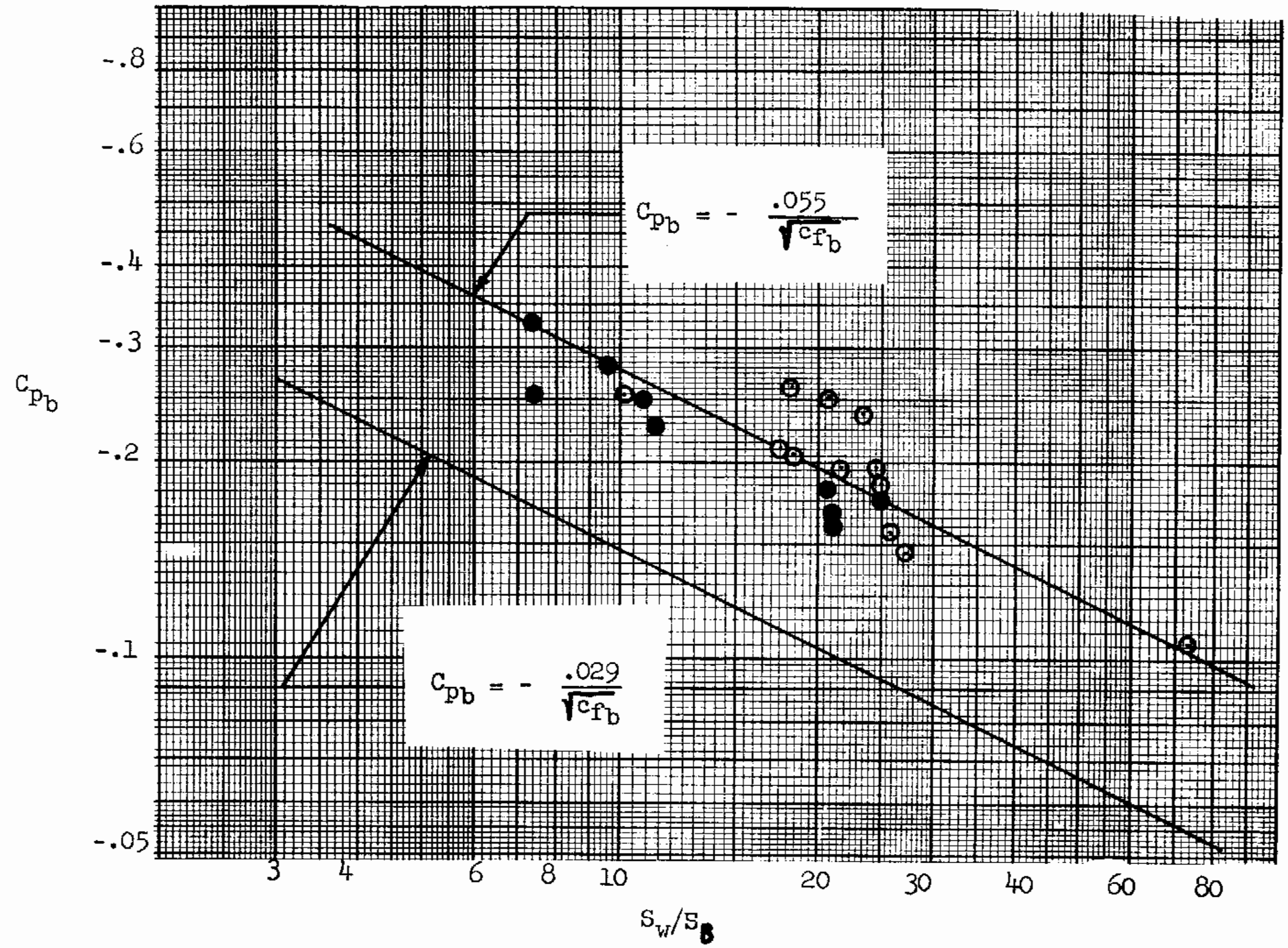

FIGURE 1. Correlation of Base Pressure Data Based on Skin Friction Coefficient.

vehicle geometries. The method was based on correlations of experimental data obtained from wind tunnel tests of models having a wider range of base geometry than those described in the previous paragraph. Two geometrical parameters were developed which account for both the viscous and non-viscous actions, although not independently:

$$\frac{(P)}{2\sqrt{\pi S_B}}$$

where (P) = perimeter of the base

S_B = base area

and

$$\frac{2S_B}{\pi L(h_b + b_b)}$$

where S_B = base area

L = overall length

h_b = base height

b_b = base width

The first expression accounts primarily for the influence of base geometry on the viscous mixing phenomenon while the latter expression accounts for both the viscous effect of boundary layer and the effect of the forebody on the external flow field. The empirical method was used during the present investigation to correlate the experimental data from several of the references of Section G of the bibliography. Figure 2 presents the results of this correlation, and shows that this method does not adequately account for the external pressure field at the base, since the data which is characteristically low as obtained for configurations typified by boattailed afterbodies. The parameter which includes effects of the external flow was modified by the inclusion of a term representing an effective angle at the base, δ. The effective angle was defined for each configuration by averaging local angularity in terms of the proportion of the perimeter over which the local angle was realized. Inclusion of the term sin δ yielded better correlation of the same data, as shown in Figure 3.

The parameter $\frac{2 S_B}{\pi L(h_b + b_b)}$ effectively duplicates the parameter sin δ for geometries with increasing section thickness but does not adequately account for base pressures produced by configurations having significant afterbody angular deviations, such as flared or boattailed body sections. An additional correlation of the data obtained from the references of Section G was performed by retaining the parameter $(P)/2\sqrt{\pi S_B}$ to account for the viscous mixing phenomenon

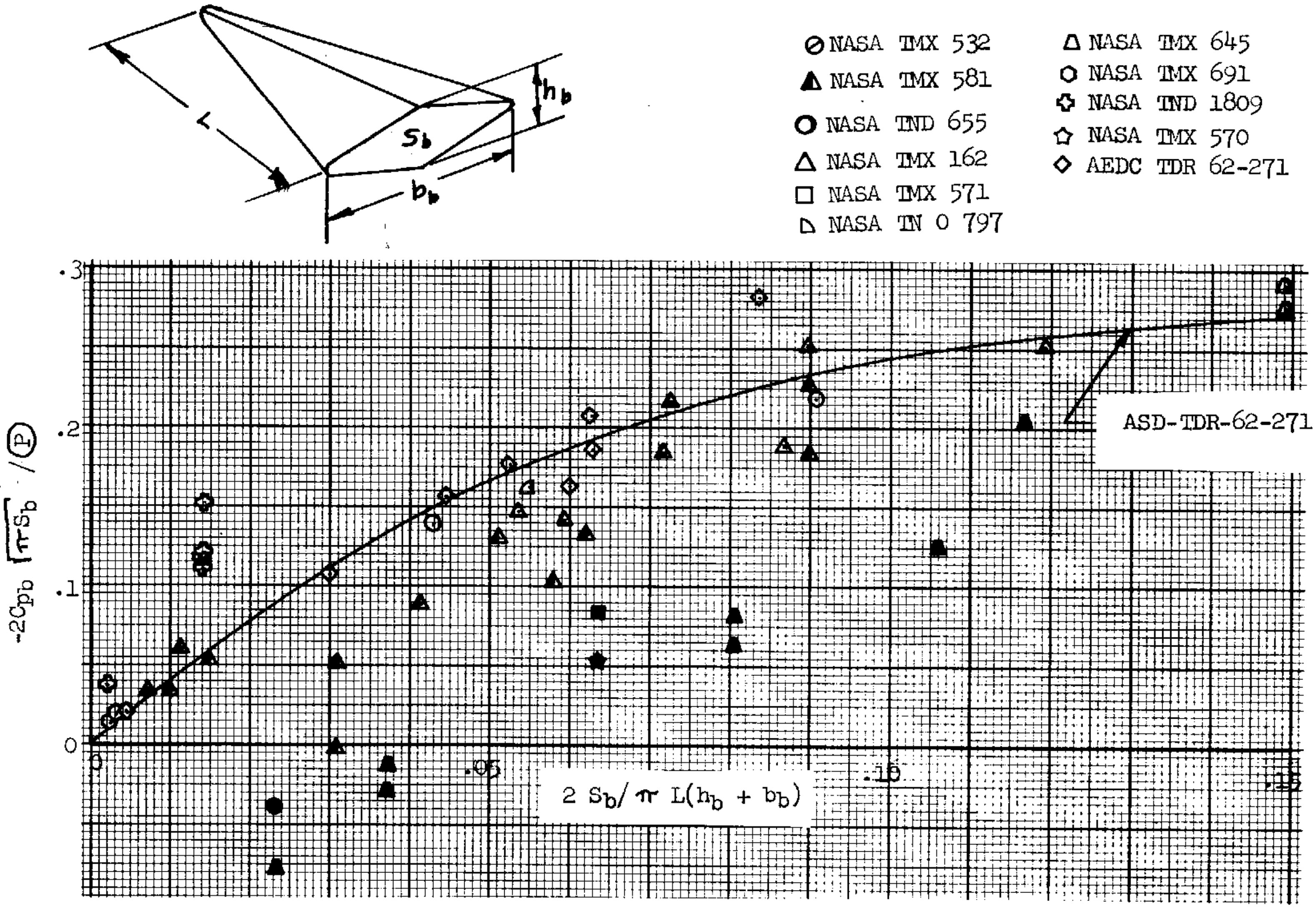

FIGURE 2 Correlation of Base Pressure Data Based on Vehicle Geometry Parameters.

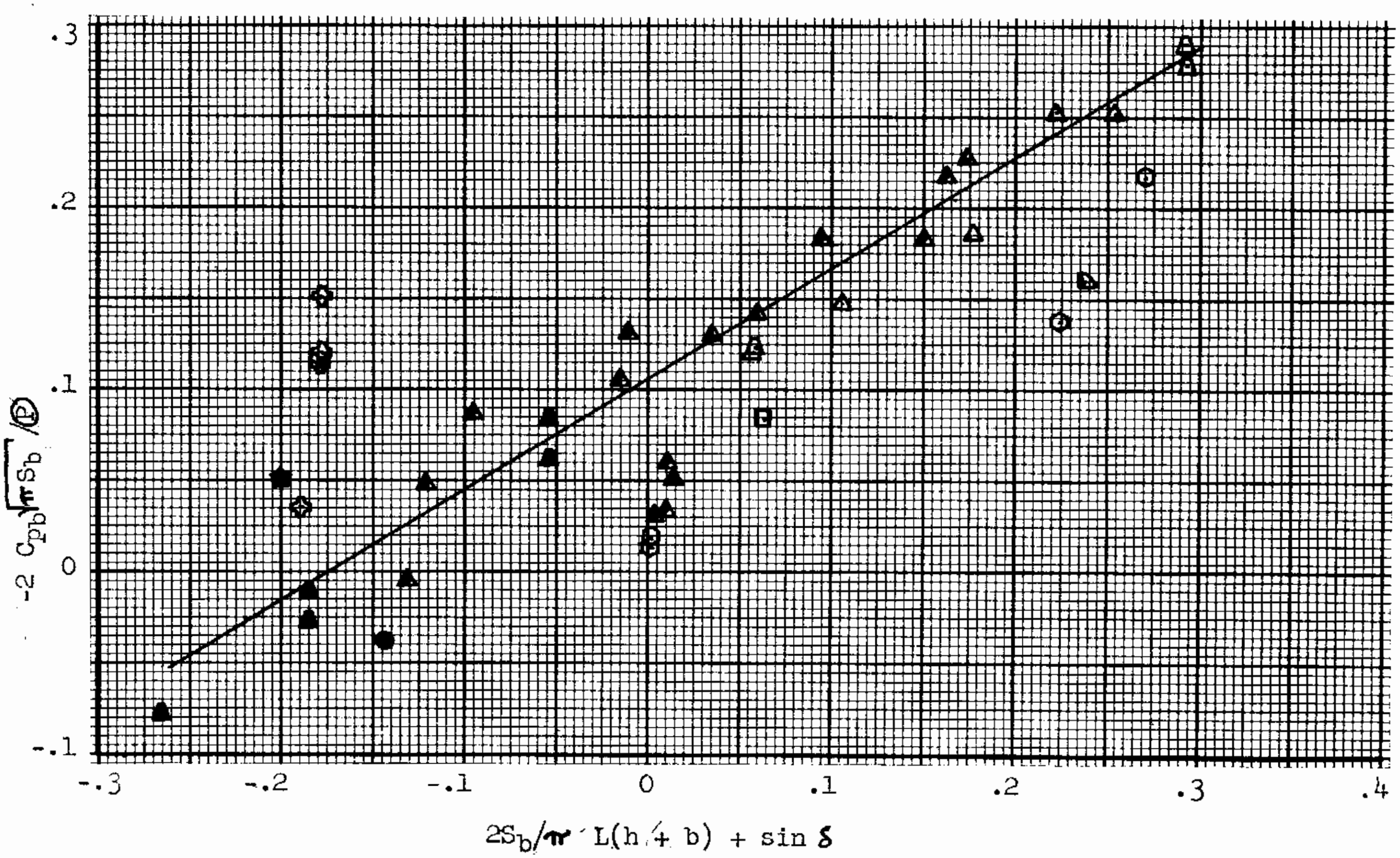

FIGURE 3 Correlation of Base Pressure Data Based on Vehicle Geometry Parameters Including Effective Base Angle.

and using the parameter sin δ to account for the effects of the external flow field. It was found that angle-of-attack data could be included in the same correlation by a simple addition of the angle-of-attack to the effective angle. The result of the correlation is shown in Figure 4.

The data presented in Figures 1 through 4 were obtained from tests of a wide range of vehicle configurations, including high-speed configurations with delta planforms, axisymmetric bodies, partial-cones and wing-body combinations. All are characterized by having blunt bases. The correlations represented by Figures 1 through 4 appear limited due to the lack of terms to adequately account for the effect of theapproaching boundary layer, the thickness of which is non-linear with approach length. Also, the effect of planform assymmetry is not sufficiently accounted for; wing-body and fin-body combinations could not be expected to have the same characteristics as a symmetrical configuration with the same value of the first geometrical parameter.

A significant amount of data scatter can be attributed to the inconsistency of experimental data due to sting interference and incomplete pressure surveys. Figure 5 presents the incremental error introduced by sting diameter interference for two configurations previously investigated. The magnitude of the errors possible indicates the limitations of correlating data representing a broad spectrum of configurations and test techniques.

The data obtained from the preliminary tests on two-dimensional configurations conducted in the low velocity smoke tunnel at San Diego State College and described in Section 2 also indicate the dependency of base pressure on both the viscous effects and the external pressure field at the base. The investigation was based on systematic variations of configuration geometry, including fineness ratio and afterbody angle. The data was correlated using parameters to account for both the viscous effect and the external flow field. Figure 6 shows a definite trend and demonstrates the degree of influence of the external pressure field on the base pressure.

1.2 DEVELOPMENT OF TWO-DIMENSIONAL ANALYTIC SOLUTION

The preceding section formulated qualitatively the parameters which influence the base pressure of blunt bodies in subsonic flow. The major effort of the analytic investigation conducted during the present study was devoted to the development of a mathematical model of the fluid dynamics of base flow. The analytic method which has been developed describes two-dimensional, steady flow separating from base geometries of arbitrary flow inclination. The method combines a viscous solution which defines the mixing process along the mixing zone dividing the separated cavity from the external potential field, and an inviscid solution which determines the geometry of the cavity and the separation streamline.

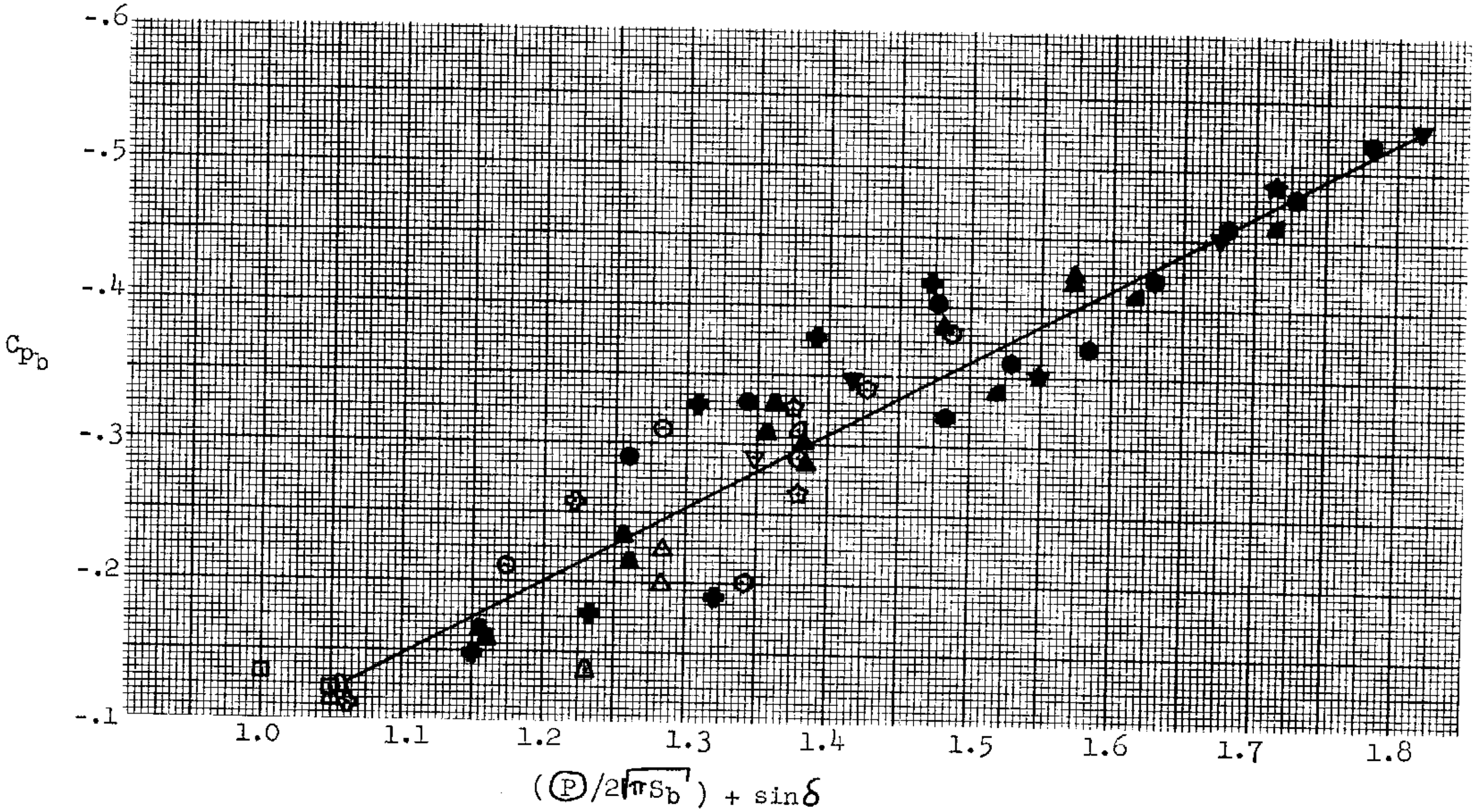

FIGURE 4 **Correlation of Base Pressure Coefficients Based on Vehicle Geometry, Including Effective Base Angle**

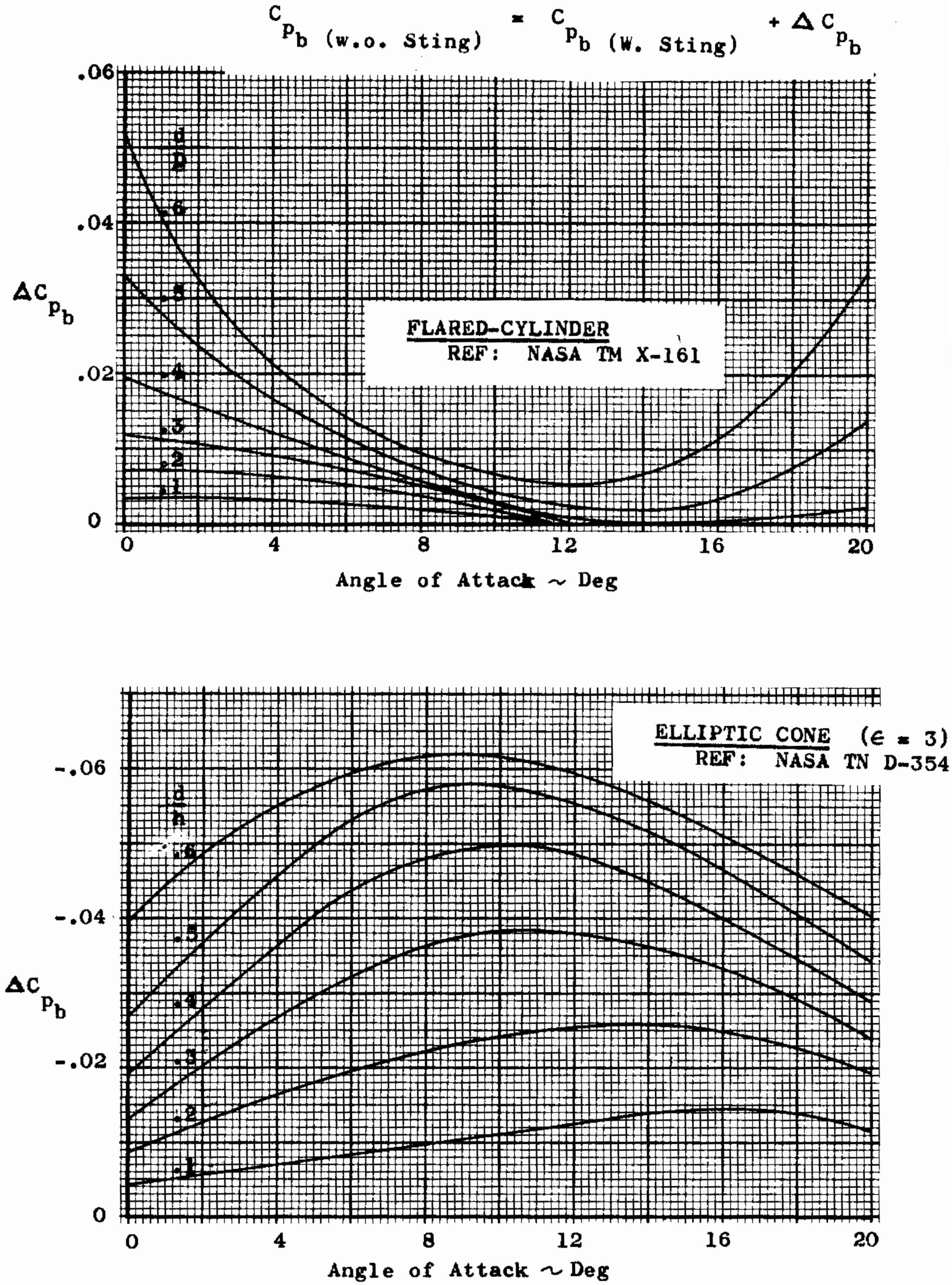

FIGURE 5 Effects of Sting Support Interference on Base Pressure

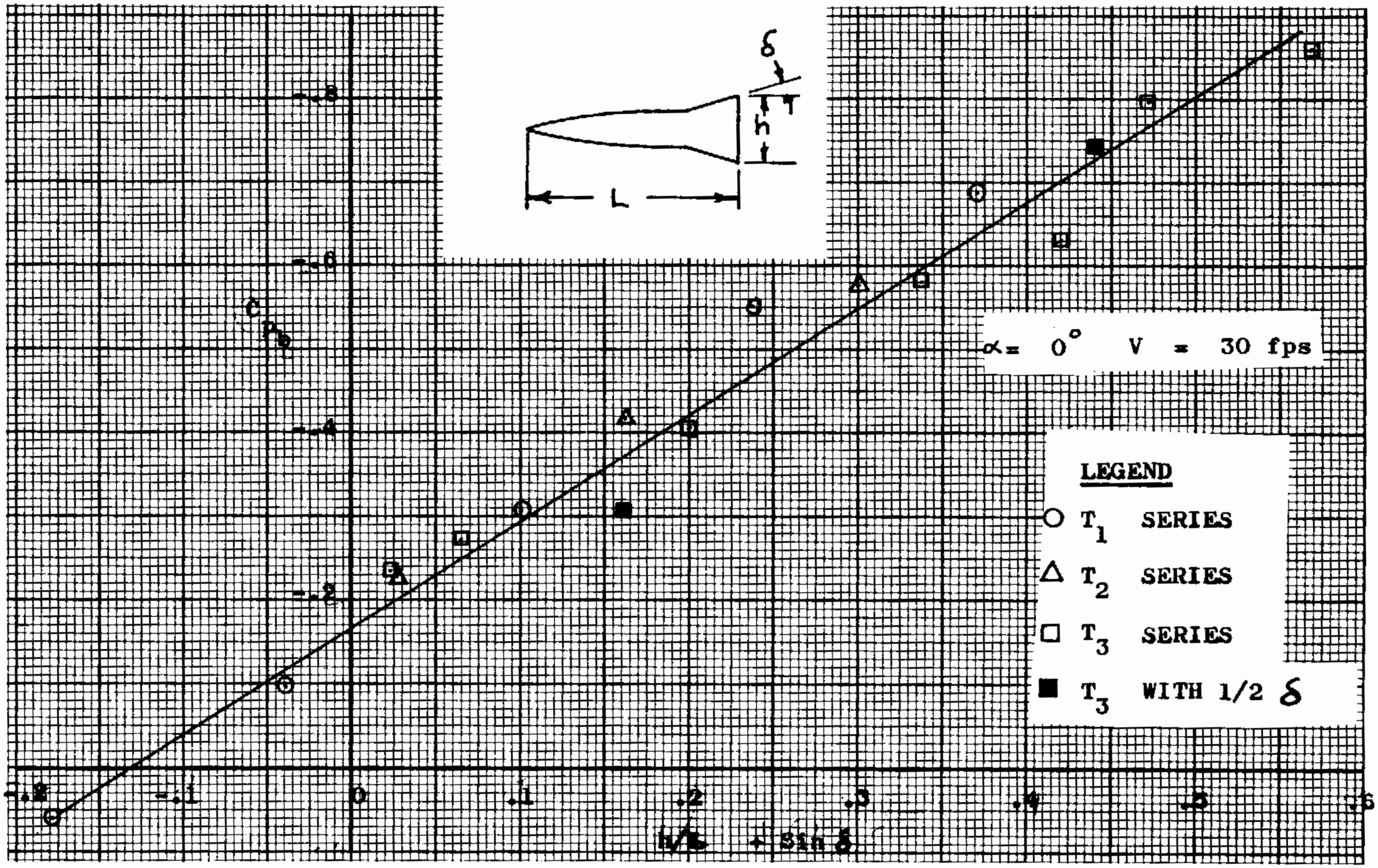

FIGURE 6 Correlation of Base Pressure Data Obtained in Smoke Wind Tunnel

1.2.1 DEFINITION OF A THEORETICAL FLOW MODEL. The present analysis of subsonic flow separating from a blunt vehicle base required the adoption of a theoretical flow model to describe the fluid mechanics of the system. This task was complicated by the fact that at least two distinct flow situations are theoretically possible, depending on base geometry and flow conditions. The first flow model, describing flow over two-dimensional bodies with blunt bases, can be characterized at Reynolds numbers above 50 by an open wake containing periodically shed vortices. The theoretical flow model, hypothesized by Von Karman, is depicted in Figure 7.

Several investigators have shown that if the periodic vortex formation is suppressed the subsonic flow is quite similar to the steady base flow at supersonic speeds. Two-dimensional subsonic flow over a rearward facing step has been analyzed using the steady flow model. Three-dimensional base configurations, especially with ratios of base perimeter to mean radius approaching the value for axisymmetric base geometries, do not exhibit the marked periodicity of the wake associated with the two-dimensional phenomenon, as will be shown in Section 2. Moreover, the subsonic base pressure determined experimentally for three-dimensional configurations are generally comparable in level with values obtained for steady two-dimensional flow, such as obtained with the rearward facing step; the base pressures for the non-steady two-dimensional flow being markedly lower. It can be theorized, therefore, that three-dimensional subsonic base flow can be adequately described using the steady flow model.

The flow model of Chapman (reference 6), was adopted for the analytic investigation of three-dimensional subsonic base flow conducted during the present program. The flow model, shown in Figure 8, considers four distinct fluid regions:

1. Flow approaching the trailing edge of the body.
2. Separation of the flow from the trailing edge.
3. Constant-pressure flow along the edge of the wake separated from a region of relatively "dead" air by a free-mixing layer.
4. Recompression of the separated flow in the wake region where the shear layers merge.

The flow model of Chapman describes the mechanism which makes the base pressure phenomenon amenable to mathematical description. The shear layer leaving the separation point entrains fluid from the dead-air cavity, tending to reduce the pressure in the cavity. The decay of cavity pressure continues until a stable condition prevails, whereby a sufficient amount of fluid in the shear layer is reversed in the recompression zone in order to preserve the mass balance in the cavity. Prediction of the cavity pressure for the

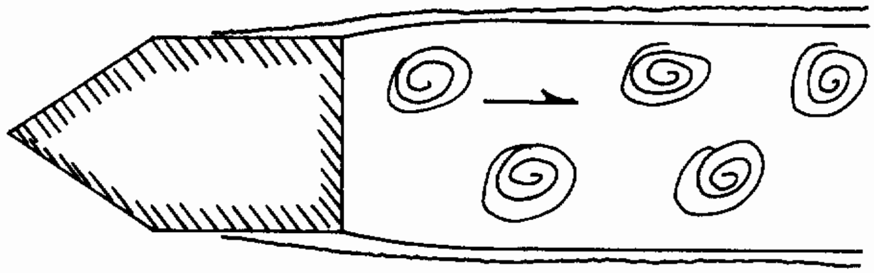

FIGURE 7 Flow Model of Von Karman; Unsteady Two-Dimensional Flow

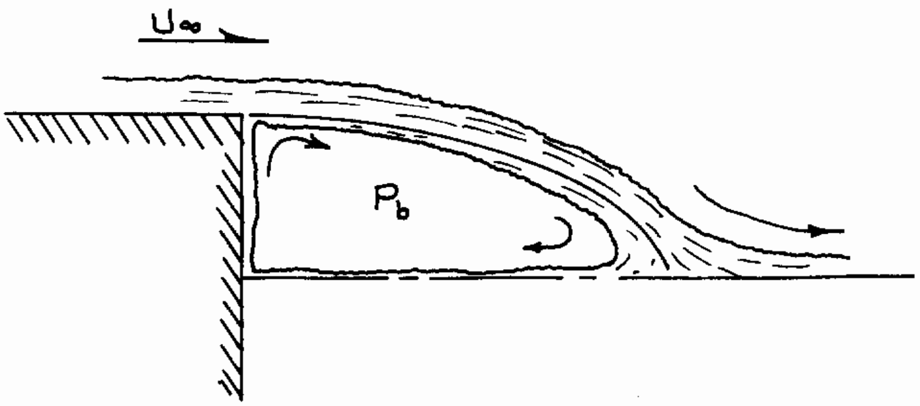

FIGURE 8 Flow Model of Chapman; Steady Two-Dimensional Flow

stable condition can be made by allowing the pressure rise across the recompression zone to adjust itself such that the correct amount of fluid in the shear layer is reversed to preserve continuity in the cavity and the remaining fluid of higher velocity is able to negotiate the pressure rise and escape into the downstream wake.

1.2.2 SOLUTION OF TWO-DIMENSIONAL STEADY BASE FLOW. Mathematical description and analyses of the flow model of Chapman have been developed by several investigators. Primary attention has been given to the supersonic flow condition; Chapman, et al (reference 7) analyzed the flow model for the case with laminar mixing along the shear layer. Korst (reference 8) analyzed the supersonic and transonic flow case for turbulent mixing along the shear layer and included in his analysis the effect of mass addition to the cavity. Neither analysis accounts for the effects of a boundary layer approaching the separation point. The solutions are therefore identified as the limiting base pressure levels, since experimental evidence indicates the boundary layer acts to raise the base pressure above the limiting base pressure predicted.

Previous analysis of the subsonic flow model has been approached primarily as an extension to the supersonic analysis. The subsonic case is considerably more complicated than the supersonic case, since straight-forward methods such as the Prandtl-Meyer theory of supersonic flow are not available in subsonic flow for predicting the geometry of the shear layer, whose length governs the amount of mixing to be accounted for in the viscous solution.

Analysis of a flow system similar to the subsonic base flow model was performed by Hsu for viscous flow of jets in ground effect (reference 17). A similar condition requiring mass balance in the cavity established the flow model. Analysis of the flow model was considerably simplified by the assumption, verified experimentally by numerous authors, that the jet in ground effect curves at a constant radius, its geometry being established completely by the height and angle of the jet nozzle exit with the ground plane. The effect of the vorticity of the standing vortex created by the recirculation of air in the cavity was investigated, but its contribution to the cavity pressure relative to the contribution of the jet mixing phenomenon was insignificant and can be ignored.

The recent analysis of Nash (reference 18) extends the work of Chapman and Korst by accounting for the effect of the approaching boundary layer on the mixing phenomenon along the separated shear layer. Analysis is made of both the supersonic and the subsonic flow regimes. An inverse solution of the problem was developed by Nash; closed form equations are presented which define the turbulent boundary layer height at the separation point required to support a given base pressure level for a given flow condition. The method applied to the subsonic flow case is limited, however, since analytic description of the shear layer geometry was not attempted and is left in the solution as a free parameter. (In application of the method, experimentally determined ~~values of the ratio of shear layer length to base height determined~~

values of the ratio of shear layer length to base height determined experimentally for a two-dimensional rearward facing step yielded accurate correlations with the experimentally determined base pressure for the step).

In the present analytic investigation, the analysis of Nash has been adopted to predict the viscous phenomenon of the steady subsonic two-dimensional base flow problem. During the present investigation, a method was developed which closes Nash's subsonic solution by providing an analytic solution for the geometry of the shear layer. The method, using inviscid free-streamline theory, allows Nash's analysis to be applied to the study of the effects of changes of base geometry involving inclination of the base flow angle, such as ramped or boattailed bases.

The two methods, Nash's viscous analysis and the inviscid free-streamline method, are discussed in the following paragraphs.

1.2.2.1 ANALYSIS OF TWO-DIMENSIONAL TURBULENT BASE FLOW. Nash's analysis of two-dimensional turbulent base flow was based on the flow model developed by Chapman. For subsonic flow, the analysis was formulated for flow over a rearward-facing step, to which the steady flow model can be applied with reservation.

The mechanism inherent to the flow model of Chapman, the coupling of the mixing or mass entrainment process along the shear-layer and the pressure rise in the recompression zone is mathematically described by Nash's analysis. The rigorous derivation of the pertinent equations which allow the base pressure level to be determined is presented in Appendix I. Two significant refinements of Nash's analysis over previous analyses are outlined below:

1.2.2.1.1 Re-attachment Condition. The re-attachment pressure rise results in the division of the flow in the free-shear layer into two streams; flow along streamlines having total pressure higher than the static recompression pressure is able to overcome the pressure rise and pass downstream, while flow along streamlines with sufficiently low total pressure is reversed. In contrast to previous analyses, the static pressure at the re-attachment point was assumed to be other than the downstream static pressure (the assumption was verified experimentally by Nash), introducing a parameter which relates the ratio of the static pressure rise at re-attachment to the difference between free-stream static pressure and the base pressure. This parametric relationship is defined:

$$\frac{P_r - P_b}{P_1 - P_b} = N \qquad (3)$$

where

P_r = static re-attachment pressure

P_b = base pressure

P_1 = free stream static pressure

In the analysis of Nash the parameter N was evaluated using experimental data obtained from investigations on flow over rearward facing steps.

1.2.2.1.2 Free-Shear Layer Development. Essential to Nash's analysis was the identification of flow properties along streamlines in the shear layer. The flow in the shear-layer was approximated by analysis of the constant pressure turbulent mixing of a two-dimensional jet or stream with a fluid at rest. The velocities along streamlines in the shear layer were determined using the mixing analysis of Kirk (reference 19) which accounts for the effects of the approaching boundary layer at the separation point. The velocity profile was predicted as a function of a development length representing both the distance from the separation point and an equivalent length accounting for the boundary layer development at the separation point.

Joining of the mixing analysis which described the total pressure on streamlines and the mass entrained along the shear layer with the re-attachment condition closed the base-flow solution. The solution in generalized from accounts for mass addition or removal (bleed rate) in the cavity. The derivation of the viscous solution presented in Appendix I results in the final equation:

$$q = \rho_{e2} \; u_{e2} \left[\frac{\sqrt{\pi}\,\ell}{(\gamma-1)\sigma M_e^2} \left\{ \ln \lambda_b - \ln \left(\frac{P_r}{P_b} \right)^{\frac{\gamma-1}{\gamma}} \right\} - \delta^{**} \frac{\ln\left(\frac{P_r}{P_b}\right)^{\frac{\gamma-1}{\gamma}}}{\ln \lambda_b} \right] \tag{I.3.10}$$

where

q = base-bleed flow rate

ρ_{e_2} = density external to free-shear layer

u_{e_2} = velocity external to free-shear layer

ℓ = length of free-shear layer

λ_b = density ratio defined by eq. (I-3.5)

P_r = pressure at reattachment

P_b = pressure in separated cavity

δ^{**} = boundary layer momentum thickness approaching separation point

γ = ratio of specific heats

Equation (I-3.10) allows the following procedure for computation of base pressure:

a. For given approaching flow conditions, a range of base pressure ratios are chosen for study.

b. A value of the parameter N is chosen, which determines the reattachment pressure for each chosen base pressure.

c. If a bleed rate is specified, the ratio of boundary layer momentum thickness to shear layer length can be determined which is necessary to produce each level of base pressure.

d. If the ratio of boundary layer momentum thickness to shear layer length is specified, the variation of base pressure with bleed mass flow can be determined.

The significance of the parameter N was not fully evaluated during the present investigation. No adequate theory has been formulated to analyze the non-isentropic mechanism of reattachment. The analytically-derived isentropic recompression criteria of Chapman and Korst yields a value of N equal to unity; the reattachment streamline is assumed to recompress to the free-stream level. Although the experimental data obtained by Nash indicated that values of N different than unity existed (between 1.5 and 1.0 subsonically) and provided refinement to the solution, the limited experimental data on reattachment pressure obtained during the present investigation (as described in Section 2.0) did not verify the results of Nash. For the present investigation, it was assumed that $N = 1$ was sufficient to analyze steady two-dimensional subsonic base flow.

~~It is noted that~~ in the viscous solution, the shear layer length remains as a free-parameter. Determination of the geometry of the shear layer analytically frees the viscous solution of its major empirical content.

1.2.2.2 FREE-STREAMLINE ANALYSIS OF SHEAR LAYER GEOMETRY. Inviscid, incompressible free-streamline theory has been applied to the study of subsonic base flow phenomena by several investigators. Free-streamline theory uses the two-dimensional, incompressible potential flow method of conformal mapping, which, by means of conformal transformation, allows the complete potential flow field to be determined from known boundary conditions. Separation from the rear of bluff two-dimensional bodies was originally studied by Kirchoff who developed a free-streamline theory whereby surfaces (streamlines) of velocity discontinuity idealize the separating free shear layers. The free-streamlines divide the flow into a wake and an outer potential field. Numerous authors have applied Kirchoff's theory to two-dimensional bluff shapes, the most notable being Roshko (references 20 and 4), who joined a free-streamline solution to the wake drag theory of Von Karman, yielding a semi-empirical method for predicting the drag of two-dimensional bodies with periodic wakes.

The class of flows mentioned above are characterized by streamlines which do not close; the streamlines extend (ideally) to infinity enclosing a wake region of finite width. The use of free-streamline theory has been applied to many other problems in fluid dynamics which involve discontinuous stream surfaces (for example, reference 21). The study of cavity flow characterized by streamlines which close, is due mainly to the original work of Riabouchinsky (reference 22).

Free-streamline theory was adopted during this investigation for the study of the geometry of the free-shear layer inherent to the flow model. The application of an inviscid method to the study of a viscous phenomenon can be questioned, but in cases where both the viscous and inviscid models are governed by a criterion which assumes constant static pressure throughout the cavity, the free-streamline method provides a close approximation of the viscous phenomenon. (The analysis of reference 21 applied free streamline theory to jet flow in ground proximity, where the jet encloses a constant pressure cavity. The geometrical relationships which evolve check very closely with experiment).

The basic flow model was modified slightly for study using free-streamline theory. The modified flow model is depicted in Figure 9. As in the analysis of Riabouchinsky flow, a cavity is formed by use of an obstacle (referred to henceforth as a fence) placed downstream of the separation corner. The fence is an artifical device required to close the streamlines; it has physical significance, however, since the streamline is forced to stagnate along the fence. The fence, therefore, can be seen to idealize the recompression zone of the viscous flow model.

The free-streamline method was applied to the base geometries depicted in Figure 10. The transformations which allow solution of the problem involved use of the Schwarz-Christoffel theorem of conformal mapping, a standard technique used in free-streamline theory (for example, see reference 23). The complete mathematical developments for each of the cases of flow over a base with zero, positive and negative flow inclination are presented in Appendix II. The inclination of the fence was allowed to remain arbitrary, which offers generality to the solution. The following geometrical relations, derived in Appendix II for the case $\Theta = 0$, are presented to illustrate the form of the equations:

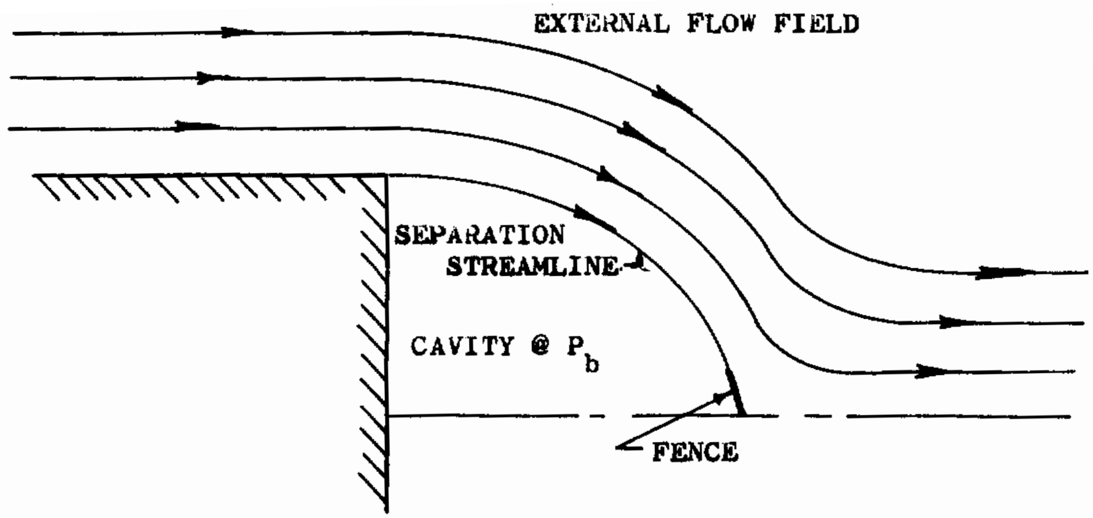

FIGURE 9 Free-Streamline Base Flow Model

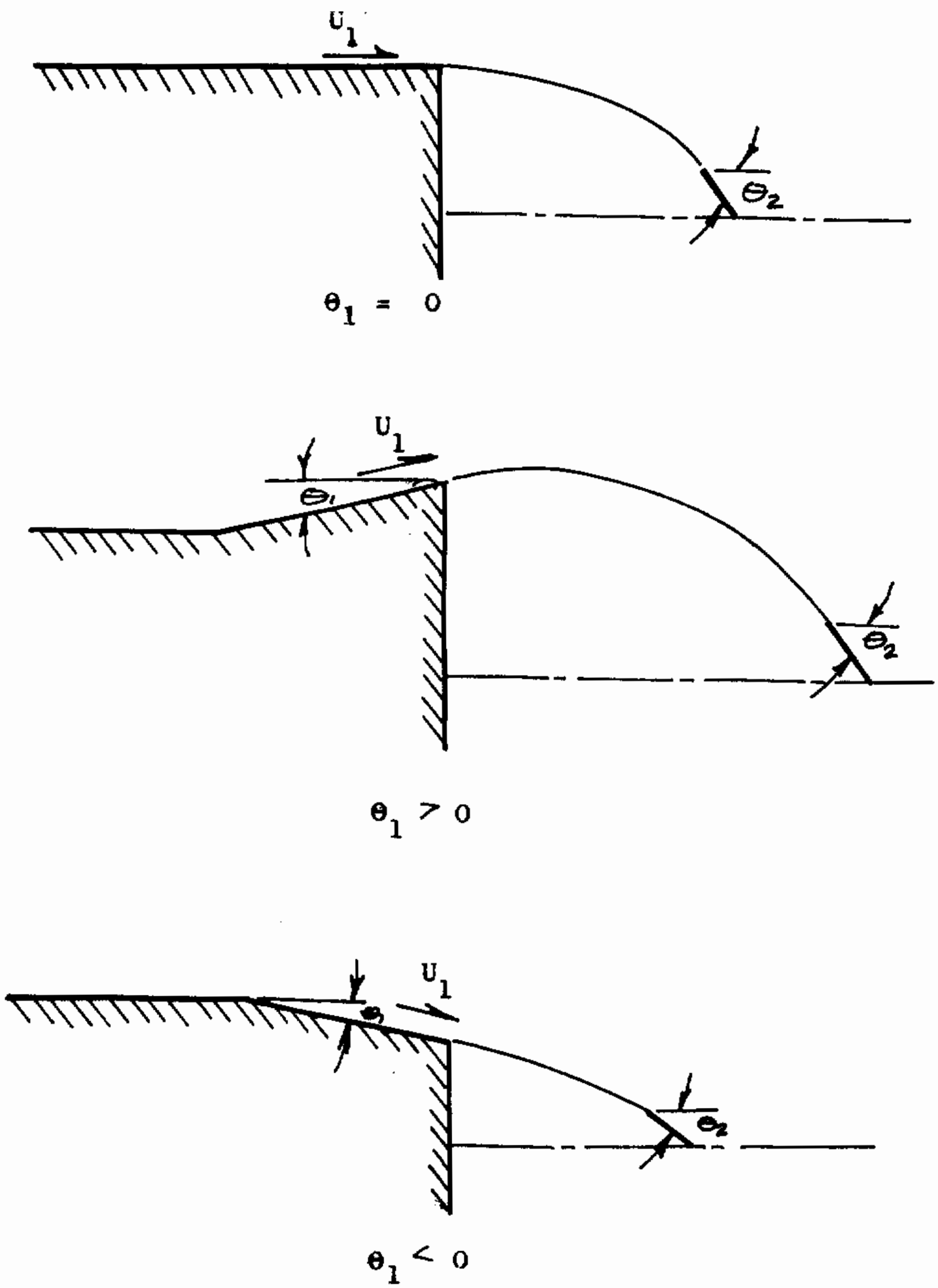

FIGURE 10 Base Geometries Analyzed Using Free-Streamline Theory

a. <u>Geometry of free-shear layer:</u>

$$\Delta X_{bc_i} = \frac{1}{U_1} \int_{\phi_{bc_i}}^{\phi_{bc_i}} \cos(\theta_{bc})\, d\phi \qquad (4)$$

$$\Delta Y_{bc_i} = \frac{1}{U_1} \int_{\phi_{bc_i}}^{\phi_{bc_i}} \sin(\theta_{bc})\, d\phi \qquad (5)$$

where

$$\theta_{bc} = \left[-\frac{\theta_2}{\pi} \tan^{-1} \left(\frac{2k\sqrt{-\phi_{bc_i}^{\,2} - (k^2+1)\phi_{bc_i} - k^2}}{2k^2 + (k^2+1)\,\phi_{bc_i}} \right) \right] \qquad (6)$$

$\Delta X_{bc_i}, \Delta Y_{bc_i}$ = incremental directed lengths along shear layer

θ_2 = angle of fence

k = constant defined by equation (II.27)

ϕ_{bc_i} = velocity potential ~ $-1 < \phi_{bc} < k^2$

U_1 = free stream velocity

b. <u>Geometry of fence:</u>

$$X_{cd} = \frac{\cos\theta_2}{U_1} \int_{\phi_c}^{\phi_d} q_{cd}\, d\phi \qquad (7)$$

$$Y_{cd} = \frac{\sin\theta_2}{U_1} \int_{\phi_c}^{\phi_d} q_{cd}\, d\phi \qquad (8)$$

where

q_{cd} = velocity along fence

$$= \left[(1-k^2) \left(\frac{-\phi_{cd}}{2k\sqrt{\phi_{cd}^2 + (k^2+1)\phi_{cd} + k^2} + 2k^2 + (k^2+1)\phi_{cd}} \right) \right]^{\frac{\theta_2}{\pi}}$$

ϕ_{cd} = velocity potential ~ $-k^2 < \phi_{cd} < 0$ (9)

c. Height of base:

$$h = \sum_{n=1}^{n=i} \Delta Y_{bc_i} + Y_{cd} \qquad (10)$$

d. Length of free-shear layer:

$$\ell = \sum_{n=1}^{n=i} \left(\sqrt{(\Delta X_{bc_i}{}^2 + \Delta Y_{bc_i}{}^2)} \right)_i + \sqrt{X_{cd}{}^2 + Y_{cd}{}^2} \qquad (11)$$

The solutions obtained, being in integral form, required numerical techniques for application to the present study. The computational method is generally as follows:

a. Inclinations of the base and the fence are chosen. (For $\theta_1 \geqq 0$, the solution was found to be generally insensitive to changes to θ_2 in the range $-\frac{\pi}{2} < \theta_2 < -\frac{\pi}{4}$; $\theta_2 = -\frac{\pi}{2}$ was chosen for simplicty in applying the solution. For $\theta_1 < 0$, a relationship was found between θ_1 and θ_2:

$$\theta_2 = -27.5° + 2.5\theta_1 \text{ (degrees)} \qquad (12)$$

which resulted in realistic solutions.)

b. A range of base pressures is chosen.

c. Corresponding to each set of values of C_{pb}, θ_1 and θ_2, values of the free-constants k_1 and k_2 are determined using the expressions presented in Appendix II. (For $\theta_1 = 0$, a single constant, k, is determined explicitly. For $\theta_1 \neq 0$, k_1 and k_2 cannot be determined explicitly. It was found that for θ 0, k_2 could be related to θ_1 by:

$$k_2 = .825 + .005\theta_1, \ (\theta_1 \text{ in degrees}) \qquad (13)$$

For $\theta_1 > 0$, it was found that k_2 could be related to θ_1 by:

$$k_2 = \frac{1.939}{\theta_1 - 66.7} + 1.003 + .00033\,\theta_1 \ (\theta_1 \text{ in degrees}) \qquad (14)$$

These relations, along with the relations found for θ_2, allowed k_1 to be determined by a numerical iteration technique.)

d. The free-streamline equations presented in Appendix II determine explicitly the geometry of the corresponding free-shear layers with respect to the height of the base. Also, the corresponding height of the fence with respect to that of the base is determined. (The relations discussed previously for determining θ_2 and k_2 as a function of k_1 were developed in an attempt to minimize the fence height, required to maintain realistic correspondence with the recompression zone).

Figure 11 presents typical plots of the free-shear layer geometry for specific values of C_{p_b}, base angle and fence angle.

1.2.2.3 COMBINATION OF VISCOUS AND INVISCID SOLUTIONS. Combination of the two solutions described in the previous paragraphs offers an analytic method by which the base pressure level for a two-dimensional subsonic flow model can be predicted. The sensitivity of the base pressure level to changes in such parameters as base flow inclination, boundary layer thickness and free-stream conditions can be systematically studied.

The independent solutions, the viscous base flow analysis of Nash and the inviscid free-shear layer geometry, were programmed for numerical solution on digital computing equipment. Programming of the viscous solution was restricted to the no-bleed (q_b=0) case. (Inclusion of the solution for arbitrary bleed-rates would provide a means for study of the effects of mass addition on two-dimensional base flow and with new experimental data, means could be conceived for extending the analysis to three-dimensional base flow).

The digital solution of the combined two-dimensional subsonic base pressure solution is diagrammed in Figure 12. The two-dimensional analytic solution provided a technique which was used to correlate the data obtained during the experimental program discussed in Section 2. The experimental data also provided empirical data which allowed the two-dimensional solution to be extended to generalized three-dimensional base geometries, as discussed in Section 3.

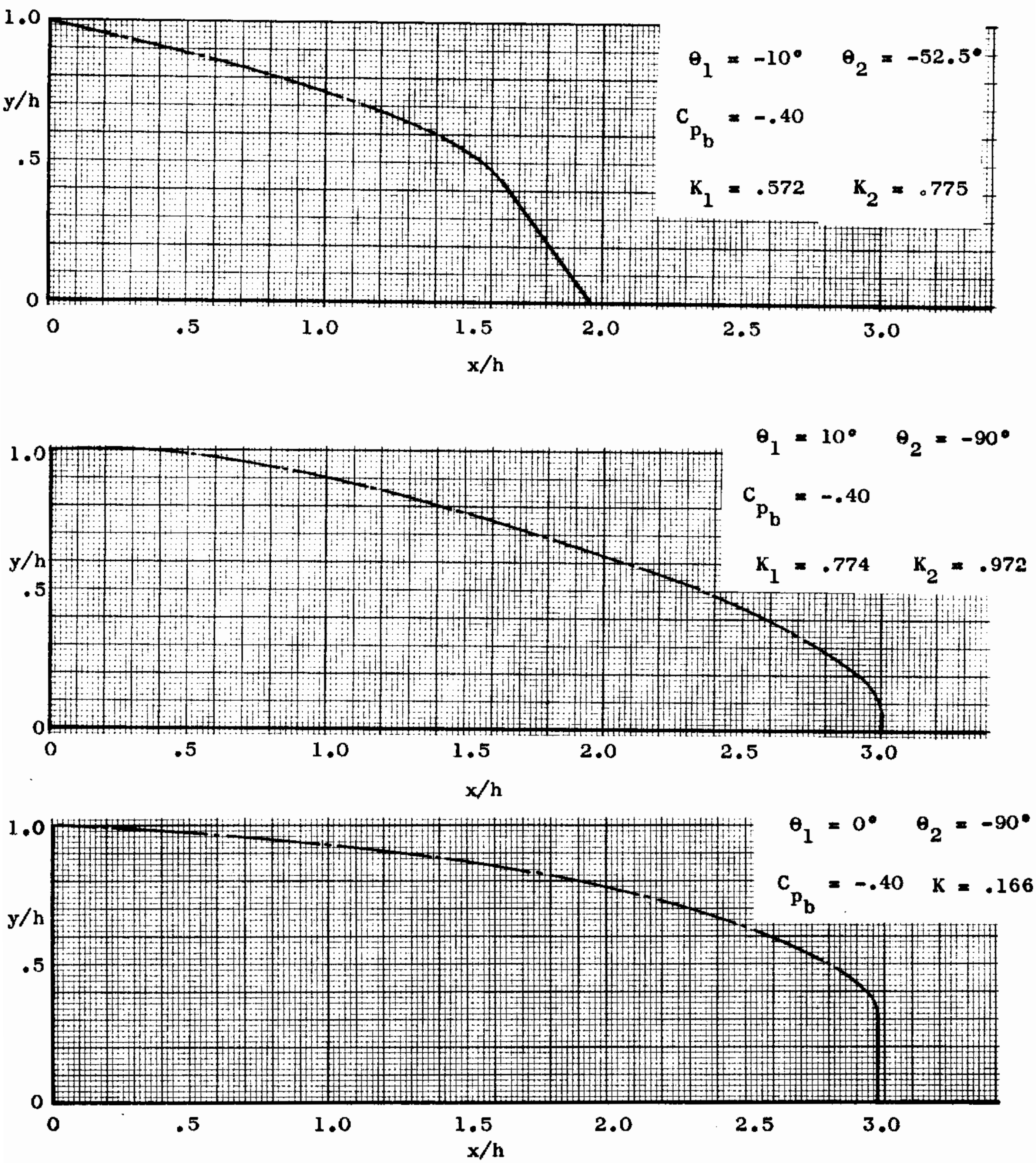

FIGURE 11   Example of Predicted Geometry of Free-Shear Layer

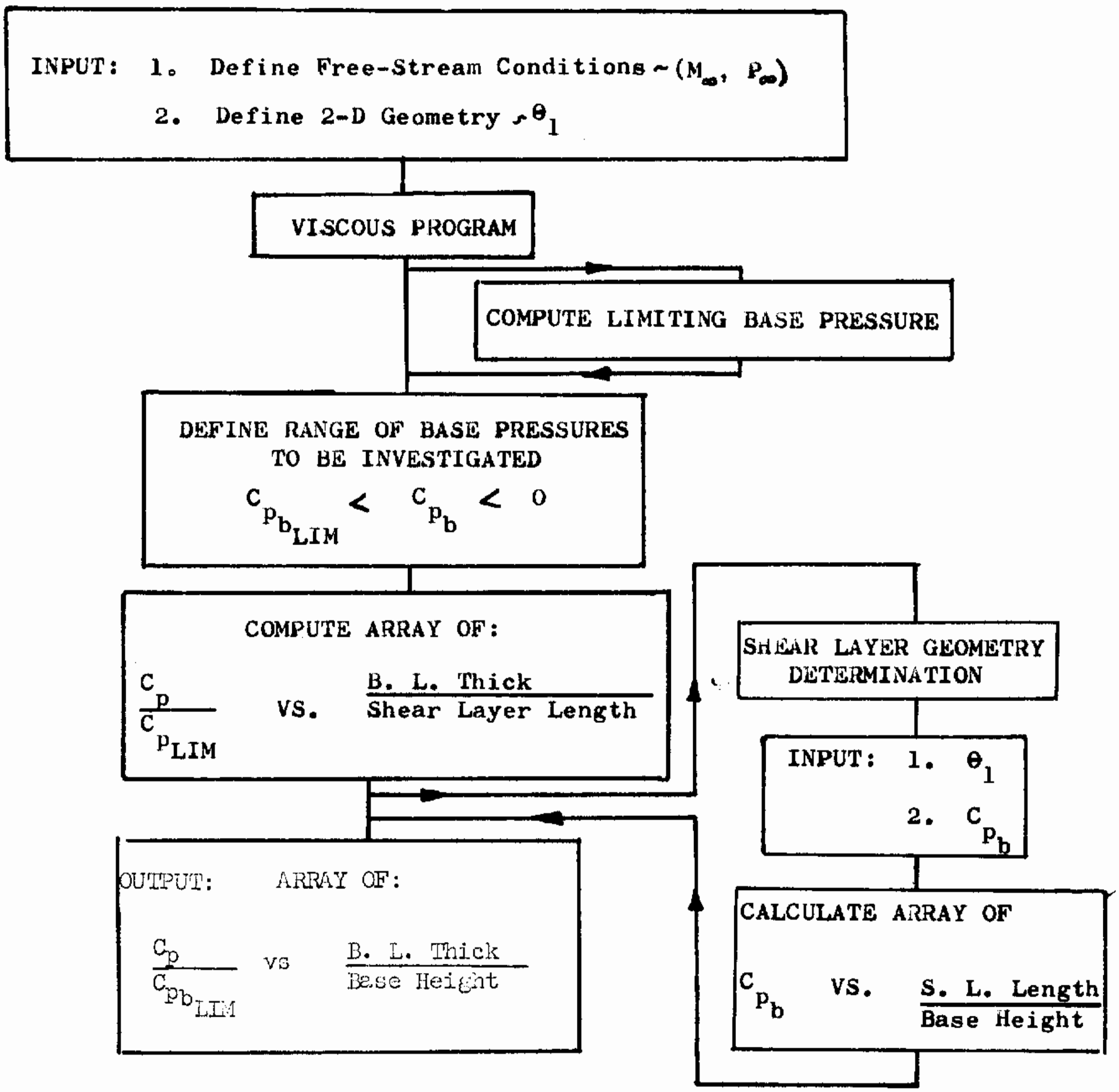

FIGURE 12 Diagram of Digital Computer for Two-Dimensional Analytical Solution

2/ EXPERIMENTAL PROGRAM

Subsonic wind tunnel tests were performed to determine the pressures and wake flow characteristics in the base regions of blunt-based bodies. Aerodynamic forces and surface pressures were measured concurrently to provide additional data. The test series was designed to provide experimental data to augment the analytic investigation and the development of a generalized prediction technique.

These tests were conducted in the San Diego State College Smoke Wind Tunnel, the Convair 8' x 12' wind tunnel and the California Institute of Technology 32" x 45" Merrill Wind Tunnel. Only two-dimensional tests were made in the smoke tunnel, both two-dimensional and three-dimensional tests were made in the Convair tunnel, and only three-dimensional tests were made in the Cal Tech tunnel. The Reynolds numbers tested were approximately 1.8×10^5 and $.6 \times 10^5$ per foot in the smoke tunnel, and $.7 \times 10^6$ to 2.2×10^6 per foot in the Convair tunnel and in the Cal Tech tunnel. The maximum dynamic pressure tested with the two-dimensional models was 60 lbs/sq ft and with the three-dimensional models 150 lbs/sq. ft. The data from these tests, in graphical and tabular form, are presented in Volume II along with a run index for each tunnel, listing the order in which the tests were made.

2.1 SUMMARY OF WIND TUNNEL PROGRAM

2.1.1 SMOKE TUNNEL TESTS. Reference 24 summarizes the smoke tunnel investigation. The data obtained from testing of two-dimensional configurations, with varying thicknesses and base flow angularities, is presented in Volume II.

2.1.2 GD/CONVAIR AND CAL TECH TESTS

2.1.2.1 PRESSURE DATA. The two-dimensional configurations depicted in Figures 13 and 14, with varying degrees of thickness and base flow angle, were tested to determine the effects of base angle Reynolds number, angle of attack, transition strip location and horizontal splitter plate on the base pressure coefficient.

The three-dimensional configurations, depicted in Figures 15 through 18, were tested to determine the effects of base angle, nose bluntness, fin interactions and base planform assymmetry, trailing edge sweep, angle-of-attack and Reynolds number on base pressure coefficient.

A summary of the average values of base pressure coefficient measured for the different models and their configurations is presented in Tables I and II.

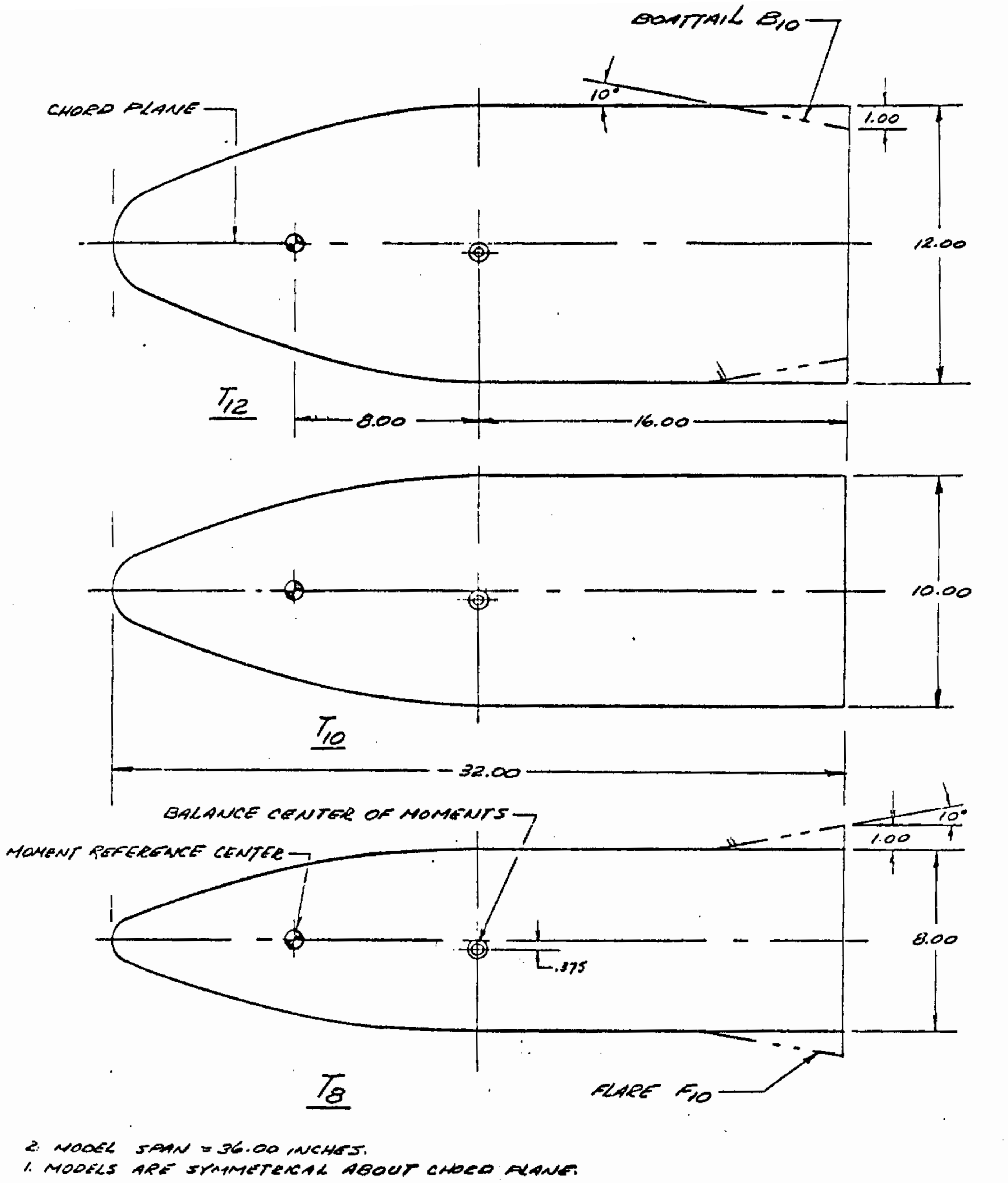

FIGURE 13 Two-Dimensional Models

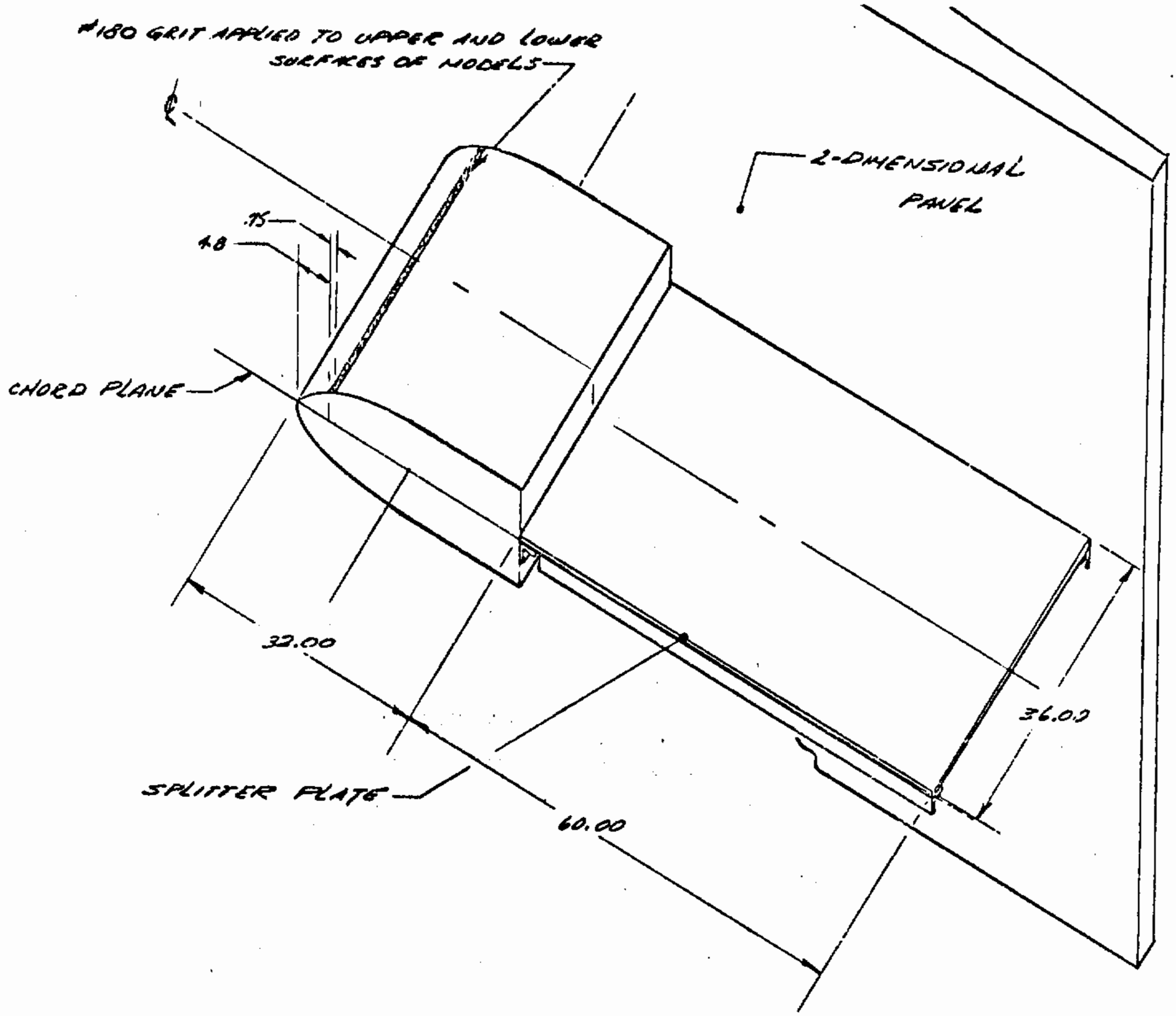

FIGURE 14 Two-Dimensional Configuration Transition Grit and Splitter Plate Location.

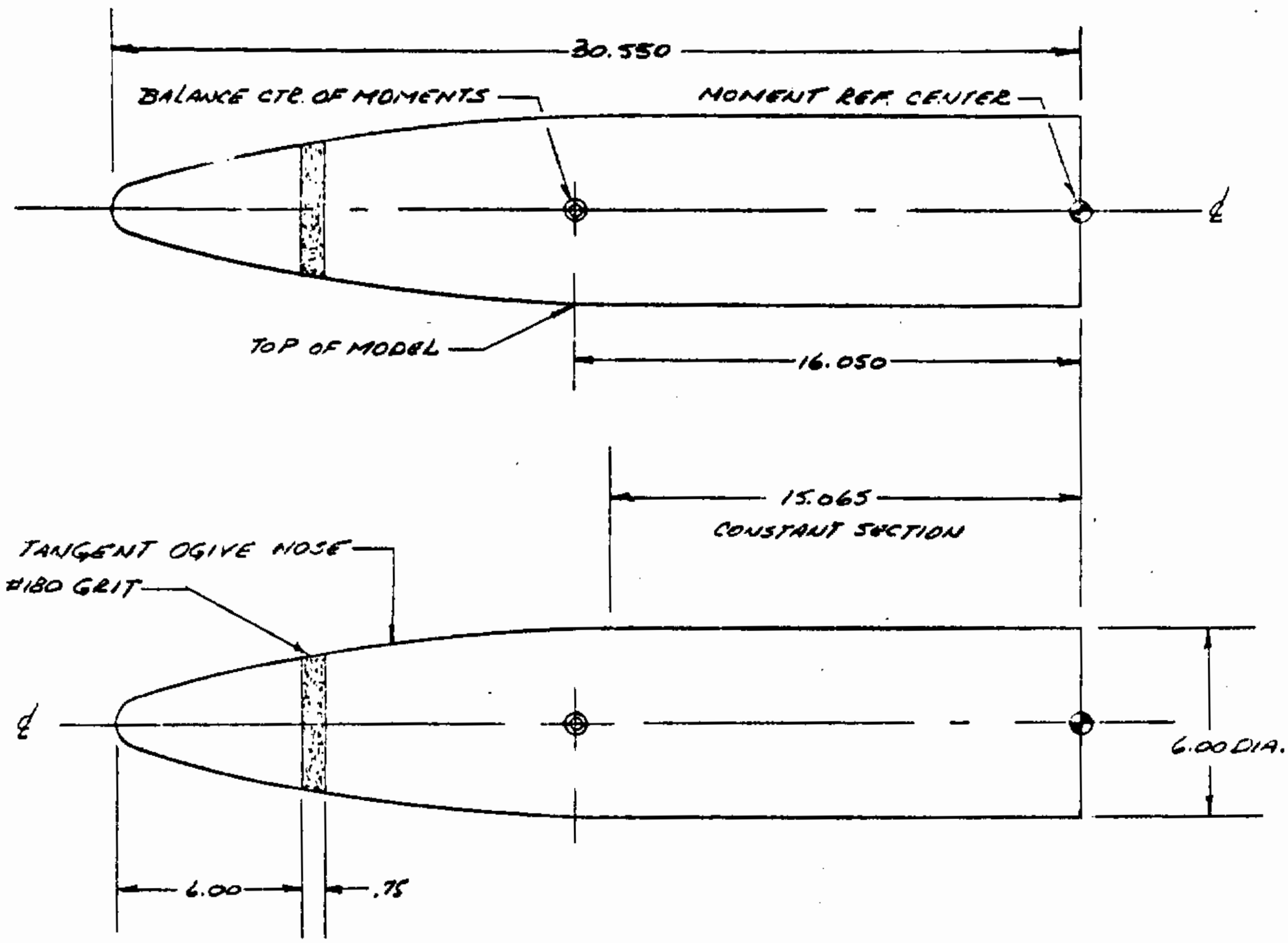

FIGURE 15 Three-Dimensional Body - M_1

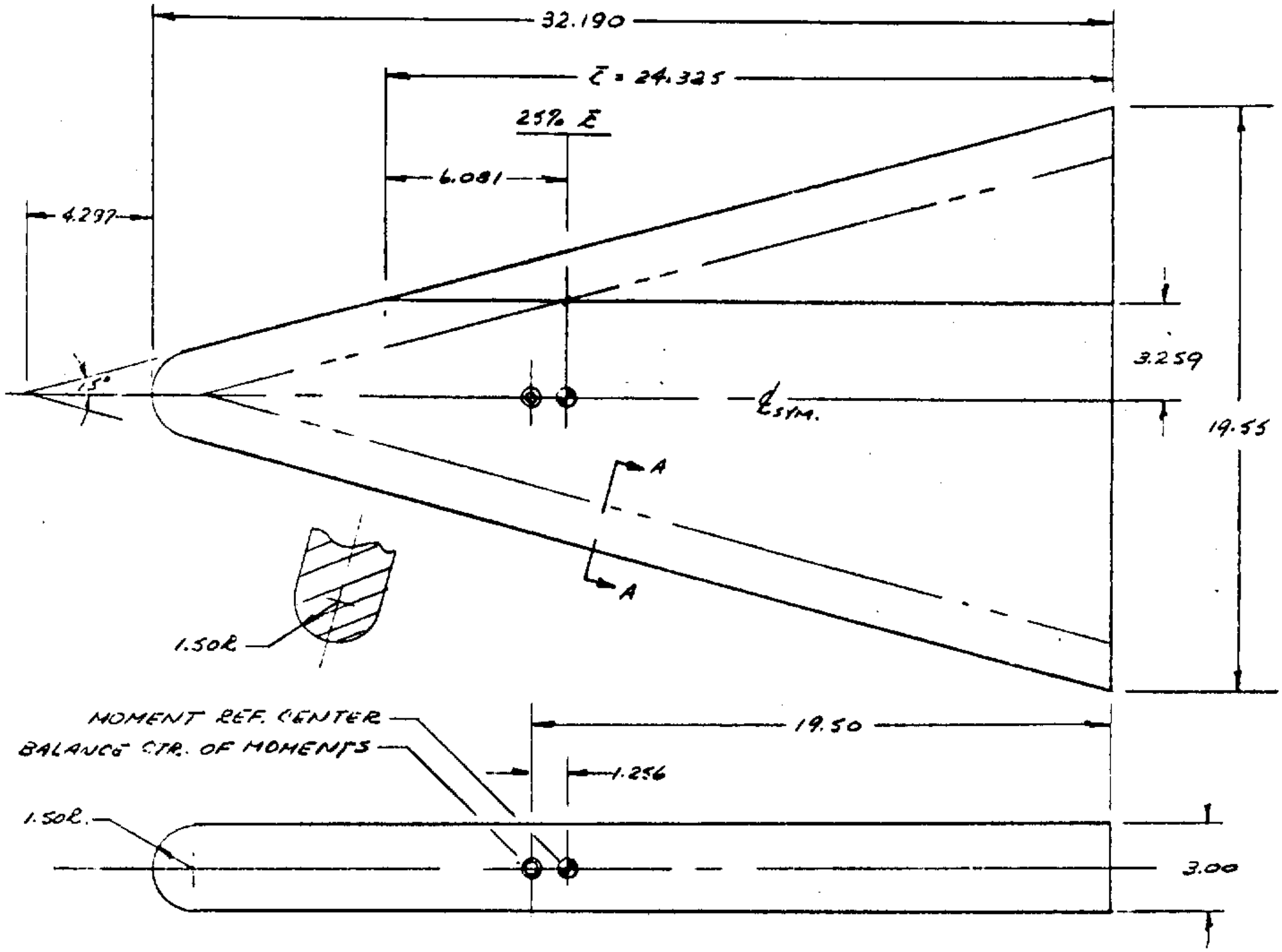

FIGURE 16 Three-Dimensional Wing - W_3

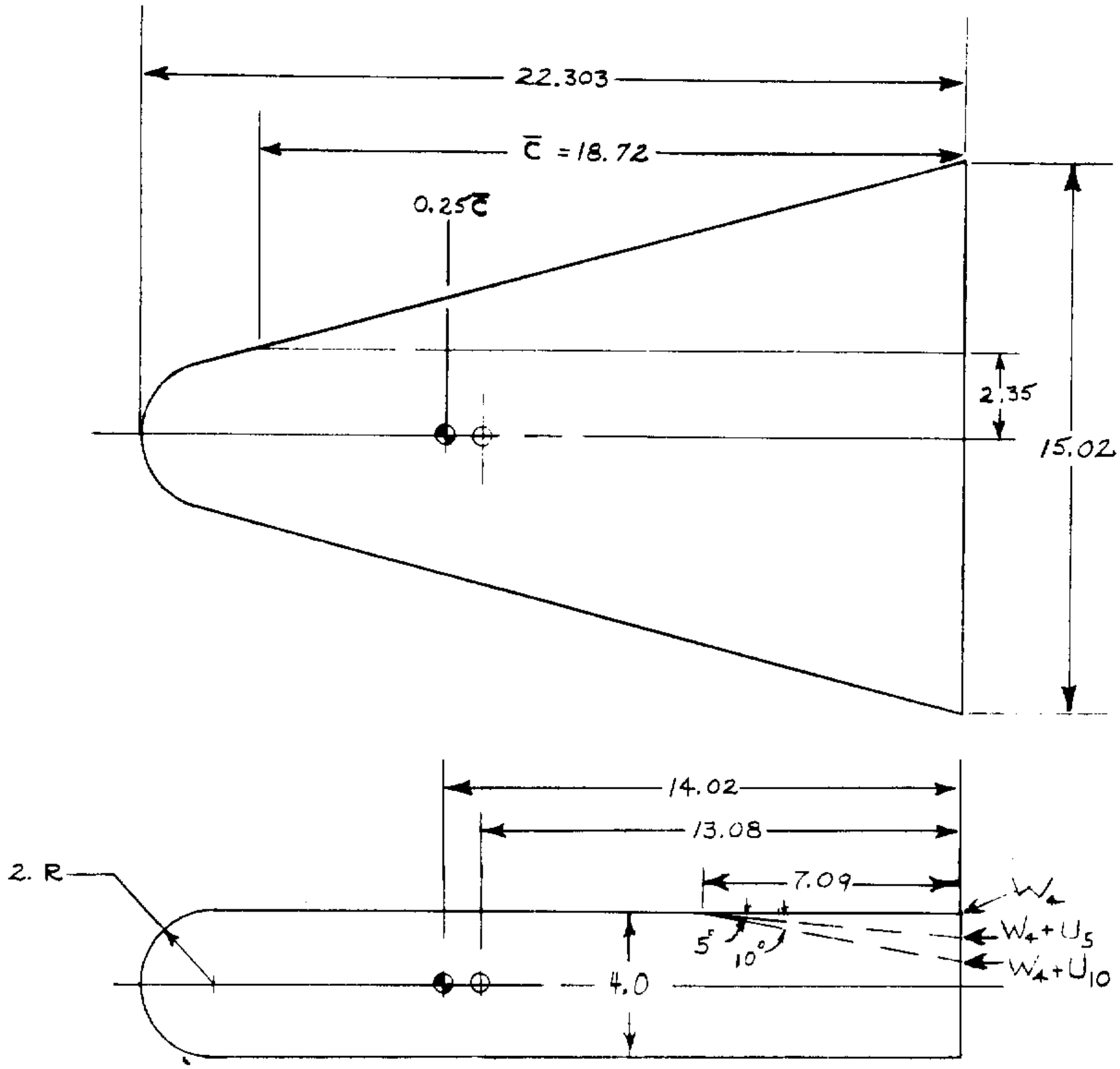

FIGURE 17 Three-Dimensional 4 Inch Wing - W_4

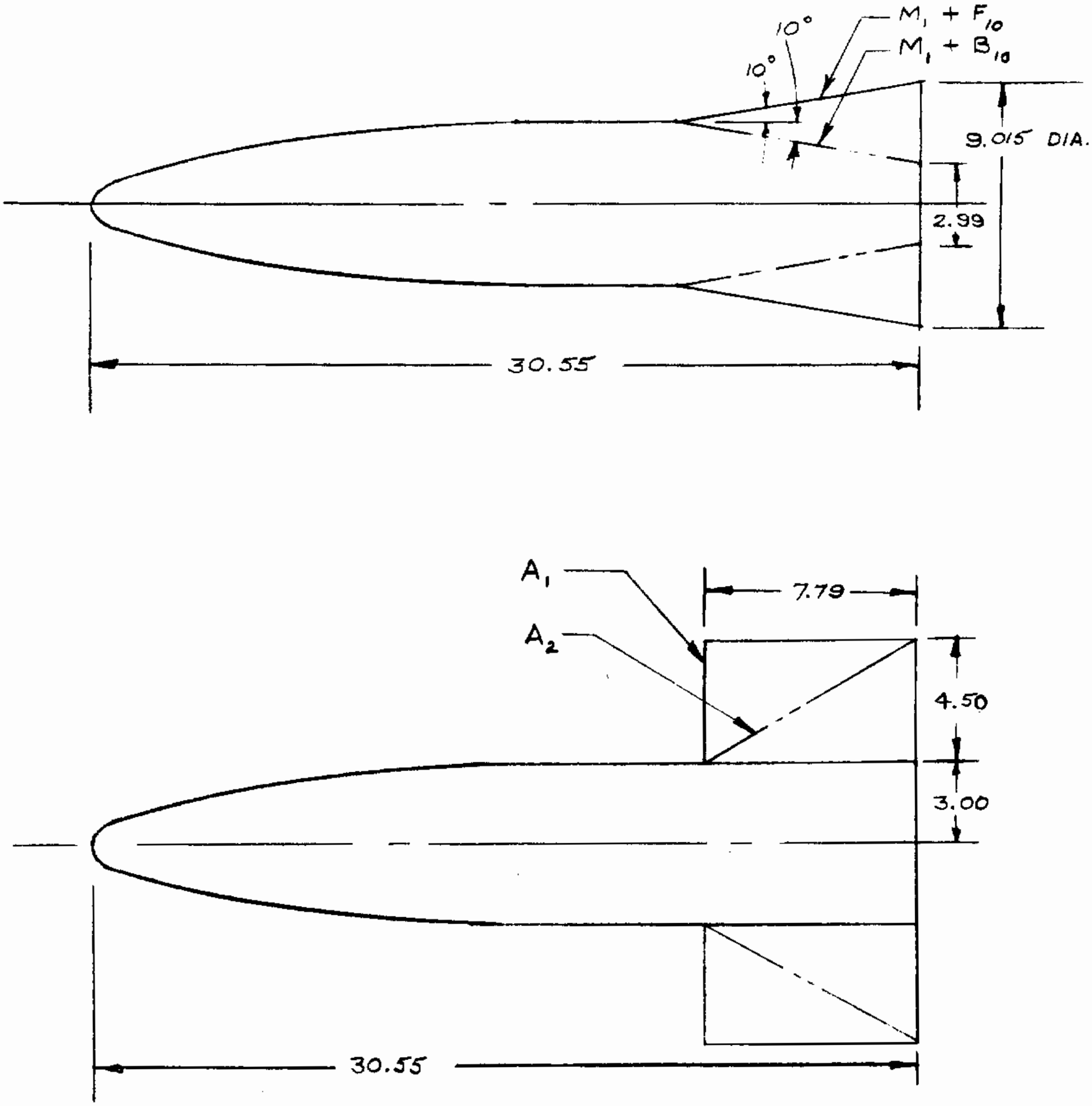

FIGURE 18 Three-Dimensional Body with Boattail and Fin Configurations

TABLE I
2-D Configurations
(Convair Tests)
Average Base Pressures

Run	Configuration	q	Avg. Base Pressure $\alpha = 0$	$\alpha = 3$	$\alpha = 6$
2*	T_{10}	60	-.81465	-.80504	-.80526
3*	T_{10}	30	-.79695	-.77259	-.75329
5	T_{10}	60	-.80981	-.79609	-.79339
6	T_{10}	30	-.76839	-.77885	-.75801
7	T_{10+P}	15	-.44628		
7	T_{10+P}	30	-.45163		
7	T_{10+P}	45	-.42149		
7	T_{10+P}	60	-.4374		
9	T_8+F_{10+P}	60	-.53598		
9	T_8+F_{10+P}	30	-.57199		
10	T_8+F_{10}	60	-.99236	-.97204	-.94929
11	$T_{12}+B_{10+P}$	60	-.33162		
11	$T_{12}+B_{10+P}$	30	-.33294		
13	$T_{12}+B_{10}$	60	-.63833	-.60587	-.58788
14	$T_{12}+B_{10}$	30	-.55122	-.55250	-.55250
15	T_{12}	60	-.81488	-.82467	-.80561
16	T_{12}	30	-.84950	-.84081	-.81711

*Runs 2 and 3 do not have transition grit.

TABLE II
3-D Configurations
Average Base Pressures
(Corrected for Tares)
(Cal Tech Tests)

Run	Configuration	q	Average Base Pressure $\alpha = 0$	$\alpha = 5$	$\alpha = 10$
CT 1	M_1	30	-.15149	-.18685	-.23737
CT 2	M_1	45	-.16046	-.18663	-.2346
3	M_1+B_{10}	45	+.02802	+.001401	-.03799
4	M_1+B_{10}	30	+.03144	+.000238	-.04876
5	W_3	45	-.46919	-.46863	
6	W_3	30	-.46658	-.48719	
9	$W_3+1/2M_2$	45	-.28234	-.29310	
10	$W_3+1/2M_2$	30	-.28484	-.29113	
11	W_3+S_{30}	45	-.59690	-.62249	
12	W_3+S_{30}	30	-.64110	-.64153	
13	W_3+S_{45}	45	-.60846		
14	W_3+S_{45}	30	-.60882		
17	W_4	45	-.45678	-.48823	
18	W_4	30	-.44993	-.47334	
19	W_4+U_{10}	45	-.31957	-.37312	
20	W_4+U_{10}	30	-.31381	-.37429	
21	W_4+U_5	45	-.37416	-.38928	
22	W_4+U_5	30	-.37046	-.38110	

TABLE II (cont'd)

Run	Configuration	q	Average base pressure $\alpha = 0$	$\alpha = 5$	$\alpha = 10$
CT 23	M_1+A_1	45	-.24974	-.26180	
24	M_1+A_1	30	-.27222	-.24870	
25	$M_1+1/2A_1$	45	-.20351	-.21980	-.26184
26	$M_1+1/2A_1$	30	-.22262	-.22628	-.25971
27	M_1+A_2	30	-.31583	-.31885	-.31513
28	M_1+A_2	45	-.33103	-.32458	-.32155
29	$M_1+1/2A_2$	45	-.26184	-.25307	-.26794
30	$M_1+1/2A_2$	30	-.26910	-.26122	-.27192
31	M_1+R	30	-.14482	-.15966	-.21490
32	M_1+R	45	-.14624	-.16599	-.22482
33	M_1+F_{10}	45	-.3000	-.29783	
34	M_1+F_{10}	30	-.29866	-.29524	

2.1.2.2 FORCE AND MOMENT DATA. Force and moment data were obtained from both the GD/Convair and Cal Tech wind tunnel tests. Figure 19 presents force and moment data obtained for an axisymmetric configuration and is typical of the data obtained. It should be noted that the base area of the 3-D body configurations and the planform area of the wing configurations is used for reference area for the respective configurations. The pitching moments for the body configurations are destabilizing due to the choice of the model reference moment center located at the model base.

2.1.2.3 AIRFLOW VISUALIZATION. French-chalked vertical splitter plates were used for wake flow visualization on selected two-dimensional configurations tested in the Convair wind tunnel. Figure 20 presents a typical photograph of the flow pattern set up in the wake of a two-dimensional configuration with zero base flow angle.

The flow patterns obtained using the french-chalk method are difficult to interpret. The wake was found to be unsteady when probed with hot-wire anemometers. The flow patterns may indicate a time-averaged gross flow pattern established by slow response of the french-chalk method. A different interpretation can be made by referring to the static pressure distribution measured near the centerline of the wake region. In all of the french-chalk plates an apparent streamline can be identified which appears to separate streamlines recirculating into the base region and streamlines flowing downstream. In each case, the apparent "dividing" streamline is directed to the point in the wake of lowest static pressure. This may indicate a type of boundary layer flow, where the liquid french-chalk is influenced by the low static pressure levels which are found along the wake centerline.

The flow patterns do indicate a high level of vorticity adjacent to the base. These vortices were stationary and represented the only steady portion of the wake.

2.1.2.4 PRESSURE WAKE SURVEYS. Total and static pressure surveys were obtained using a pressure rake in the wakes of selected two and three-dimensional configurations tested in the Convair wind tunnel. Plots of lines of constant value of the parameter $\frac{H - P_\infty}{q_\infty}$, a measure of the total head loss in the wake region, were made for each configuration. The original data obtained from the wake total pressure survey was crossplotted to obtain plots of total pressure versus vertical station at each longitudinal survey station.

2.1.2.5 HOT-WIRE ANEMOMETER WAKE SURVEYS. Hot-wire anemometer data was obtained by surveying the wake of selected two-dimensional configurations (with and without horizontal splitter plate) and three-dimensional configurations. The data was recorded on oscillograph and magnetic tape.

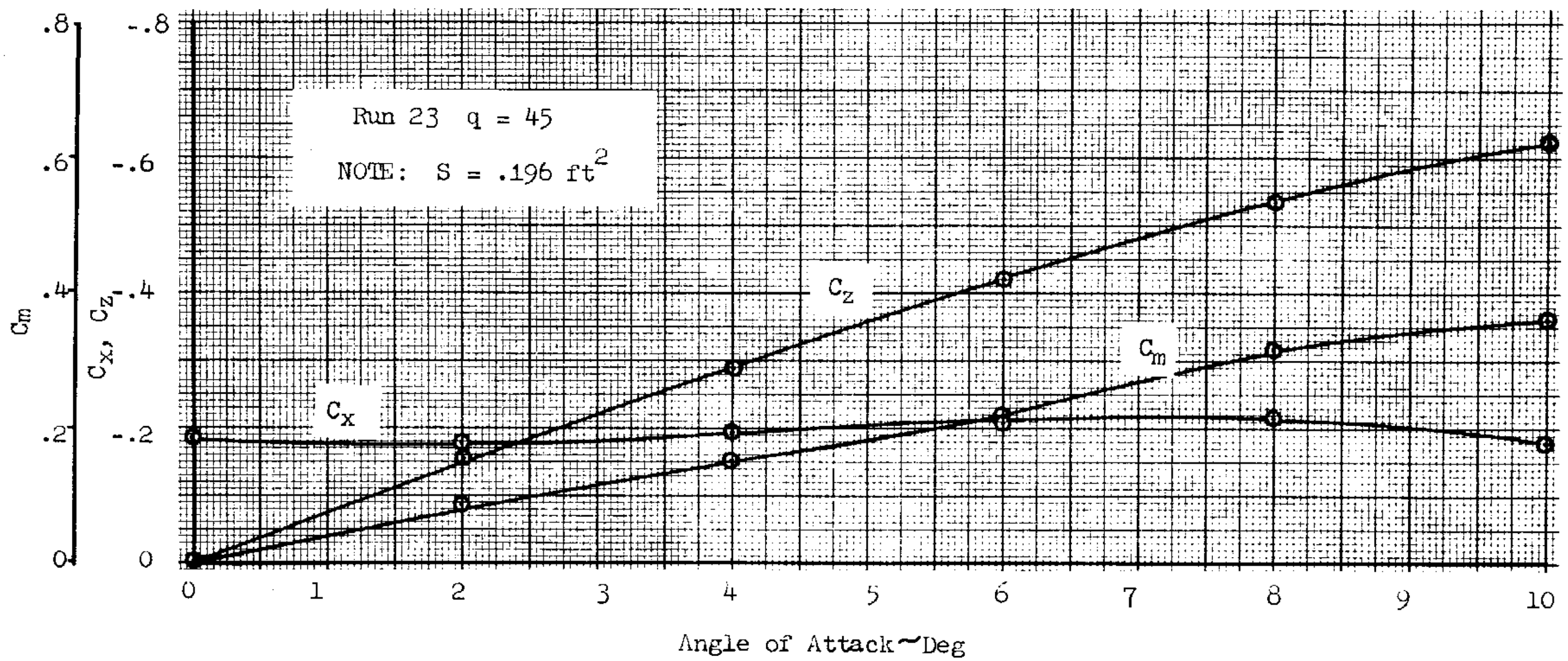

FIGURE 19 **Typical Force and Moment Data - 3-D Body**

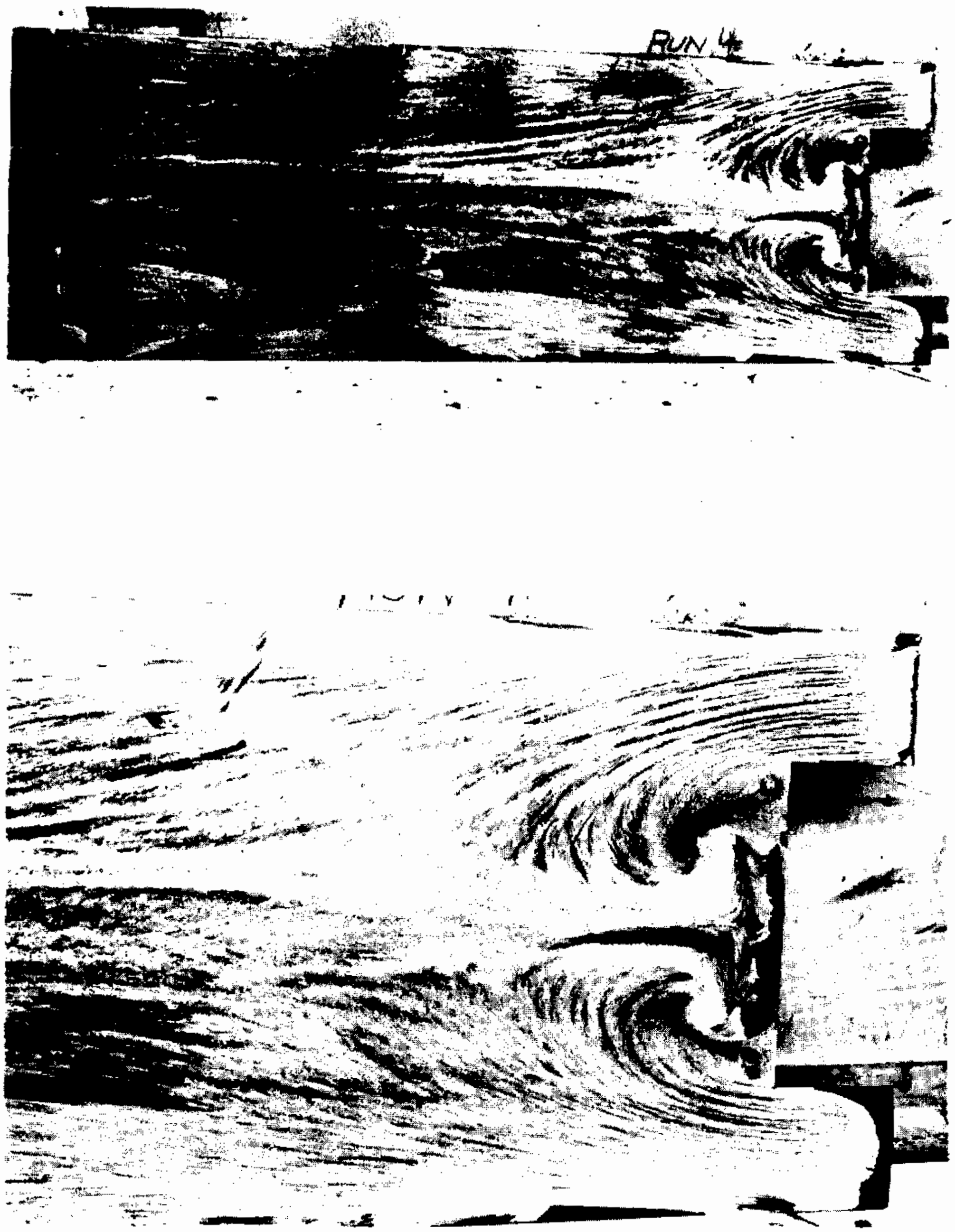

FIGURE 20 Typical Visualization of Flow Past a 2-D Model with Zero Base Angle

2.2 CORRELATION OF WAKE FLOW PROPERTIES

The wake flow data discussed in Sections 2.1.2.4 and 2.1.2.5 represents the results of the portion of the experimental program concerned with the investigation of the flow properties of wakes generated by two - and three-dimensional blunt based geometries in subsonic flow. The purpose of the wake flow investigation was primarily to verify the applicability of the idealized two-dimensional steady base flow solution described in Section 1 to the analysis of three-dimensional base flow.

In order to identify the nature of three-dimensional base flow, the experimental program included considerable testing of the two-dimensional configurations tested with and without a horizontal splitter plate. In addition to the base pressure measurements, extensive wake flow measurements, including hot-wire data and total and static pressure surveys, were conducted to investigate the nature of steady and non-steady two-dimensional wake flow and of three-dimensional wake flow. The following paragraphs present correlations of the data obtained for the three types of wake flow phenomenon.

2.2.1 TWO-DIMENSIONAL WAKES.

2.2.1.1 WAKE VELOCITY FLUCTIONATIONS. The non-steady nature of flow in the wake of two-dimensional isolated bases is demonstrated most effectively by the measurement of velocity fluctuations using hot-wire anemometry. Figure 21 presents a trace of velocity fluctuations measured in the wake of a two-dimensional configuration with zero base angle. The trace exhibits a marked periodicity with a frequency of approximately 70 cps. Similar measurements of fluctuations in the wake of the two-dimensional configurations with 10° flare and 10° boattail, along with the data from the two-dimensional configuration with zero base angle, were correlated with the data of previous investigations using the non-dimensional Strouhal number, as presented in Figure 22.

The term "steady" as applied to the wake flow phenomenon being discussed refers primarily to the nature of the shear layers which separate at the base; the formation of a trailing vortex system is suppressed and the wake is turbulent with an absence of periodicity. Figure 23 presents a trace of the velocity fluctuations measured in the wake of a two-dimensional configuration with a horizontal splitter plate; no periodicity can be observed and the fluctuations can be described as completely random.

2.3.1.2 STATIC PRESSURE. Figure 24 presents the static pressure along the centerline of a two-dimensional configuration tested with and without a horizontal splitter plate. Behind the isolated section, the static pressure decreases away from the base reaching a minimum at a distance of approximately 1-1/2 times the semi-thickness of the section. This low pressure "trough" is believed to coincide with the point at which the vortices form (reference 5). Downstream of the trough the static pressure rises and levels off at some value below ambient static pressure. (It can be shown theoretically that the static pressure along the centerline of a vortex street is lower than free-stream static pressure by an amount depending on the strength of the street).

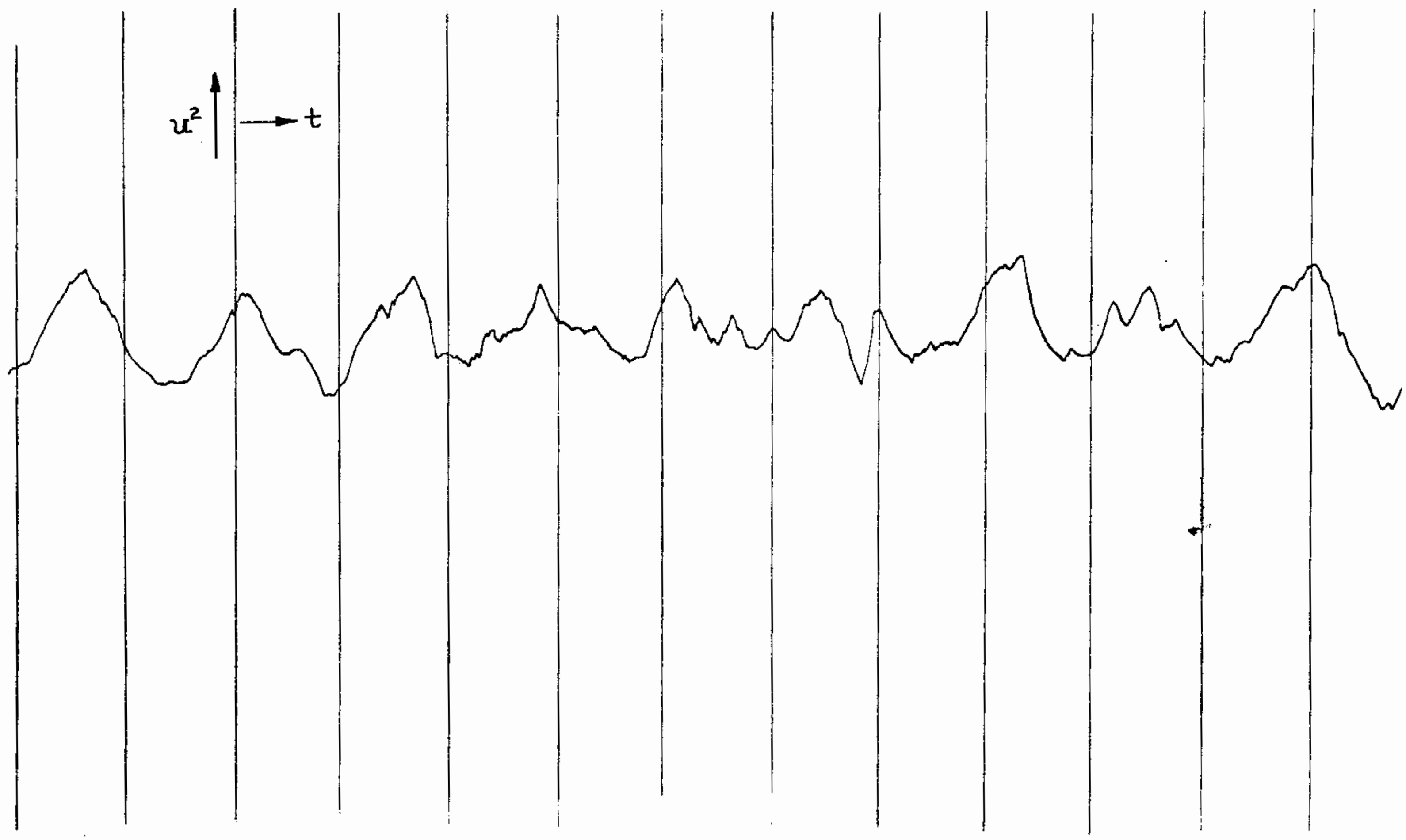

FIGURE 21 Velocity Fluctuations in the Wake of a Two-Dimensional Configuration with Zero Base Angle 7-3/8" aft of base Time Lines = .01 sec

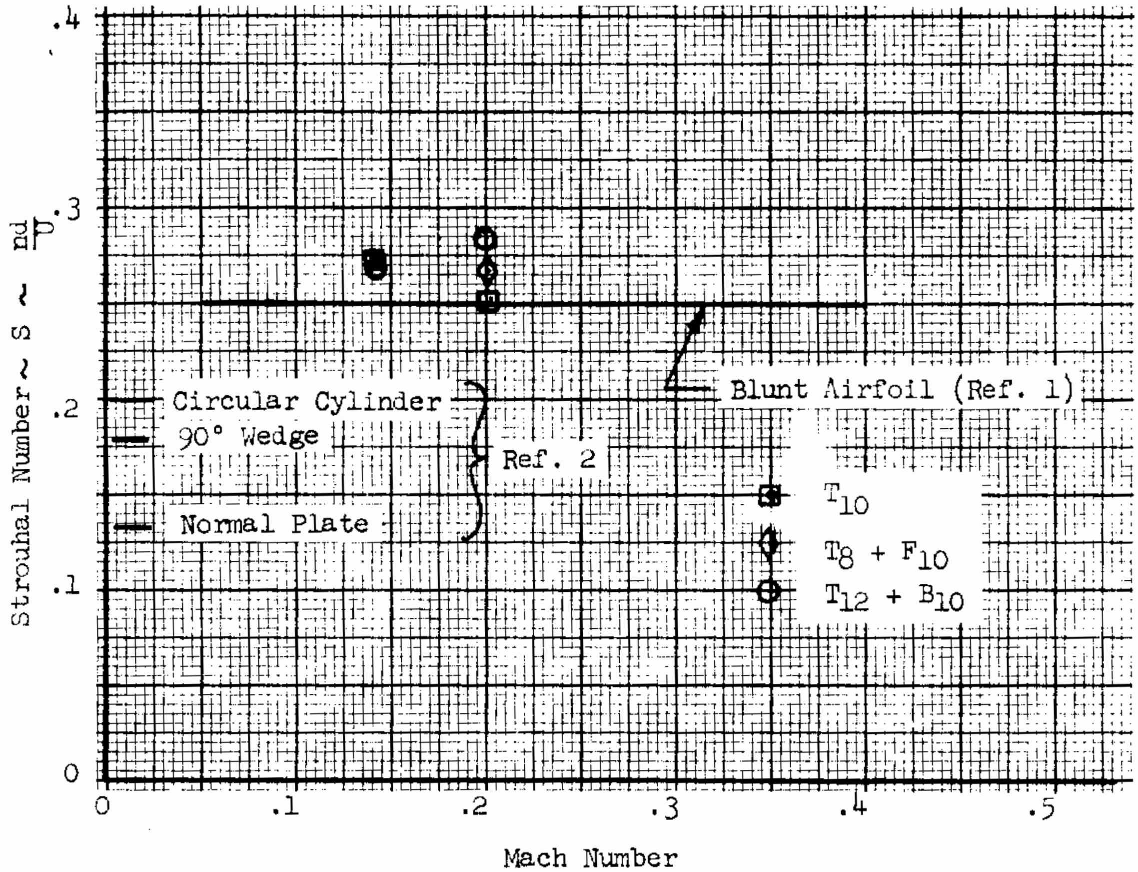

FIGURE 22 Correlation of Non-Dimensional Wake Periodicity of Two-Dimensional Isolated Blunt Bases in Subsonic Flow

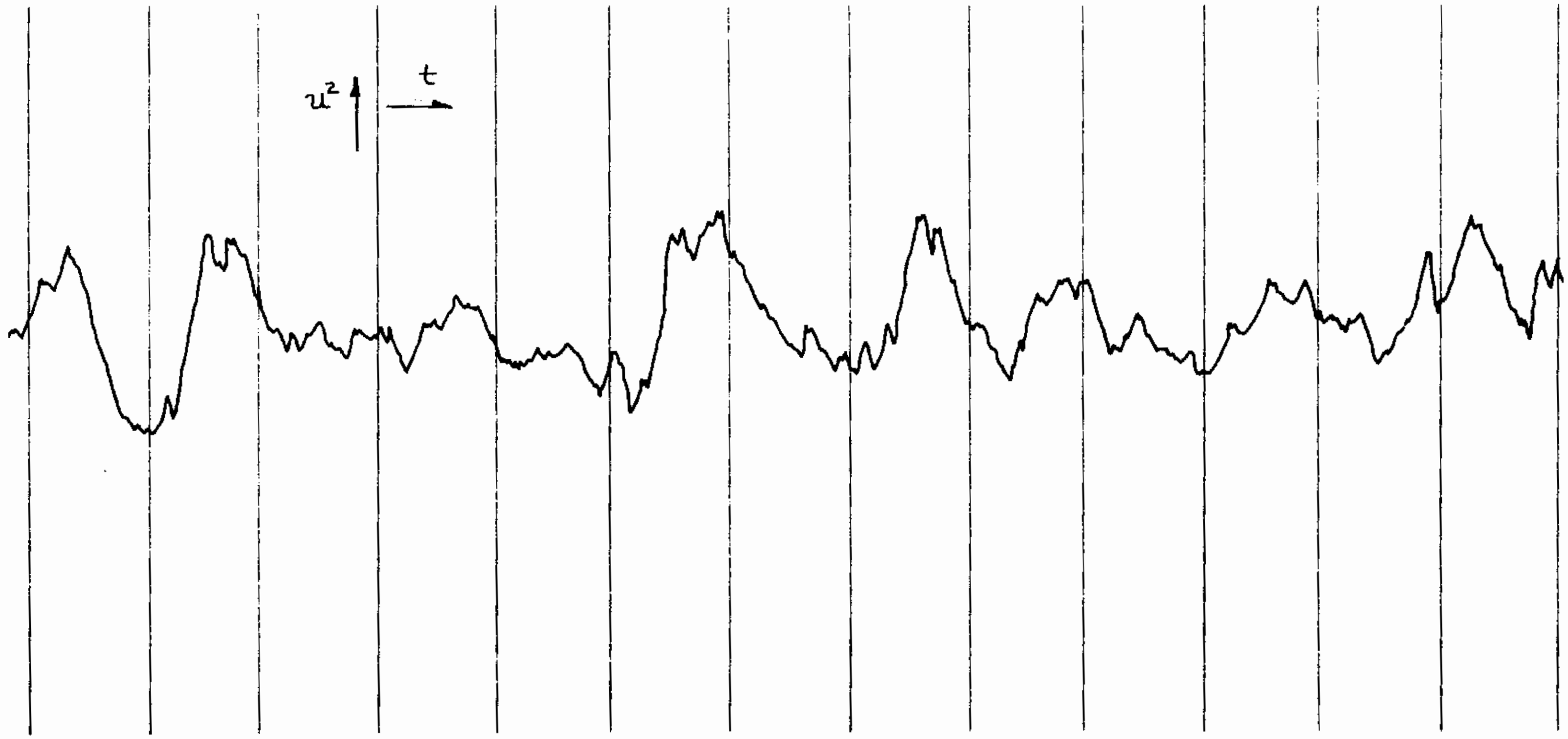

FIGURE 23 Velocity Flucatuations in the Wake of a Two-Dimensional Configuration with Horizontal Splitter Plate 7-3/8" Aft of Base Time Lines = .01 sec

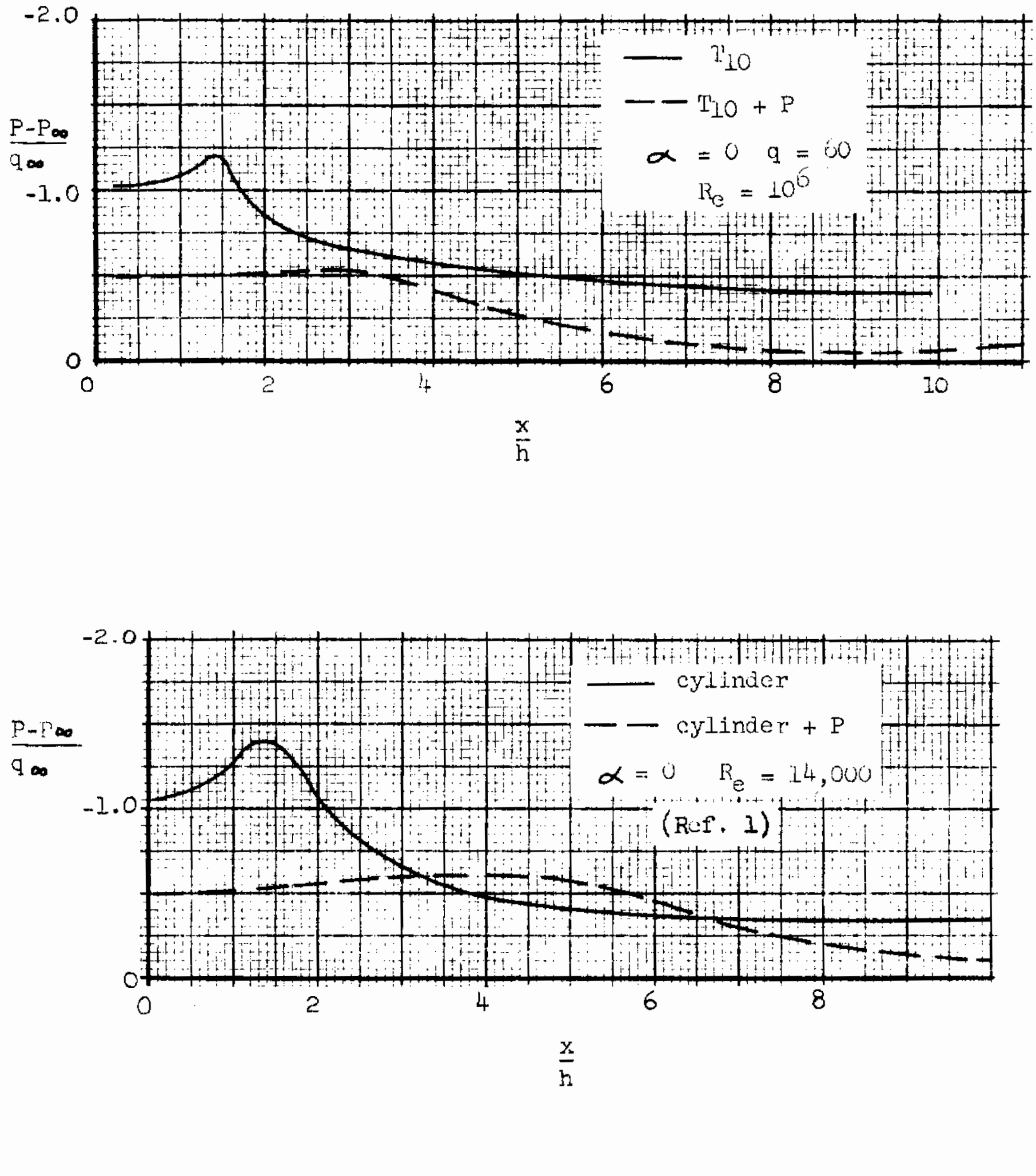

FIGURE 24 Effect of Horizontal Splitter Plate on Centerline Static Pressure Behind Two-Dimensional Blunt Base Configurations in Subsonic Flow.

The static pressure along the splitter plate behind the two-dimensional configuration is markedly different, with a region of fairly constant pressure extending from the base and eventually recovering to a value near ambient. The existence of a constant pressure "cavity", as postualted by the idealized steady flow model, is indicated.

Figure 24 also presents a comparison of centerline static pressures behind a circular cylinder with and without a horizontal splitter plate, obtained from reference 5. A very similar result is shown.

2.2.1.3 TOTAL PRESSURE. The use of a total-pressure rake to survey the wakes behind the configurations tested in the CVAL tunnel resulted in the wake total pressure contours, such as those presented in Figure 25. The parameter $\frac{H - P_\infty}{q_\infty}$ is a measure of the total head loss in the wake and also provides a measure of wake width. The differences of the fluid mechanics of the unsteady "open" wake and the steady "closed" wake are indicated. The integrated effect of the losses represented by the contours is directly related to the marked differences in base pressure or resultant base drag of the two base flow phenomenon.

2.2.2 THREE-DIMENSIONAL WAKES. The previous section has attempted to establish the character of the steady and non-steady subsonic two-dimensional base flow phenomenon. The properties of three-dimensional subsonic base flow will be examined using the two-dimensional data for comparison.

2.2.2.1 WAKE VELOCITY FLUCTUATIONS. Figures 26 through 28 present traces of the velocity fluctuations in the wakes of the three-dimensional configurations. The fluctuations measured in the wake of the axisymmetric three-dimensional body, appear to be random and exhibit characteristics similar to those measured in the turbulent wake of the two-dimensional configuration with horizontal splitter plate, (Figure 23). The fluctuations measured in the wakes of the thick delta wing configurations exhibit a degree of periodicity superimposed on the turbulent fluctuations. It appears that as the base planform tends toward a two-dimensional geometry, the wake contains regions with nearly two-dimensional unsteady properties. The locally shed vortices diffuse rapidly due to the turbulent wake emanating from the three-dimensional regions, although a discernible amount of energy is present in the wake at the periodic frequency.

A thorough correlation of three-dimensional wake flow properties would include an analysis of wake fluctuations using power spectral techniques. Periodicity (or the absence of periodicity) could be identified conclusively and correlated with geometrical parameters. Due to the limited scope of the present program, this was not attempted.

2.2.2.2 STATIC PRESSURE. Figure 29 compares the static pressures in the wake behind the axisymmetric configuration with the static pressure distribution in the wake behind the two-dimensional configuration with horizontal splitter plate. The distribution near the centerline behind the axisymmetric body is similar to

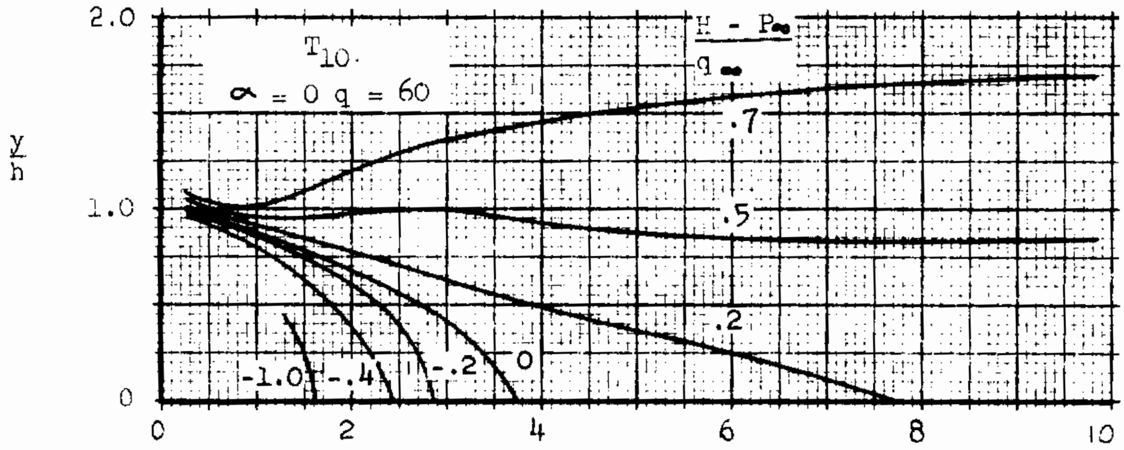

a. "Open" Wake

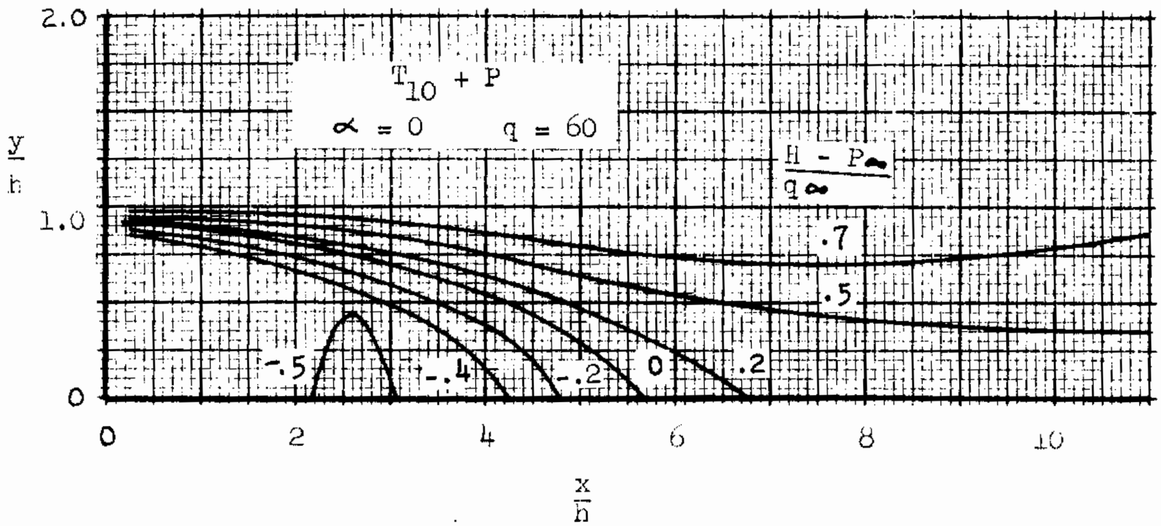

b. "Closed" Wake

FIGURE 25 Total Pressure Contours in the Wakes of Two-Dimensional Configurations With and Without Horizontal Splitter Plates

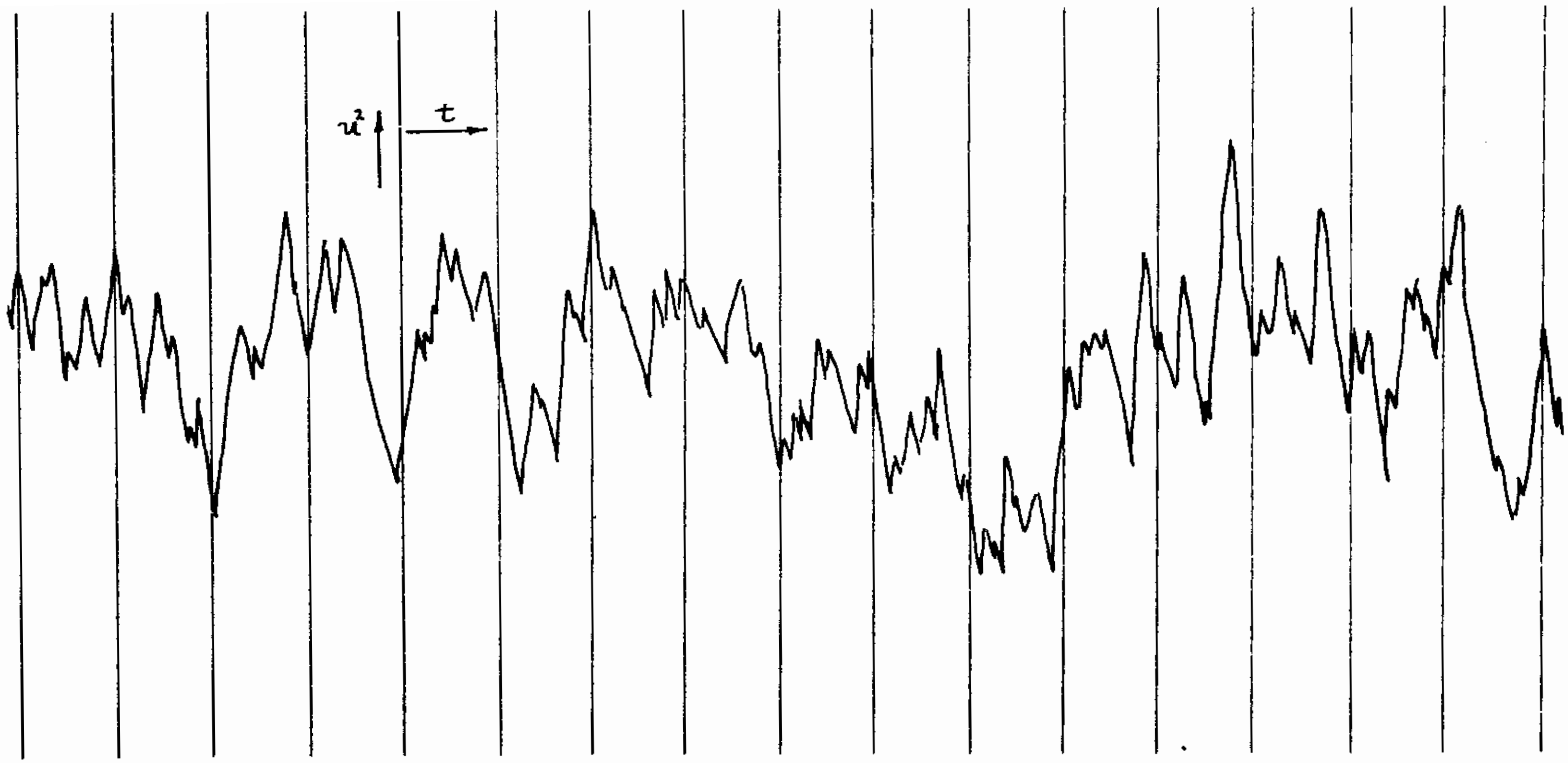

FIGURE 26 Velocity Fluctuations in the Wake of an Axisymmetric Configuration
6" Aft of Base Time Lines = .01 sec

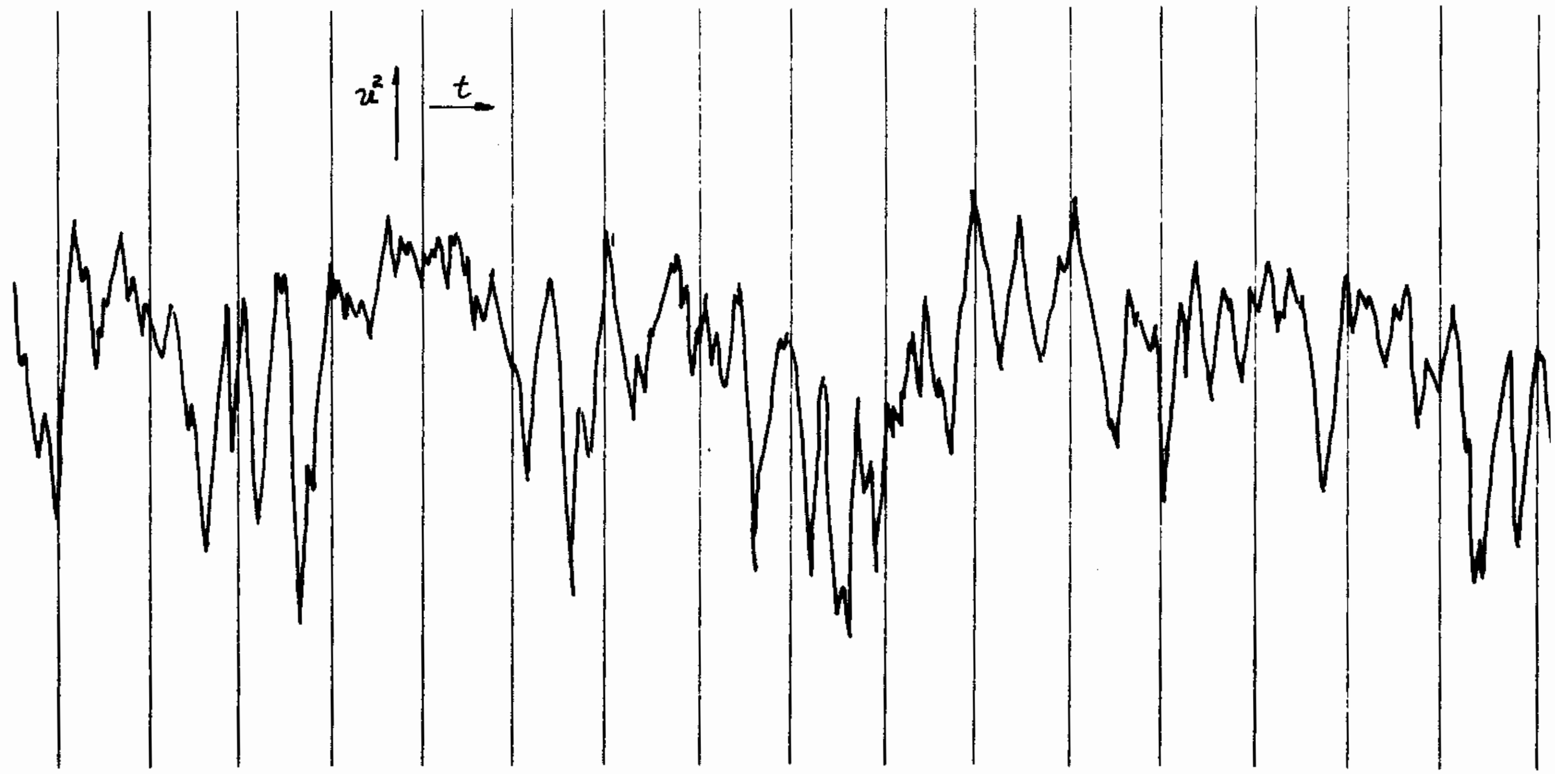

FIGURE 27 Velocity Flucations in the Wake of a Thick Delta Wing Configuration (W_3) 5" Aft of Base Time Lines = .01 sec

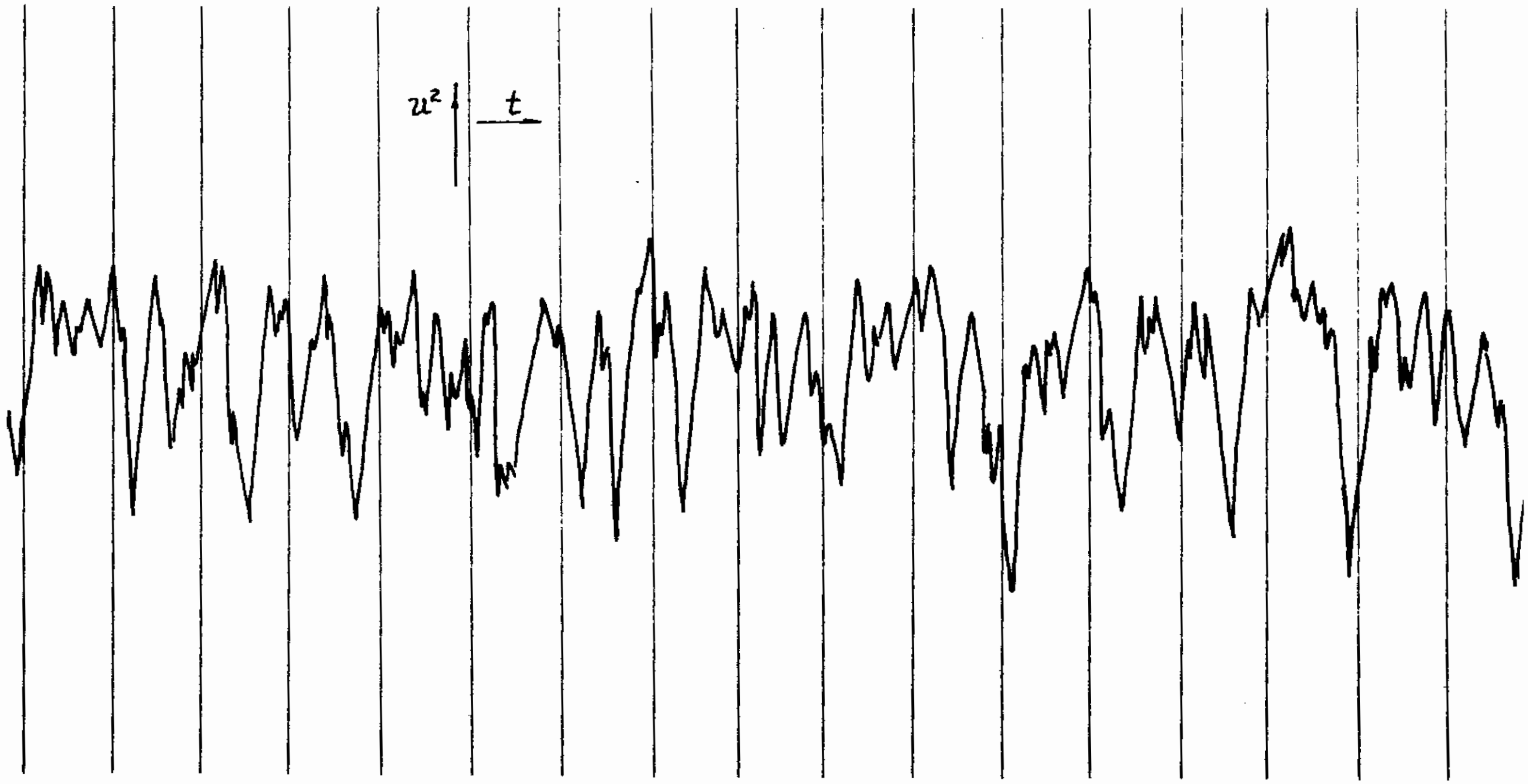

FIGURE 28 Velocity Fluctuations in the Wake of a Thick Delta Wing Configuration (W_4) 8" Aft of Base Time Lines = .01 sec

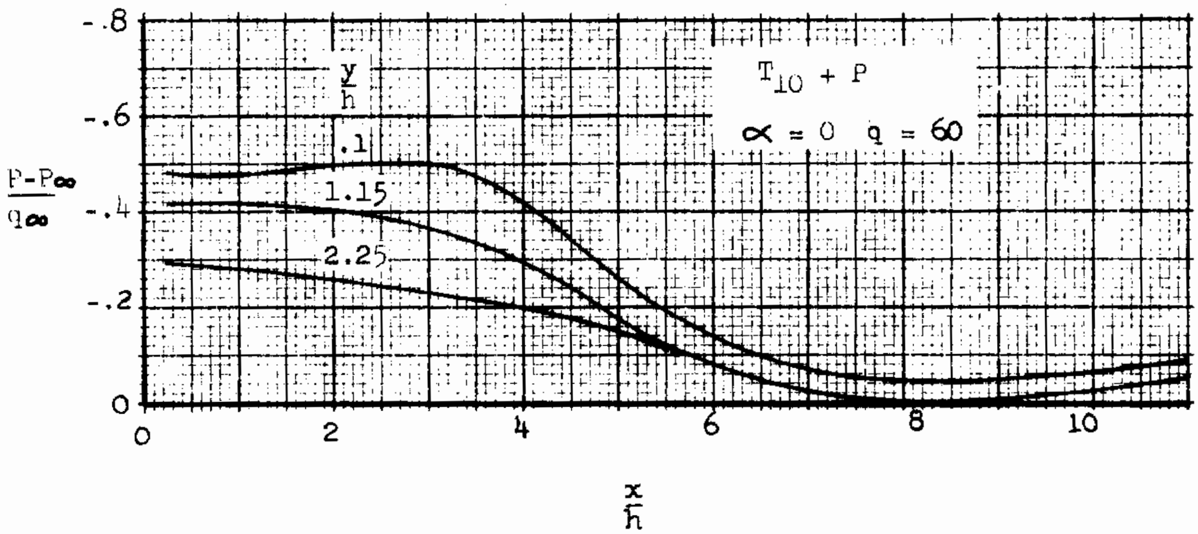

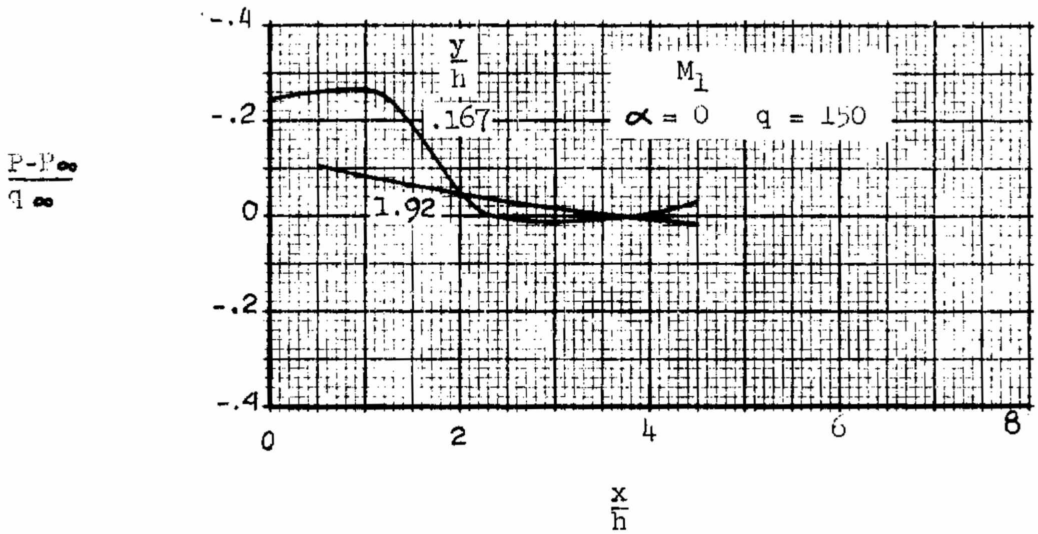

FIGURE 29 Comparison of Static Pressure Distributions in the Wakes of an Axisymmetric Configuration (M_1) and a Tw-Dimensional Configuration with Horizontal Splitter Plate (T_{10} + P)

the distribution found for the steady closed wake of the two-dimensional configuration with splitter plate. A constant pressure "cavity" is suggested.

Figure 30 presents the static pressures in the wake behind a thick delta wing configuration, measured at three spanwise stations with respect to the centerline. In each case, the distribution close to the horizontal plane of symmetry exhibits the presence of a "trough" with the pressure recovering downstream to a constant level lower than ambient. At these stations the distributions are typical of the two-dimensional non-steady wake, similar to that of the isolated two-dimensional configurations. Although surveys at outboard stations were not made, it can be expected that near the tips the static pressure distribution is similar to that behind the axisymmetric configuration.

The static pressure distributions follow the trend noted in the analysis of three-dimensional wake velocity fluctuations; the wake properties tend toward that of the non-steady two-dimensional phenomenon as the base geometry becomes more two-dimensional. It is to be expected that near the center of a configuration such as a thick delta, the wake would be essentially two-dimensional.

2.2.2.3 TOTAL PRESSURE. Figure 31 compares the distribution of total pressure in the wake of the axisymmetric configuration with the total pressure behind the two-dimensional configuration with horizontal splitter plate; the distributions exhibit similar characteristics, although the streamwise variation of the axisymmetric wake occurs over a shorter distance than the two-dimensional steady wake, which might be attributed to the effect of curvature on the steady flow mechanism. Figure 32 presents the total pressure distribution in the wake behind a thick delta wing configuration, again measured at the three spanwise locations. The distributions behind the wing are inconclusive since the total pressure distributions are not as markedly two-dimensional near the vertical plane of symmetry as the velocity fluctuations and static pressure distributions.

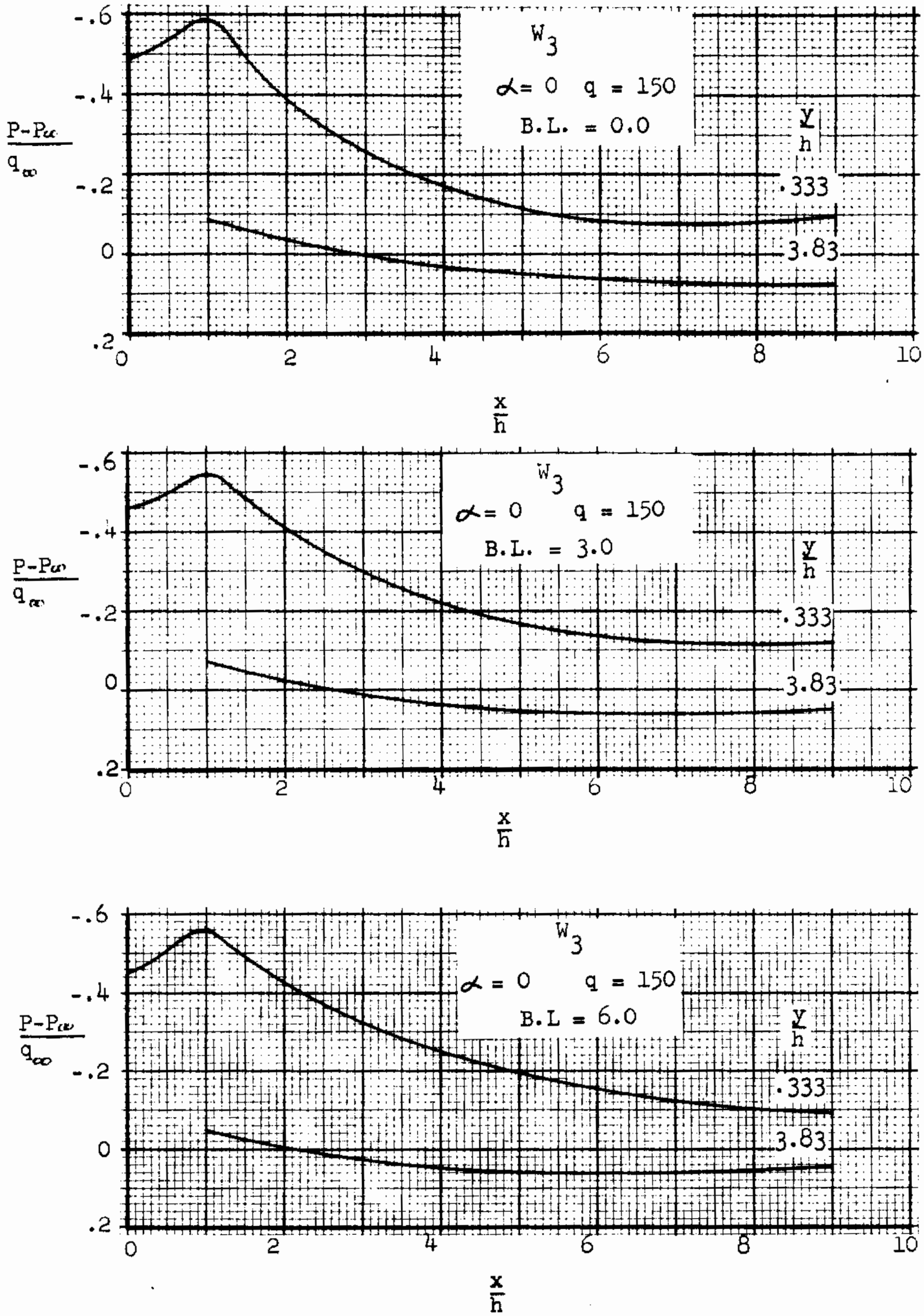

FIGURE 30 **Spanwise Variation of Static Pressures in the Wake of a Thick Delta Wing Configuration**

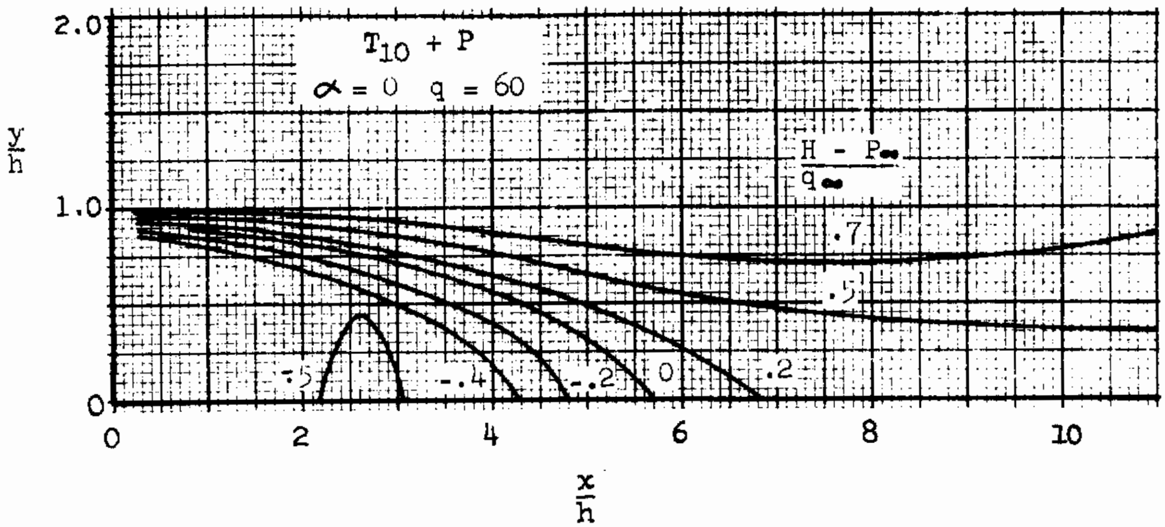

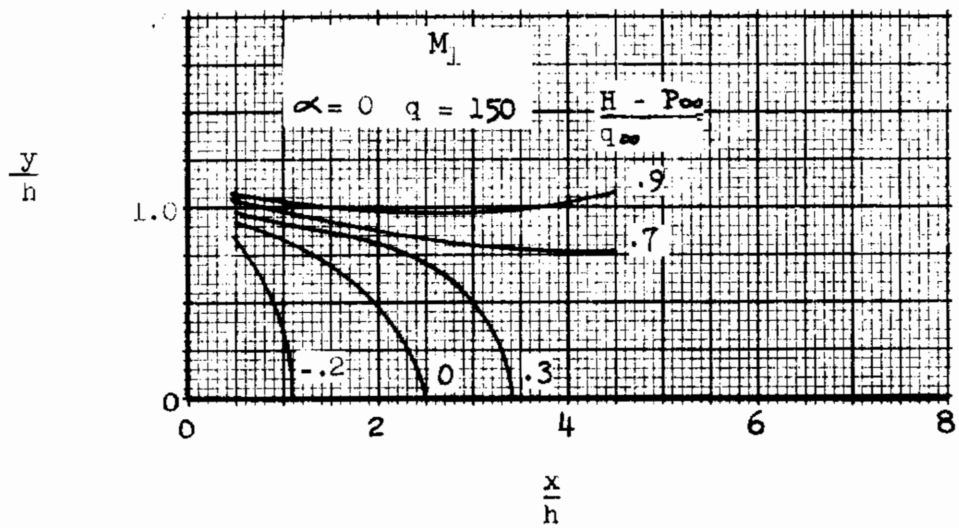

FIGURE 31 Comparison of Total Pressure Contours in the Wakes of an (M_1) and a Two-Dimensional Configuration with Horizontal Splitter Plate (T_{10} + P)

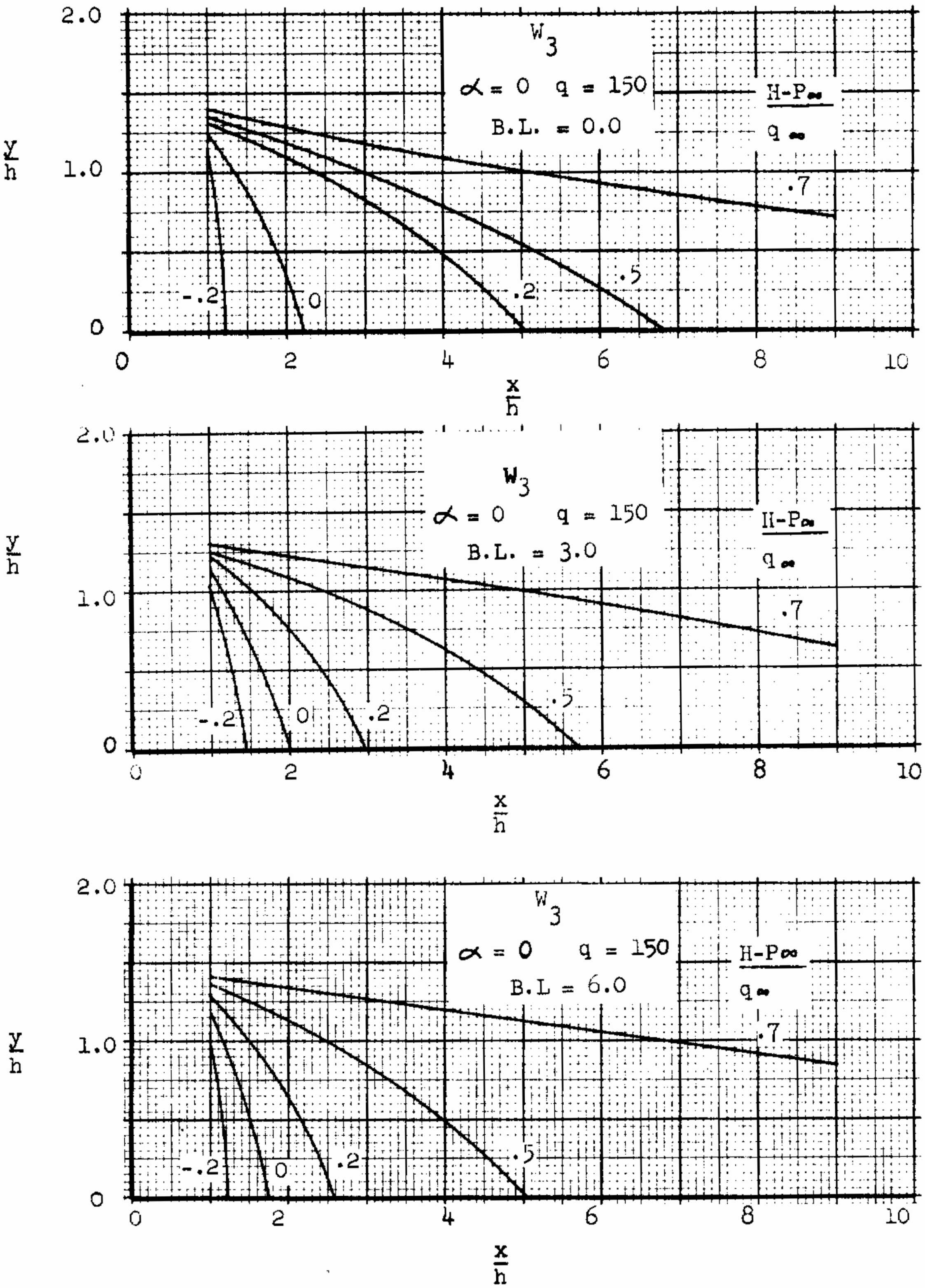

FIGURE 32 Spanwise Variations of Total Pressure Controus in the Wake of a Thick Delta Wing Configuration

3/ DEVELOPMENT OF GENERAL PREDICTION TECHNIQUE

The analytic solution of two-dimensional steady base flow, described in Section 1.2, forms the basis for a method by which the base pressure level of generalized three-dimensional base geometries can be made. The two-dimensional solution allows explicit determination of the effect on base pressure caused by changes to such parameters as base flow inclination, boundary layer thickness and free-stream conditions. The two-dimensional solution was used to correlate the data obtained during the experimental program discussed in Section 2. Empirical relationships were developed which account for three-dimensional base planform effects. The incorporation of the empirical factors with the two-dimensional analytic solution resulted in the formation of a generalized prediction technique. The technique has been programmed for numerical solution on digital computer equipment.

The following paragraphs describe the development of the general prediction method and the digital program for numerical computation. The use of the method is demonstrated by correlation of experimental data with predicted values.

3.1 DEVELOPMENT OF EMPIRICAL FACTORS TO ACCOUNT FOR THREE-DIMENSIONAL EFFECTS

The empirical analyses review in Section 1.1 indicated that the subsonic base pressure of three-dimensional blunt-based configurations is influenced by the effects of three independent parameters; boundary layer thickness at separation, angularity of the flow at separation, and three-dimensional planform effects. The two-dimensional analytic solution provides a tool to predict the effect of the boundary layer thickness and, partially, the effect of the base flow angularity (the free-streamline solutions are used to predict only shear-layer geometry, which, along with approaching boundary layer thickness, determines the effect of viscous mixing on the base pressure level). The effects of base flow angularity on the external flow field (the inviscid effect) and of base planform were recognized to be difficult to determine analytically and were therefore left to be evaluated empirically.

In order to use the two-dimensional solution to determine the empirical relations required, the following assumptions were formulated and applied:

1. The inviscid effect of base flow angularity (and, in turn changes to the external flow field) on base pressure level could be accounted for by empirical corrections to the limiting base pressure (e.g. minimum base pressure at a given free-stream condition in the absence of an approaching boundary layer) predicted for zero-angle flow. (The two-dimensional analysis solution predicts the limiting base pressure based on values of the local flow properties upstream of the separation point; for other than zero-angle flow, specific values would be required for each configuration. For zero-angle flow, free-stream conditions are sufficient to predict the limiting base pressure).

2. Three-dimensional planform effects could be accounted for by empirical corrections to the two-dimensional zero-angle limiting base pressure calculated at the particular free-stream condition under consideration.

3. The value of the actual base pressure (ratioed to the appropriate limiting base pressure) corresponding to a given value of boundary layer thickness is the same for a three-dimensional configuration as for the two-dimensional analytic model at the same value of effective base flow angle.

The two-dimensional analytic solution was used to correlate the wind tunnel data for several of the configurations tested during the experimental program. The following paragraphs describe the development of the empirical factors which allow the two-dimensional analytic solution to be extended to predict the base pressure of generalized three-dimensional base configurations.

3.1.1 EFFECT OF BASE ANGLE ON LIMITING BASE PRESSURE. The two-dimensional analytic solution was used initially to correlate the experimental data of the two-dimensional configurations tested with horizontal splitter plates, described in Section 2. Since the analytic solution relates boundary layer thickness to base pressure, values of boundary layer thickness had to be known for each experimental data point. In lieu of experimentally determined values, the boundary layer momentum thickness at the separation point was predicted analytically for the given configuration and test conditions using the formula for turbulent incompressible flow over a flat plate obtained from reference 27:

$$\delta_{**}(X) = 0.036\ X \left(\frac{X\ U_\infty}{\nu}\right)^{-\frac{1}{5}} \qquad (15)$$

Figure 33 indicates close agreement between the predicted and experimental values of base pressure for two-dimensional steady flow with zero base angularity. (It is noted that the assumption N=1 for the reattachment condition in the analytical viscous solution, as discussed in Section 1.2.2.1.1, results in better agreement than the empirical value of N suggested by Nash).

The two-dimensional analytic solution was used to analyze the variation of base pressure with boundary layer thickness and base angle of a given free-stream condition; Figure 34 presents the results for values of base angle between -10° and +10°. This analytical data suggested a method by which an empirical factor to account for the effect of base angularity on limiting base pressure could be developed. The following procedure was used:

1. Values of the boundary layer momentum thickness for the two-dimensional configurations with horizontal splitter plate and base angles of -10°, 0° and 10° were determined at the test conditions using the formula presented above.

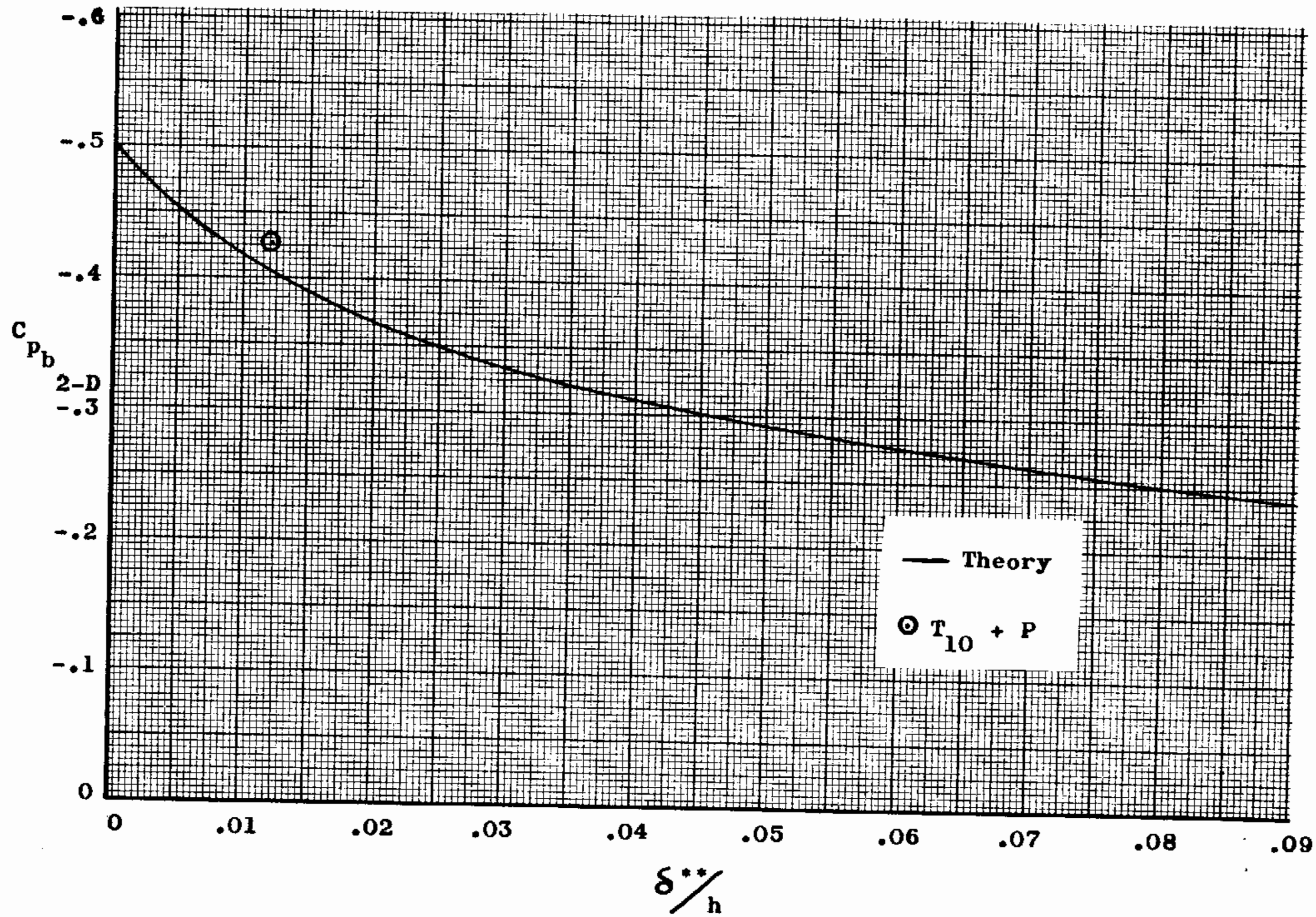

FIGURE 33 Predicted Effect of Boundary Layer Thickness on Base Pressure for Steady Two-Dimensional Flow and Comparison with Experiment

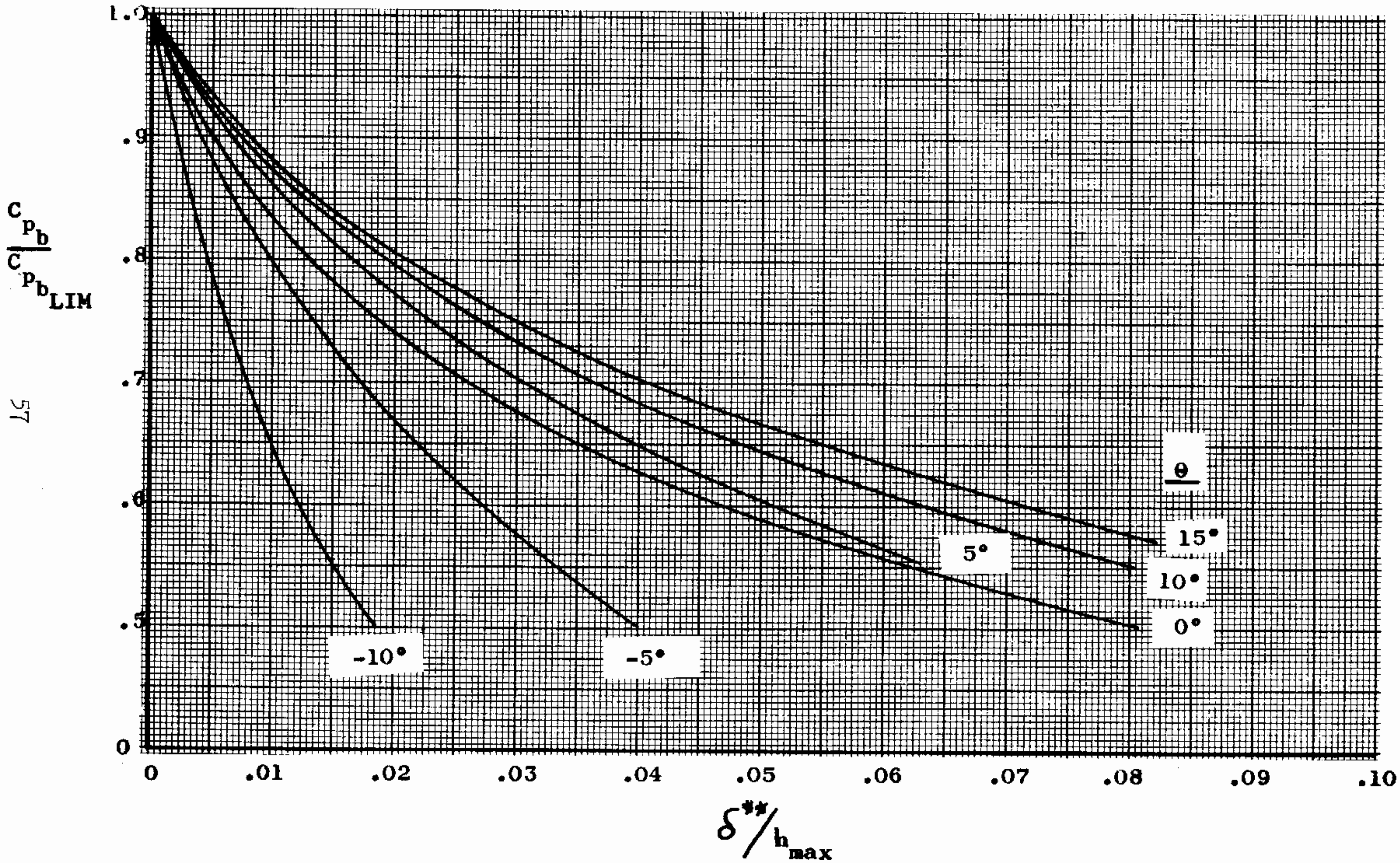

FIGURE 34 Viscous Effects of Base Angle and Boundary Layer Thickness on Base Pressure for Steady Two-Dimensional Flow

2. Values of the parameters (C_{pb}/C_{pblim}) were determined for each case using the data of Figure 34. (As discussed previously, the limiting base pressure as determined is independent of base angle. The assumption was made that the analytic solution results in the proper ratio of (C_{pb}/C_{pblim}) at a given value of boundary layer thickness, even though C_{pblim} varies with θ_1).

3. Empirical values of $(C_{pblim})_\theta$ were obtained for each configuration by division of the experimental values of average base pressure by the corresponding value of the ratio of (C_{pb}/C_{pblim}).

Figure 35 presents the resulting limiting base pressure as a function of base angle for two-dimensional steady base flow.

The same procedure was followed to determine the effect of base angularity for three-dimensional base flow. (The boundary layer thicknesses for the three-dimensional configurations were calculated using the two-dimensional formula; the validity of the method is verified in reference 28.) Empirical values of the limiting base pressure for axisymmetric bases with base angularity were obtained using the experimental data for the axisymmetric configurations with base angles of -10°, 0° and 10°. Figure 36 compares the data for the axisymmetric three-dimensional effect and the two-dimensional effect. The curves indicate that although the limiting base pressure for the two-dimensional and three-dimensional configurations at $\theta=0$ are considerably different, the slope of the curve, or effect of the angle, is nearly equal. Further, the slope of each can be expressed numerically as -1 psf/rad. (It is interesting to note that although the slope of the curves which present the effect of base angle on the experimentally-determined average base pressures of the two-dimensional configurations with splitter plate and of the axisymmetric configurations (Figures 32 and 46, Volume II) is different from the slope derived empirically for the limiting base pressures, the slope of the curve for the experimentally determined base pressures of the isolated two-dimensional configurations is approximately -1 psf/rad. (Figure 31, Volume II). It can be hypothesized that for the open wake case, the effect of base angle is independent of viscous effects, which is suggested by Roshko's work, reference 5).

The results represented by Figure 36 indicated an empirical relationship which was adopted for application to base geometries of arbitrary planform. The limiting base pressure of any configuration can be determined if the limiting base pressure of the corresponding planform at zero base angle can be found, using the relation:

$$\left(C_{pblim}\right)_{\theta_{eff}} = \left(C_{pblim}\right)_{\theta=0} - \theta_{eff} \qquad (16)$$

where θ_{eff} is the effective base angle, expressed in radians, averaged around the base perimeter using the method presented in Figure 37. The deter-

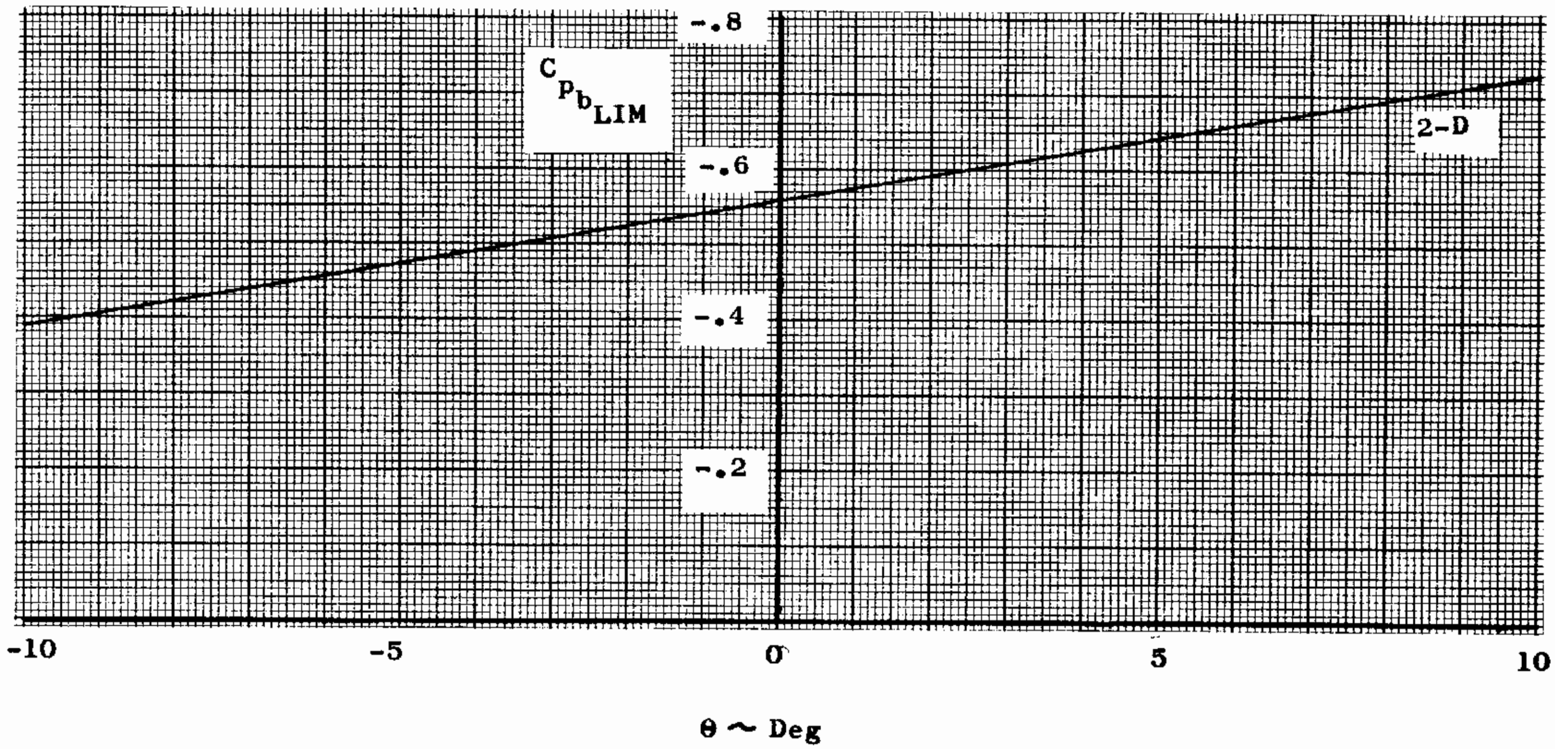

FIGURE 35 Effect of Base Angle on Limiting Base Pressure for Two-Dimensional Steady Flow

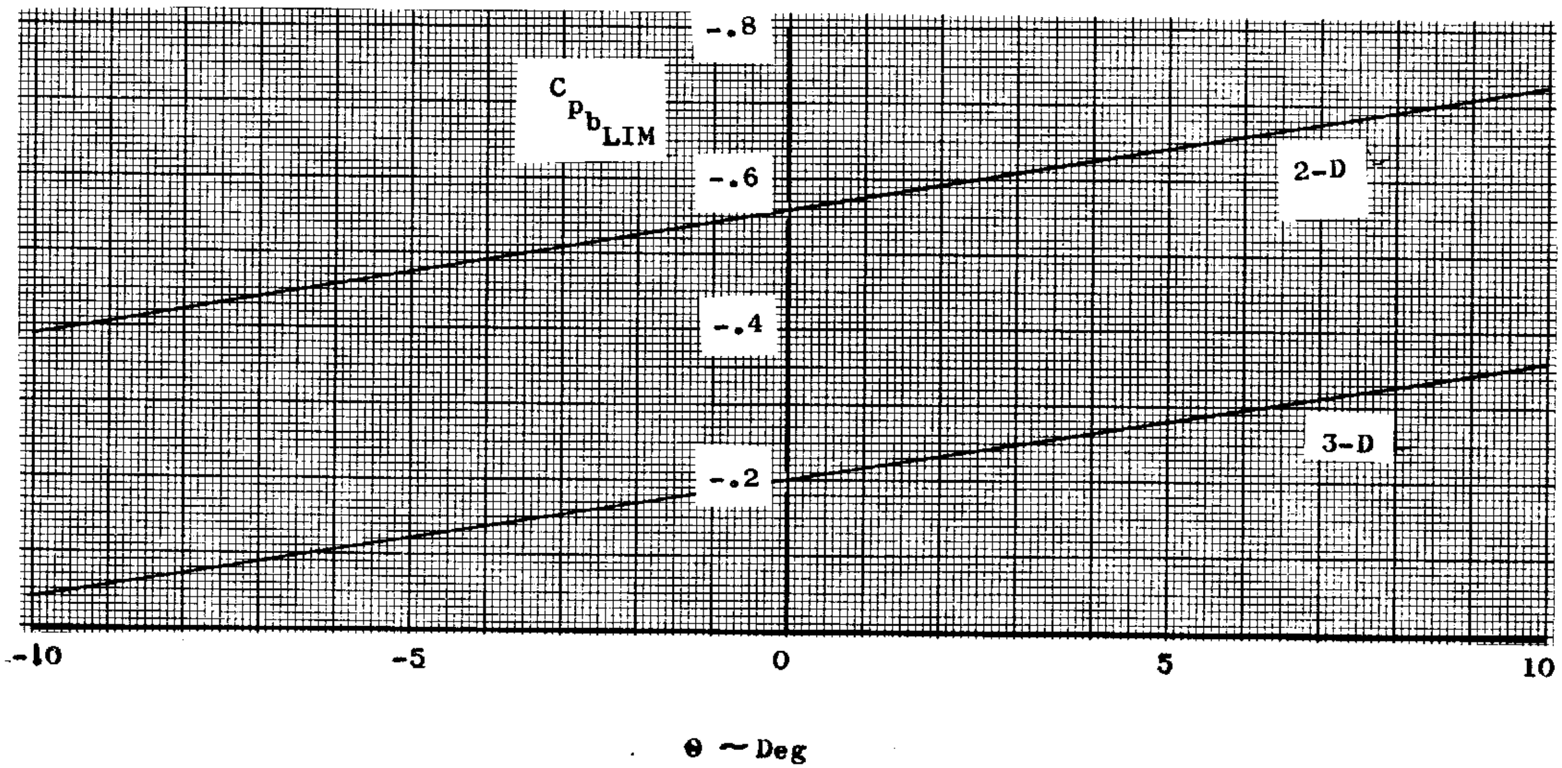

FIGURE 36 Effect of Base Angle on Limiting Base Pressure for Axisymmetric Configurations

GIVEN: Symmetrical geometry, such as shown:

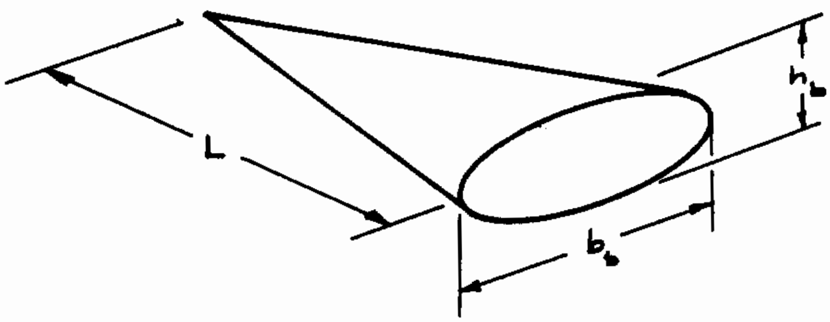

TO FIND: θ_{eff} and h_{eff}

PROCEDURE:

1. Divide base perimeter into sufficient equal length increments to define geometry:

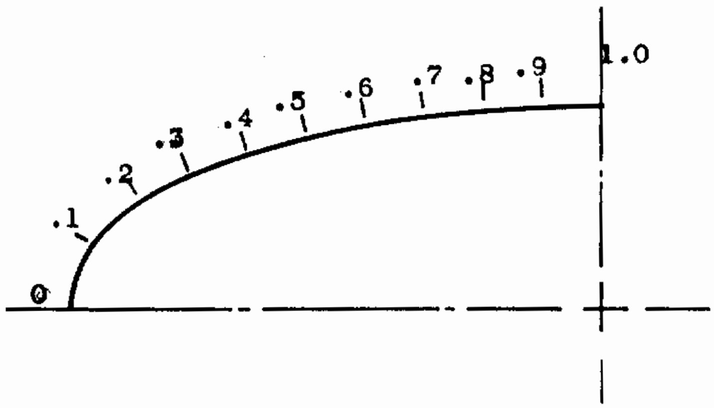

FIGURE 37 Method for Determination of Geometrical Parameters of Symmetrical Three-Dimensional Base Configurations

2. At each point, define an approach streamline which lies on the intersection of the surface and a plane which is normal to the line tangent to the perimeter at the point under consideration. The flow angle and effective base height of each streamline at separation is determined as shown below:

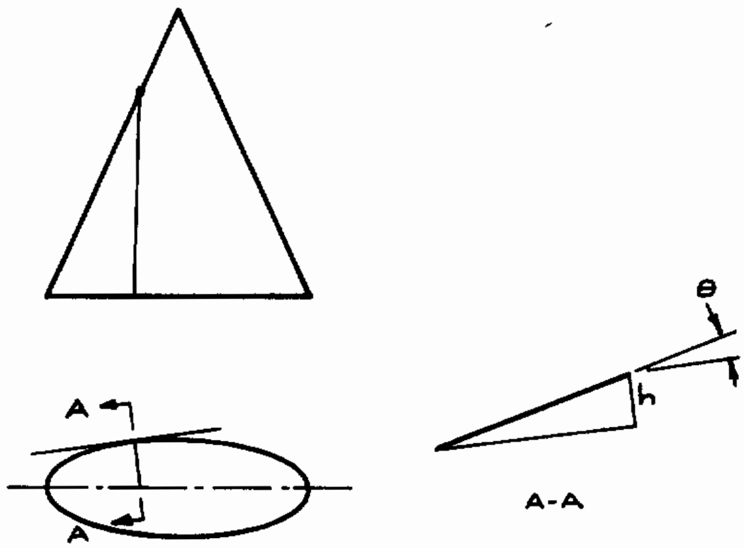

3. The average of the θ's and h's (averaged over perimeter as shown below), yields valves of θ_{eff} and h_{eff}:

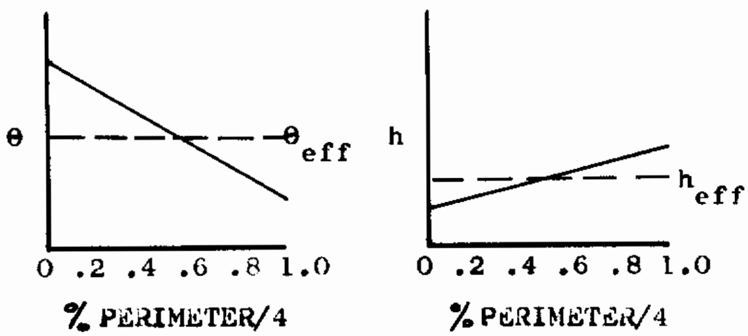

FIGURE 37 Method for Determination of Geometrical Parameters of Symmetrical Three-Dimensional Base Configurations (Continued)

mination of the limiting base pressure for $\theta = 0$ requires an additional empirical factor which is described in the following paragraphs.

3.1.2 EFFECT OF THREE-DIMENSIONAL BASE PLANFORM ON LIMITING BASE PRESSURE. The effect of base planform on the limiting base pressure of configurations with zero base angle was determined empirically using the two-dimensional analytic solution applied to three-dimensional configurations under the assumption that viscous effects are equivalent. The following procedure was used:

1. A value of average or effective boundary layer thickness was calculated for each of the three-dimensional configurations based on an average development length (the M.A.C. was used for the delta planforms). An effective base height was determined for the thick delta wings using the procedure shown in Figure 37.

2. Values of the parameter $(C_{pb}/C_{p_{blim}})$ were determined from the two-dimensional solution at the free-stream conditions and at the effective value of θ for each configuration.

3. Using the experimental values of average C_{pb}, and empirical value of $(C_{p_{blim}})_\theta$ was obtained for each configuration.

4. Using the previously derived relation to account for base angle the limiting base pressure at $\theta = 0$ for each configuration was obtained:

$$(C_{p_{blim}})_{\theta=0} = (C_{p_{blim}})_{\theta_{eff}} + \theta_{eff} \qquad (17)$$

The values thus obtained were ratioed to the value of 2-D limiting base pressure determined at the same free stream conditions. The values were correlated using the parameter presented in Section 1.1, $ⓟ/2\sqrt{\pi S_B}$, which, for symmetrical base planforms, describes the three-dimensionality of the base. Figure 38 presents a plot of the empirical data. A hyperbolic curve was fitted to the data points, which becomes asymptotic to a line representing the pressure predicted for a two-dimensional isolated base with non-steady flow, the limiting value assumed to be accounted for by planform effects.

Although the relationship presented was derived at one free-stream condition, it was assumed that the relation can be applied throughout the range where the analytic solution is valid.

3.1.3 OUTLINE OF PREDICTION METHOD. The two empirical relationships along with the two-dimensional analytic solution combine to form a method by which pressure for any symmetrical base planform can be predicted. (Extension to non-symmetrical base planforms, including the effect of fins, will be discussed later.) Application of the method is outlined as follows:

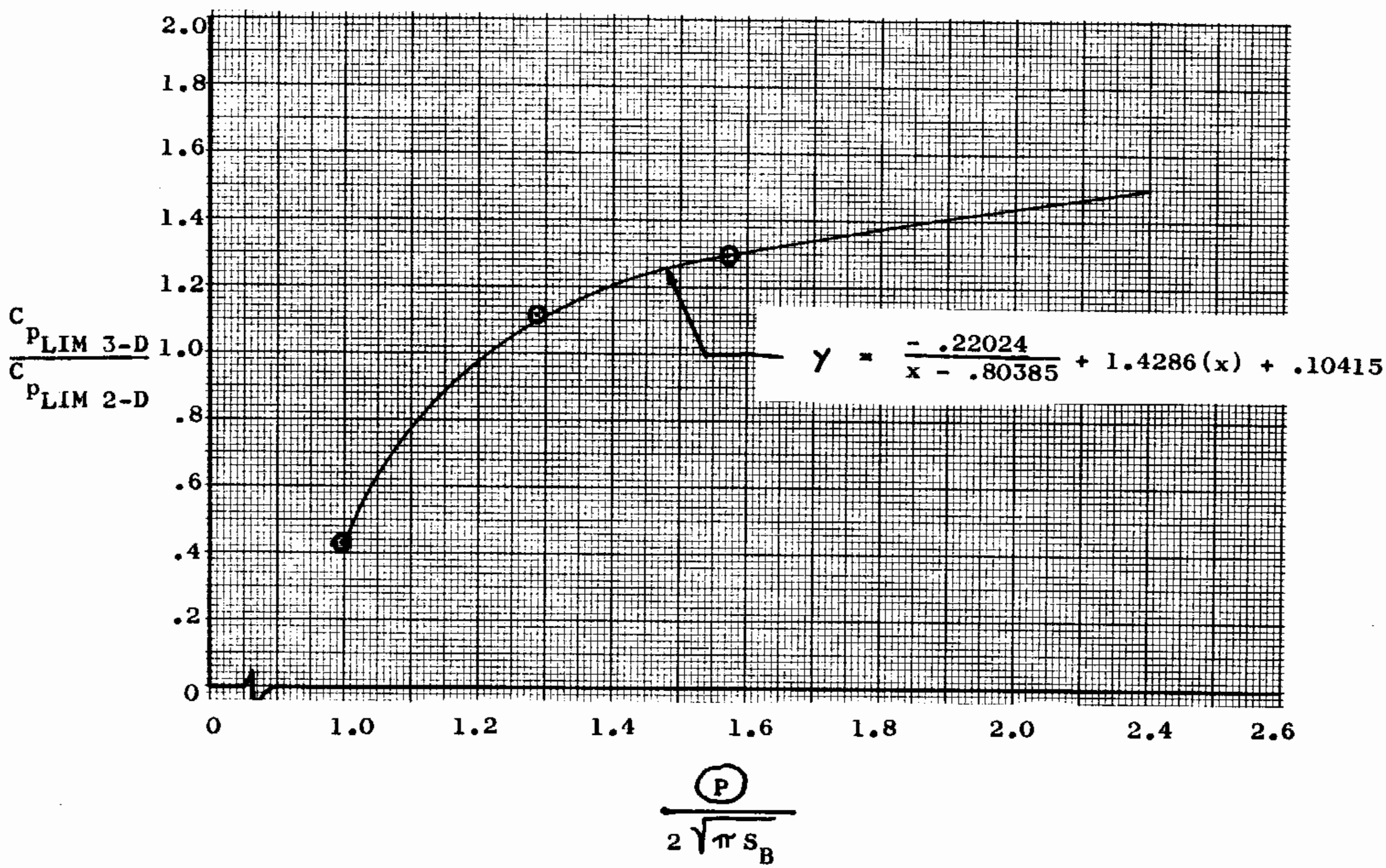

FIGURE 38 Effect of Base Planform on Limiting Base Pressure for Symmetrical Three-Dimensional Base Configurations

1. Given a vehicle configuration, the following geometrical parameters are defined, using the method presented in Figure 37:

   a. Effective base angle ~ θ_{eff}
   b. Base geometry parameter ~ $Ⓟ/2\sqrt{\pi S_B}$
   c. Effective base height ~ h_{eff}
   d. Mean approach length ~ ℓ_{eff}

2. At given free-stream conditions, a value of δ^{**}/h_{eff} is predicted.

3. Using the two-dimensional solution at the given free-stream condition and θ_{eff}, values of $(C_p/C_{p_{lim}})_\theta$ versus δ^{**}/h_{eff} and $C_{p_{lim_{2D}}}$ are obtained.

4. Using the value of $Ⓟ/2\sqrt{\pi S_B}$ determined, a value of

   $$\left(\frac{C_{p_{lim}}\ 3D}{C_{p_{lim}}\ 2D}\right)_{\theta=0}$$

   is obtained, from which $\left(C_{p_{lim_{3D}}}\right)_{\theta=0}$ can be determined.

5. A value of $\left(C_{p_{lim}}\right)_{\theta_{eff}}$ is determined using the relation:

   $$\left(C_{p_{lim}}\right)_{\theta_{eff}} = \left(C_{p_{lim}}\right)_{\theta=0} - \theta_{eff} \tag{16}$$

6. Two-dimensional values of the ratio $(C_p/C_{p_{lim}})_{2D}$ are corrected to three-dimensional at each value of δ^{**}/h_{eff} by:

   $$\left(C_p/C_{p_{lim}}\right)_{\theta_{3D}} = \left(C_p/C_{p_{lim}}\right)_{\theta_{2D}} \cdot \left(\frac{C_{p_{lim}\ 2D}}{C_{p_{lim}\ 3D}}\right)_{\theta=0} \tag{18}$$

7. The predicted base pressure at the corresponding value of δ^{**}/h_{eff} calculated is found by interpolating between values of the array geneated in the previous step.

3.1.4 EXTENSION OF METHOD TO UNSYMMETRICAL BASE PLANFORMS. The empirical factors developed and incorporated into the prediction method were based on data obtained from symmetrical base planforms. It was found, however, that the method could be applied to unsymmetrical bases and bases with fins by treating those bases as combinations of subregions, where the geometry and corresponding base pressure of each subregion could be determined by the general method. Averaging of the base pressures of the subregion by a simple area relation resulted in a predicted effective base pressure which provided good correlation with the experimental data of the configurations tested, namely the wing-body combination and the body-fin combinations. Figure 39 outlines the technique for describing the geometry of bases which are combinations of subregions.

It was also found that unsymmetrical boattailing of a symmetrical planform, such as the thick delta with 5° and 10° boattailing, shown in Figure 17, could not be accounted for by describing the resulting base region by the methods developed for symmetrical planforms (in particular, defining an average flow angularity around the base perimeter). Better correlation with experiment was achieved by first defining the geometry of the symmetrical unboattailed base and then correcting the value of effective angle by the amount of boattail, even though the boattailing was applied only to the upper surface, which represents less than half of the base perimeter. The effect is predominately influenced by changes to the external flow field which in the present analysis is accounted for by changes to the limiting base pressure of a given configuration. The total flow field apparently adjusts to the influence of the local major change in flow angularity, resulting in nearly the same pressure level as would be predicted for symmetrical boattailing to top and bottom surfaces. The limited amount of data made thorough evaluation of the effect impossible. It is suggested that the procedure found in correlating the data of the thick delta configuration be applied to predicting the effects of unsymmetrical boattailing on similar base planforms. Figure 40 outlines the method for defining vehicle geometry for this case.

3.2 DESCRIPTION OF GENERAL PREDICTION TECHNIQUE COMPUTER PROGRAM

The general prediction method, as outlined in Section 3.1.3, was programmed for solution on the IBM 7094 digital computer. The program is documented in Appendix III; Section III-1 presents a flow diagram of the basic program logic, Section III-2 presents a listing of the source program, Section III-3 outlines input procedures and Section III-4 presents sample output.

3.3 CORRELATION OF EXPERIMENTAL DATA WITH GENERAL PREDICTION TECHNIQUE

The general prediction computer program was used to correlate with the experimental data obtained from wind tunnel testing of all three-dimensional configurations. Geometric input parameters were determined for each configuration using the techniques described in previous paragraphs and presented in Figures 37, 39 and 40. Values of the atmospheric variables corresponding to the appropriate test conditions were used as input.

Figure 41 presents a comparison of experimental and predicted values of average base pressure for each of the configurations tested.

GIVEN: Configurations described as combinations of bodies and base subregions, such as shown:

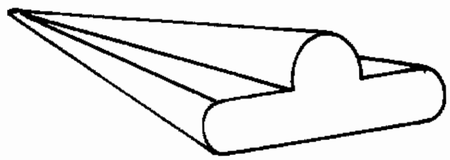

COMBINATION OF BODIES

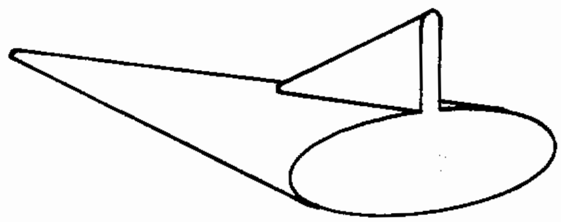

BODY PLUS FIN

DEFINE: Geometry of base.

PROCEDURE:

1. Divide base into sub-regions as shown below for typical examples:

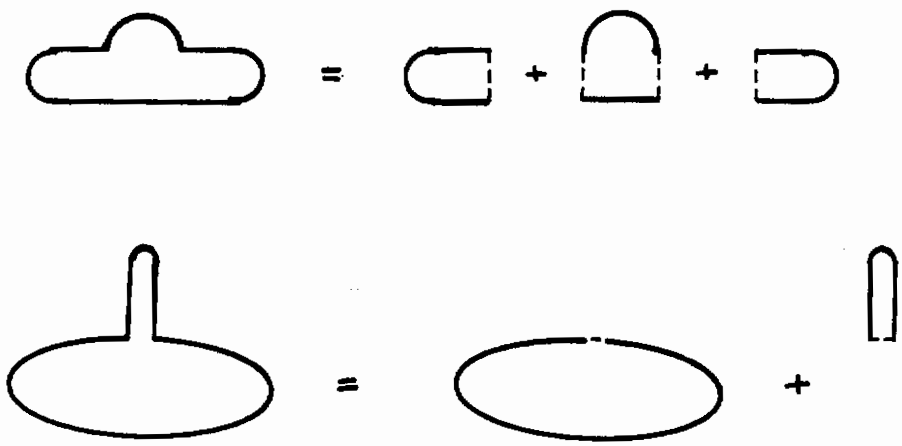

2. For each sub-region, define $\frac{(P)}{2\sqrt{\pi S_B}}$, $\%S_{B_{Total}}$ and θ_{eff}, h_{eff} and L_{eff} using method developed for symmetrical geometries.

NOTE: θ_{eff} for each sub-region determined from average of θ over wetted perimeter only.

FIGURE 39 Method for Determination of Geometrical Parameters for Configurations Made Up of Combinations of Base Regions

GIVEN: Configuration with unsymmetrical boat-tailing, such as shown below:

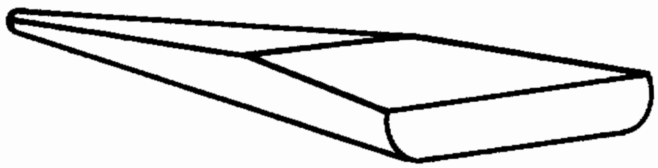

TO FIND: Geometry of configuration ~ $\frac{\textcircled{P}}{2\sqrt{\pi S_B}}$, θ_{eff}, h_{eff}

PROCEDURE: 1. Determine geometry, $\left(\frac{\textcircled{P}}{2\sqrt{\pi S_B}}\right)^*$, $\left(\theta_{eff}\right)^*$, $\left(h_{eff}\right)^*$ of symmetrical configuration (without boat-tailing) such as shown below:

2. Define geometry of boat-tailed configuration as follows:

A. $\frac{\textcircled{P}}{2\sqrt{\pi S_B}} = \left(\frac{\textcircled{P}}{2\sqrt{\pi S_B}}\right)^*$

B. $h_{eff} = \left(h_{eff}\right)^*$

C. $\theta_{eff} = \left(\theta_{eff}\right)^* - \theta_b$

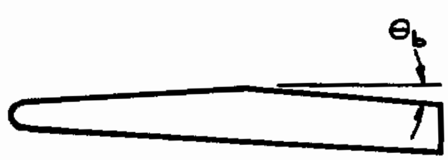

FIGURE 40 Method for Determination of Geometrical Parameters for Configurations Having Unsymmetrical Boat-tailing

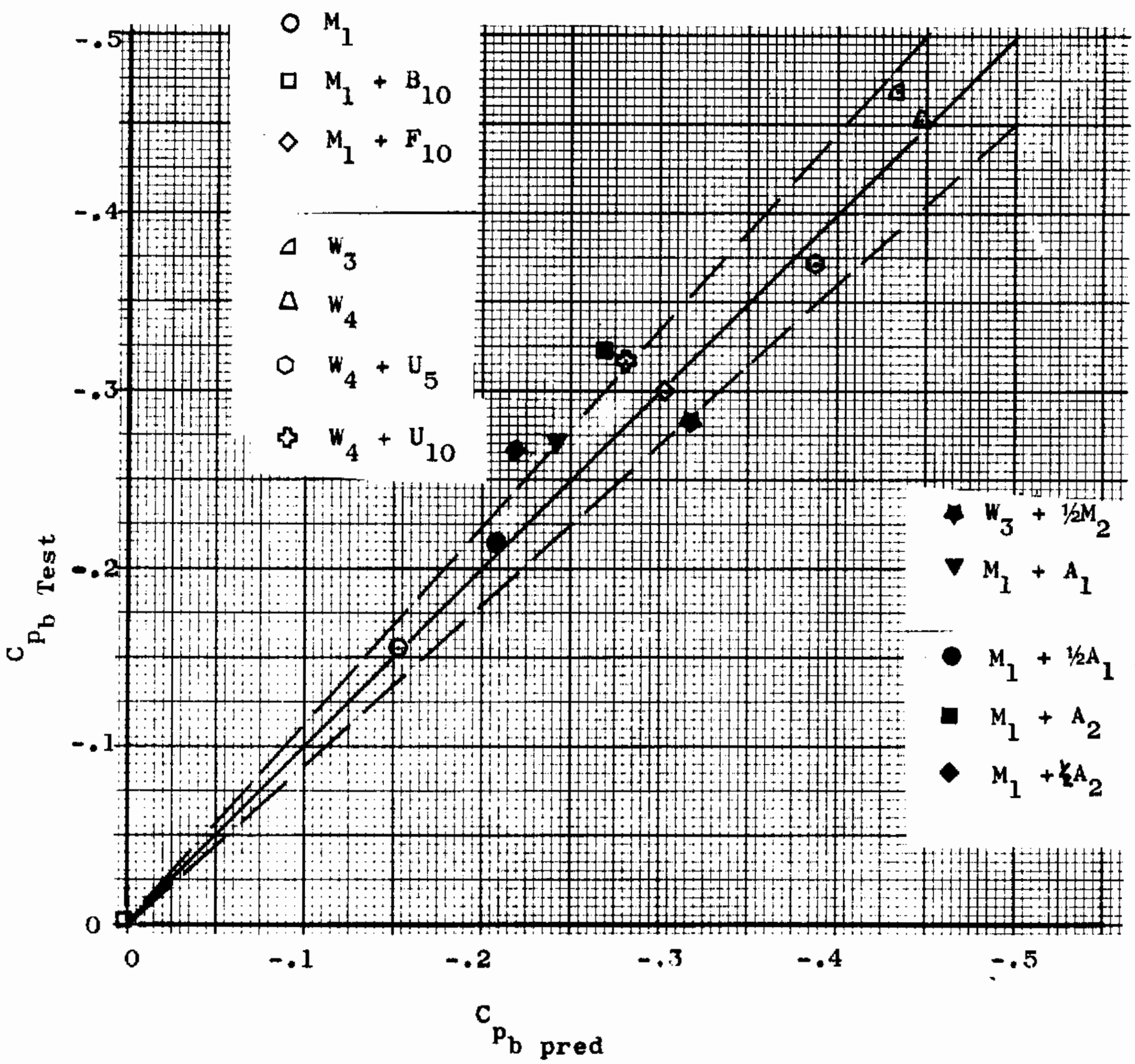

FIGURE 41 Correlation of Experimental Data with Prediction

3.4 EFFECT OF TRAILING EDGE SWEEP

The effect of a trailing edge sweep on base pressure of a blunt lifting surface was investigated experimentally, as described in Section 2. However, it was found during correlation of the data that the trend in base pressure attributed to sweep effects (see Figure 51, Volume II) was also substantially influenced by the effect of base planform. This effect was introduced since the swept trailing edge configurations were the thick delta wing (W_3) with extensions to the trailing edge (see Figures 16 and 17, Volume II). It is apparent that the base planform (described by the parameter $Ⓟ/2\sqrt{\pi S_B}$ affectively increased with the increase of the trailing edge sweep, resulting in a decrease of base pressure similar to that noted for simple changes of planform. The effect of sweep angle could not, therefore, be determined conclusively.

4/ CONCLUSIONS

4.1 The two-dimensional analytic solution provides an accurate mathematical description of the fluid mechanics of steady subsonic base flow. The development of a free-streamline solution to theoretically define the geometry of the shear layer closes the viscous solution of Nash. The applicability of the combined solution has been shown by the close agreement with experimental values of base pressure and shear layer length obtained from testing of flow over a rearward-facing step.

4.2 The applicability of the steady flow model and analytic solution to isolated three-dimensional blunt bases has been demonstrated most effectively for axisymmetric base geometries. The correlation of the wake flow properties of the two-dimensional steady flow and axisymmetric base flow and the similarity in the effect on base pressure of the influence of boundary layer thickness and base angularity between the two cases indicates that a steady-flow analysis can be used to predict base pressure for axisymmetric geometries.

4.3 The steady-flow analytic solution can be extended to general three-dimensional base planforms, even though in certain configurations a mixed base flow phenomenon is known to exist (in planforms with ratios of width to height of approximately three or greater, two-dimensional unsteady base flow is found in the interior base region). The viscous effect of approaching boundary layer can be evaluated by the analytic solution. The empirical relationships which have been developed to account for planform effects were based on a limited amount of experimental data. While it is concluded that the relations provide an accounting for the pertinent parameters which influence base pressure, it can be expected that the accuracy of the prediction technique as developed may differ for certain geometries, such as diamond-shaped base planforms.

4.4 ~~It can be concluded that~~ the inconsistencies encountered during the limited effort to correlate a portion of the existing experimental data previously obtained with the general prediction technique were due primarily to the inability to properly account for the effects of sting-support interference and also to accurately define the test conditions. ~~It is felt that~~ the type of support-system used during the experimental program of the present study virtually eliminated interference effects.

5/ RECOMMENDATIONS

5.1 The general prediction technique is presented as a reliable method, subject to the following limitations in application:

a. It is recommended that the method be used primarily for predictions at flight conditions where compressibility effects are not significant. However, the method will provide predictions throughout the subsonic flight regime which are useful as preliminary design data; evaluation of the accuracy of the method at these conditions was not possible.

b. It is recommended that the method be restricted to the prediction of base pressure for base planforms having a value of the parameter

$(P)/2\sqrt{\pi S_B}$ of 1.6 or less.

5.2 Additional experimental investigation is recommended to augment the empirical data on the effects of base planform, base flow angularity and trailing edge sweep on three-dimensional base pressure. For thorough evaluation, the three effects should be investigated independently.

5.3 It is recommended that the feasibility of using mass addition to reduce subsonic base drag be evaluated with a combined experimental/analytical program. The two-dimensional analytic solution will provide qualitative information but an experimental program is required to verify the analytic solution and to determine three-dimensional effects.

5.4 The use of a forward-mounted support system is recommended for subsonic base pressure investigations in preference to sting-supported systems. The error due to the interference of rear-mounted stings was not evaluated during the present study but was recognized by the inconsistency of data obtained from earlier studies.

5.5 Analytical treatment of the total flow field for two-dimensional and axisymmetric geometries with arbitrary base inclinations is recommended to provide surface pressures near the separation point. This analytical data would replace the empirical relationship which accounts for base angularity.

5.6 It is recommended that an investigation be conducted to extend the present analysis to high subsonic and transonic Mach numbers. The viscous solution is valid throughout the Mach number range through the supersonic flow regime. However, redefinition of the flow model is required to include the effect of compressibility on the shear layer geometry. Transonic expansion from the separation point could conceivably be analyzed using a hodograph technique.

6/ REFERENCES

1. A. Fage and F. C. Johansen, "On the Flow of Air Behind an Inclined Flat Plate of Infinite Span", R&M No. 1104, British A.R.C., 1927.

2. A. Fage and F. C. Johansen, "The Structure of Vortex Sheets", R&M No. 1143, British A.R. C., 1927.

3. A. Fage, "The Air Flow Around a Circular Cylinder in the Region where the Boundary Layer Separates from the Surface", R&M 1179, British A.R.C., 1928,

4. A. Roshko, "On the Development of Turbulent Wakes from Vortex Sheets", NACA TN 2913, March 1953.

5. A. Roshko,"On the Drag and Shedding Frequency of Two-Dimensional Bluff Bodies", NACA TN 3169, July 1954.

6. D. R. Chapman, "An Analysis of Base Pressure at Supersonic Velocities and Comparison with Experiment", NACA Report 1051, 1951.

7. D. R. Chapman, D. M. Kuehn, and H. K. Larson, "Investigation of Separated Flows in Supersonic and Subsonic Streams with Emphasis on the Effects of Transition", NACA Report 1356, 1956.

8. H. H. Korst, R. H. Page and M. E. Childs, "A Theory for Base Pressure in Transonic and Supersonic Flow", Univ. of Illinois ME Tech Note 392-2, March 1955.

9. H. H. Korst, W. L. Chow and G. W. Zumwalt, "Research on Transonic and Supersonic Flow of a Real Fluid at Abrupt Increases in Cross Section (With Special Consideration of Base Drag Problems)", Univ. of Illinois ME Tech Note 392-5, December 1959

10. S. F. Hoerner, "Base Drag and Thick Trailing Edges", Journal of the Aeronautical Sciences, October 1950.

11. E. E. Honeywell, "Compilation of Power-Off Base Drag Data and Empirical Methods for Predicting Power-Off Base Drag", GD/Pomona TM No. 334-337, 1959.

12. D. B. Seager and J. E. Meyer, "An Investigation of the Subsonic Aerodynamic Characteristics and the Landing Flare Manuever for Hypersonic Re-entry Configurations", ASD-FDL Tech. Documentary Report No. ASD-TDR-62-271, August 1962.

13. H. H. Kurzweg, "Interrelationship Between Boundary Layer and Base Pressure", Journal of the Aeronautical Sciences, November 1951.

14. R. Lehnert and V. L. Schermerhorn, "Correlation of Base Pressures and Wake Structure of Sharp and Blunt-Nosed Cones with Reynolds Numbers Based on Boundary Layer Thickness", Journal of the Aeronautical Sciences, March 1959.

15. L. S. Stivers and L. L. Levy, "Longitudinal Force and Moment Data at Mach Numbers from 0.60 to 1.40 for a Family of Elliptic Cones with Various Semi-Apex Angles", NASA TN D-1149, December 1961.

16. O. E. Sipe and D. B. Seager, "Tests to Determine Subsonic Aerodynamic Characteristics of Hypersonic Re-entry Configurations", ASD TR 61-485, 1961.

17. C. C. Hsu, "Viscous Effects on Balanced Jets in Ground Proximity", Technical Report 241-1, Hydronautics, Inc., January 1963.

18. J. F. Nash, "An Analysis of Two-Dimensional Turbulent Base Flow, Including the Effect of the Approaching Boundary Layer," Aeronautical Research Council (G.B.) R&M No. 3344, 1963.

19. F. N. Kirk, "An Approximate Theory of Base Pressure in Two-Dimensional Flow at Supersonic Speeds", RAE Tech. Note Aero. 2377, December 1959.

20. A. Roshko, "A New Hodograph for Free-Streamline Theory", NACA TN 3168, July 1954.

21. T. Strand, "Inviscid-Incompressible-Flow Theory of Static Peripheral Jets in Proximity to the Ground", JAS, V. 28, No. 1, January 1961.

22. D. Riabouchinsky, "On Unsteady Fluid Motions with Free Surfaces", Proc. Loud. Math. Soc., Vol. 19, pg 206-215, 1921.

23. L. M. Milne-Thomson, "Theoretical Hydrodynamics", The MacMillian Co., 1955.

24. W. V. Carter and J. E. Butsko, "An Investigation of Subsonic Two-Dimensional Base Pressures and Flow Field Visualizations Conducted in a Smoke Wind Tunnel", GDA-DDE-64-074, September 1964.

25. W. Herman and J. E. Butsko, "A Wind Tunnel Investigation of Subsonic Two-Dimensional and Three-Dimensional Base Pressure and Wake Flow Characteristics", GD/C-DCD-64-003, May 1965.

26. J. F. Nash et al, "Experiments on Two-Dimensional Base Flow at Subsonic and Transonic Speeds", Nat. Phys. Lab. (G.B.) Aero Report 1070, January 1963.

27. H. Schlichting, "Boundary Layer Theory", McGraw-Hill Book Co., Inc., 1960.

28. H. V. Eckert, "Simplified Treatment of the Turbulent Boundary Layer Along a Cylinder in Compressible Flow", Journal of the Aeronautical Sciences, January, 1952.

7/ BIBLIOGRAPHY

Index of Topical Divisions

A. General Subsonic Base Flow

B. General Fluid Dynamics

C. Turbulent Mixing

D. Laminar Mixing

E. Wakes and Vortex Streets

F. Separation Phenomena

G. Experimental Subsonic Base Pressure and Base Drag Data

H. Related Flow Mechanisms and Phenomena

I. Transonic and Supersonic Base Flow

J. Experimental Model and Sting Data

A. General Subsonic Base Flow

1. "Base Drag and Thick Trailing Edges", Hoerner, S. F., Journal of the Aeronautical Sciences, October 1950.

2. "On the Wake and Drag of Bluff Bodies", Roshko, A., Journal of the Aeronautical Sciences, February 1955.

3. "Compilation of Power-Off Base Drag Data and Empirical Methods for Predicting Power-Off Base Drag", Honeywell, E. E., GD/Pomona TM No. 334-337, 1959.

4. "Heat Transfer from the Rear of Bluff Objects to a Low Speed Air Stream", Sogin, H. H., Tulane Univ. ARL 62-361, June 1962.

5. "An Investigation of the Subsonic Aerodynamic Characteristics and the Landing Flare Maneuver for Hypersonic Re-entry Configurations", Seager, D. B. and Meyer, J. E., ASD-FDL Tech. Documentary Report No. ASD-TDR-62-271, August 1962.

6. "Study of Flow Over Afterbodies of Aircraft or Rockets", Carriere, P., Zeitschrift fur Flugwissen Schaften, V-10, n.7. (GDA translation from German), 1962.

7. "A Review of Research on Two-Dimensional Base Flow", Nash, J. F., Aero Research Council R&M No. 3323, 1963.

8. "An Analysis of Two-Dimensional Turbulent Base Flow, Including the Effect of the Approaching Boundary Layer", Nash, J. F., National Physical Laboratory Aero Rep. 1036, July 1962.

9. "Experiments on Two-Dimensional Flow Over a Normal Wall", Arie, M., Rouse, H., Journal of Fluid Mechanics.

10. "Experimental Investigation of Flow Separation Over a Step", Tani, I., 1956.

11. "Theoretical and Experimental Investigation of Flow Behind Single and Double Backward Facing Steps", Abbott, D. E. and Kline, S. J., Stanford Univ. Rept. No. MD-5, June 1961.

12. "Experimental Investigation of Flow Separation Associated with a Step or a Groove", Tani, I. and Komada, H., Report No. 364, N-88322, University of Tokyo.

13. "Theory of Bluff Bodies", Imai, I. Tech Note BN-104, University of Maryland, June 1957.

14. "Recent Research on the Problem of Base Pressures", Carriere, P., NASA TT F-8873, May 1964.

15. "Experiments on the Flow Past a Circular Cylinder at Very High Reynolds Number", Roshko, A., Journal of Fluid Mechanics, pg 345, 1960.

16. "Fluctuating Lift and Drag Acting on a Cylinder in a Flow at Super-critical Reynolds Numbers", Fung, Y. C., Journal of the Aerospace Sciences, November 1960.

B. General Fluid Dynamics

1. "A New Hodograph for Free Streamline Theory", Roshko, A., NACA TN 3168, July 1954.

2. "Pressure and Force Characteristics on Non-Circular Cylinders as Affected by Reynold's Number with a Method Included for Determining the Potential Flow about Arbitrary Shapes", Polhamus, Geller and Grunwald, NASA TR R-46, 1959.

3. "The Theory of Subsonic Plane Flow", Woods, L. C., Cambridge University Press, 1961.

4. "Advanced Mechanics of Fluids", Rouse, H., John Wiley & Sons, 1959.

C. Turbulent Mixing

1. "Turbulent Jet Expansion", Forthman, E., NACA TM No. 789, March 1936.

2. "Investigations of Free Turbulent Mixing", Liepmann, H. W. and Laufer, J., NACA TN 1257, August 1947.

3. "Two Dimensional Jet Mixing of a Compressible Fluid", Pai, S. I., Journal of Aeronautical Sciences, V. 16 N. 8, pp. 463-69, 1949.

4. "A Mixing Theory for the Interaction Between Dissipative Flows, and Nearly Isentropic Streams", Crocco, L. and Lees, L., JAS October 1952.

5. "Compressible Two-Dimensional Jet Mixing at Constant Pressure", Korst, Page and Childs, Univ. of Illinois TN 392-1, 1954.

6. "Analysis of Free-Shear Layer with Finite Initial Thickness and its Application to Base Flow", Toba, K., Report No. N65-13315, Douglas Aircraft Co.

D. Laminar Mixing

1. "Laminar Mixing of a Compressible Fluid", Chapman, D. R., NACA Rep. 958, 1950.

E. Wakes and Vortex Streets

1. "On the Development of Turbulent Wakes from Vortex Sheets", Roshko, A., NACA TN 2913, March 1953.

2. "On the Drag and Shedding Frequency of Bluff Bodies", Roshko, A., NACA TN 3169, July 1954.

3. "The Stability of Vortex Streets with Consideration of the Spreading of Vorticity of the Individual Vortices", Domm, V., Journal of the Aeronautical Sciences, pg 750, November 1955.

4. "A Proposal Concerning Laminar Wakes Behind Bluff Bodies at Large Reynold's Number", Batchelor, G. K., Journal of Fluid Mechanics pg 388, October 1956.

5. "Vortex Shedding from Thin-Flat Plates Parallel to the Free Stream", Bauer, A. B., Journal of the Aerospace Sciences, pg 340, April 1961.

6. "On Steady Laminar Flow with Closed Streamlines at Large Reynolds Number", Batchelor, G. K., Journal of Fluid Mechanics, pg 177, 1956.

7. "Boundary Layers Whose Streamlines are Closed", Wood, W. W., Journal of Fluid Mechanics, pg 77, 1957.

F. Separation Phenomena

1. "Investigation of Separation of the Turbulent Boundary Layer", Schubauer, G. B. and Klenbanoff, P. S., NACA TN No. 2133, August 1950.

2. "Experimental Investigation of Localized Regions of Laminar Boundary Layer Separation", Bursnall, W. J. and Loftin, L. K., NACA TN No. 2338, April 1951.

3. "On Determining Turbulent Boundary-Layer Separation in Incompressible and Compressible Flow", Schuh, H., Journal of the Aeronautical Sciences, May 1955.

4. "Flow Separation in Three Dimensions", Maskell, E. C., Royal Aircraft Establishment Report. No. Aero 2565, November 1955.

5. "An Experimental Investigation of Regions of Separated Laminar Flow", Gault, D. E., NACA TN 3505, 1955.

6. "Investigation of Separated Flows in Supersonic and Subsonic Streams with Emphasis on the Effect of Transition", Chapman, Kuehn and Larson, NACA Report 1356, 1958.

7. "On Dissipative Mechanisms Within Separated Flow Regions (with Special Considerations to Energy Transfer Across Turbulent, Compressible Pr = 1, Mixing Regions)", Golik, R. J., Univ. of Illinois Thesis 63-2923, 1962.

8. "Separated Supersonic Flow", Cooke, J. C., RAE Tech Note No. Aero 2879, March 1963.

G. Experimental Subsonic Base Pressure and Base Drag Data

1. "Effects of Stabilizing Fins and a Rear Support Sting on the Base Pressure of a Body of Revolution in Free Flight at Mach Numbers from 0.7 to 1.3", Hart, R. G., NACA TM L52 E06, September 1952.

2. "Experimental Investigation of Drag of Afterbodies with Exiting Jet at High Subsonic Mach Numbers", Salm:, R. J., NACA RM E 54I 13, November 1954.

3. "Flight Investigation at Mach Numbers from 0.6 to 1.7 to Determine the Drag and Base Pressure on a Blunt-Trailing Edge Airfoil and Drag of Diamond and Circular Arc Airfoils at Zero-Lift", Morrow, J. D. and Katz, E., NACA TN 3548, November 1955.

4. "Free Flight Investigation of the Base Pressure and Drag of a Flare Stabilized Blunt-Nosed Re-entry Body Having a Fineness Ratio of 3.11 at Mach Numbers from 0.70 to 1.90", Mayhue, R. J. and Blanchard, W. S., NASA TM X-214, March 1960.

5. "A Preliminary Investigation of Modified Blunt 13 Degree Half-Cone Re-entry Configurations at Subsonic Speeds", Kenyon, G. C. and Edwards, G. G., NASA TM X-501, March 1961.

6. "The Longitudinal Aerodynamic Characteristics of a Re-entry Configuration Based on a Blunt 13-Degree Half Cone at Mach Numbers to 0.92", Kenyon, G. C. and Sutton, F. B., NASA TM X-571, July 1961.

7. "Aerodynamic Performance and Static-Stability Characteristics of a Blunt-Nose, Boattailed, 13° Half Cone at Mach Numbers from 0.6 to 5.0", Rakich, J. V., NASA TM X-570, July 1961.

8. "Low Speed Aerodynamic Characteristics of a Model of the DS-1 Glider" Allen, C. Q., NASA TM X-573, August 1961.

9. "Longitudinal Force and Moment Data at Mach Numbers from 0.60 to 1.40 for a Family of Elliptic Cones with Various Semi-apex Angles", Stivers, L. S. and Levy, L. L., NASA TN D-1149, December 1961.

10. "Collection of Zero-Lift Drag Data on Bodies of Revolution from Free-Flight Investigations", Stoney, W. E., NASA TR R-100, 1961.

11. Effects of Cross-Section Shape on the Low-Speed Aerodynamic Characteristics of a Low-Wave-Drag Hypersonic Body", Spencer, B., and Philips, W. P., NASA TN D-1963, October 1963.

12. "Experiments on Two-Dimensional Base Flow at Subsonic and Transonic Speeds", Nash, J. F, Nash, J. F., Quincey, V. G. and Callinan, J., National Physical Laboratory Report 1070, January 1963.

13. "Tests to Determine Subsonic Aerodynamic Characteristics of Hypersonic Re-entry Configurations", Sipe, O. E. and Seager, D. B., ASD TR 61-485, 1961.

14. "A Fundamental Study of the Problems Associated with the Approach and Landing of Advanced Flight Vehicles", Seager, Litrownik, Prince, and Schwartz, WADD TR 60-711, 1960.

15. "The Subsonic Aerodynamic Characteristics of Some Blunt Delta Configurations with 75° Sweepback", Edwards, G. G. and Savage, H. J., NASA TM X-581, 1961.

16. "Static Longitudinal Aerodynamic Characteristics at Transonic Speeds of a Blunted Right Triangular Pyramidal Lifting Re-entry Configuration at Angles of Attack up to 110°, Mugler, J. P. and Olstad, W. B., NASA TN D-797, 1961.

17. "Static Longitudinal Aerodynamic Characteristics at Transonic Speeds of a Thick Delta-Wing Supersonic-Glider Configuration for Angles of Attack up to 100°, NASA TM X-532, 1961.

18. "Transonic Longitudinal and Lateral Aerodynamic Characteristics of a Preliminary Concept of a First Stage Horizontal - Take-Off and Horizontal - Landing Recoverable Booster with a 70° Delta Wing", Pierpont, P. K., NASA TM X-691, 1962.

19. "Aerodynamic Effects of Modifying Wing Inboard Trailing-Edge Camber of a Model at High Subsonic Speeds", Re, R. J., NASA TN D-1809, 1963.

20. "The Aerodynamic Characteristics of Several Thick Delta Wings at Mach Numbers to 6 and Angles of Attack to 50°", Rakick, J. V. and McDevitt, J. B., NASA TM X-162, 1960.

21. "Static Longitudinal and Lateral Stability Characteristics of a Right Triangular Pyramidal Lifting Re-entry Configuration at Transonic Speeds", Olstad, W. B. et al, NASA TN D-655, 1961.

H. Related Applications

1. "Viscous Effects on Balanced Jets in Ground Proximity", Hsu, C. C., Hydronautics, Inc. Technical Report 241-1, January 1963.

2. "Jet Effects on Base and Afterbody Pressures of a Cylindrical Afterbody at Transonic Speeds", Cubbage, J. M., NASA RM L56C21, 1956.

3. "Jet Effects on the Drag of Conical Afterbodies for Mach Numbers of 0.6 to 1.28", Cubbage, J. M., NACA RM L 57 B21, 1957.

4. "On the Base Pressure Resulting from the Interaction of a Supersonic External Stream with a Sonic or Subsonic Jet", Chow, W. L., Journal of the Aeronautical Sciences, March 1959.

5. "Effect of Multiple-Jet Exits on the Base Pressure of a Simple Wing-Body Combination at Mach Numbers of 0.6 to 1.27", Cubbage, J. M., NASA TM X-25, 1959.

6. "Jet Effects on the Base Pressure of a Cylindrical Afterbody with Multiple Jet Exits", Scott, W. R. and Slocumb, T. H., NASA M 3-10-59L, 1959.

7. "Static Thrust of an Annular Nozzle with a Concave Central Base", Corson, B. W. and Mercer, C. E., NASA TN D-418, September 1960.

8. "Measured Base Pressure on Several Twin Rocket-Nozzle Configurations at Mach Numbers of 0.6 to 1.40 with Effects Due to Nozzle Canting and Stabilizing Fins", Cubbage, J. M. and Andrews, E. H., NASA TN D-544, 1960.

9. "Investigation of Net Thrust and Base Pressure Characteristics of Cylindrical Afterbodies with Clustered Supersonic Nozzles at Transonic Mach Numbers", Andrews, E. H., NASA TN D-978, November 1961.

10. "Effect of Geometric Parameters on the Static Performance of an Annular Nozzle with a Concave Central Base", Mercer, C. E. and Simonson, A. J., NASA TN D-1006, February 1962.

11. "Performance of a Plug Nozzle Having a Concave Central Base With and Without Terminal Fairings at Transonic Speeds", Mercer, C. E. and Salters, L. B., Jr., NASA TN D-1804, May 1963.

12. "Base Flow Aerodynamics of a Saturn-Type Booster Stage at Mach No. 0.1 to 2.0", Allen, J. L., NASA TND-593.

13. "Base Drag Measured on an Ogive-Cylinder Model with Base Nozzle Flow", Graham, D. K. and Binion, T. W., Jr.", AEDC Tech. Doc Report No. TDR-64-87, May 1964.

I. Transonic and Supersonic Base Flow

1. "Base Pressure at Supersonic Velocities", Hill and Alpher, Journal of the Aeronautical Sciences, pg. 153, 1949.

2. "Base Pressure at Supersonic Velocities", Hill, F. K., Journal of the Aeronautical Sciences, March 1950.

3. "Interrelationship Between Boundary Layer and Base Pressure", Kurzweg, H. H., Journal of theAeronautical Sciences, November 1951.

4. "An Analysis of Base Pressure at Supersonic Velocities and Comparison with Experiment", Chapman, D. R., NACA Report 1051, 1951.

5. "Experimental Investigation of Base Pressure on Blunt Trailing-Edge Wings at Supersonic Velocities", Chapman, Winbrow and Kester, NACA TN 2611, 1952.

6. "A Theory for Base Pressure in Transonic and Supersonic Flow", Korst, Page and Childs, Univ. of Illinois ME Tech Note 392-2, March 1955.

7. "The Base Pressure Behind a Blunt Trailing Edge for Supersonic Two-Dimensional Flow", Tripp, W., Univ. of Illinois Thesis 18, 208, May 1956.

8. "A Theory for Base Pressures in Transonic and Supersonic Flow", Korst, H. H., Journal of the Aeronautical Sciences, December 1956.

9. "Base Pressure at Supersonic Speeds on Two-Dimensional Airfoils and on Bodies of Revolution with and without Fins Having Turbulent Boundary Layers", Love, E. S., NACA TN 3819, January 1957.

10. "An Investigation of Two-Dimensional Supersonic Base Pressures", Charwat, A. F. and Yakura, J. K., Journal of the Aeronautical Sciences, February 1958.

11. "Correlation of Base Pressures and Wake Structure of Sharp and Blunt-Nosed Cones with Reynolds Numbers Based on Boundary Layer Thickness", Lehnert, R. and Schermerhorn, V. L., Journal of the Aeronautical Sciences, March 1959.

12. "Investigation of Variation of Base Pressure over the Reynold's Number Range in which Wake Transition Occurs for Two-Dimensional Bodies at Mach Numbers from 1.95 to 295", Van Hise, V., NASA TN D-167, November 1959.

13. "Preliminary Base Pressures Obtained from the X-15 Airplane at Mach Numbers from 1.1 to 3.2", Saltzman, E. J., NASA TN D-1056, August 1961.

14. "Flow in the Base Region of Axisymmetric and Two Dimensional Configurations", Beheim, M. A., NASA TR R-77, 1961.

J. Experimental Model and Sting Data

1. "Pressure Distributions on Bodies of Revolution at Subsonic and Transonic Speeds", Cole, R. I., NACA TM L 52 D30, July 1952.

2. "A Comparison of the Experimental Subsonic Pressure Distributions About Several Bodies of Revolution with Pressure Distributions Computed by Means of the Linearized Theory", Matthews, C. W., NACA Report 1155, 1953.

3. "An Investigation of Sting Support Interference on Base Pressure and Forebody Chord Force at Mach Numbers from 0.6 to 1.30" Turmell, P. J., NACA RM A 54 K 16a, 1955.

4. "Effects of Sting Support Interference on the Drag of an Ogive-Cylinder Body with and without a Boattail at 0.6 to 1.4 Mach Number", Lee and Summers, NACA RM A 57 109, 1957.

5. "Low Speed Wind Tunnel Tests on 15°, 25°, 40° and 55° Semi-Vertex Angle Cones to Determine the Support Effects on Force Coefficients", Morrison, M. E., GD/Convair CVAL 167B, March 1958.

6. "Effects of Sting-Support Interference on the Base Pressures of a Model Having a Blunt-Nosed Cylinder Body and a Conical Flare at Mach Numbers of 0.65 to 2.20", Reese, D. E. and Wehrend, W. R., NASA TM X-161, February 1960.

APPENDIX I

DERIVATION OF EQUATIONS FOR VISCOUS MIXING SOLUTION

ASSUMPTIONS:

a. Viscous effects are taken into account insofar as they generate the initial velocity profile.

b. Velocity and temperature fields can be regarded as due to pressure forces alone.

c. Flow along any streamline is approximated by one-dimensional isentropic flow relations.

1/ EXPANSION AT SEPARATION CORNER

Referring to Figure 42, the relations for assumed iso-energetic shear flow are

$$u^2 + 2C_pT = u_e^2 + 2C_pT_e \tag{I.1}$$

$$1 - u^{*2} = \frac{2C_p}{u_e^2}(T - T_e)$$

Where $u^* = u/u_e$

Denoting conditions at Stations (1) and (2)

$$1 - u_1^{*2} = \frac{2C_p}{u_{e_1}^2}(T_1 - T_{e_1}) \tag{I.2a}$$

$$1 - u_2^{*2} = \frac{2C_p}{u_{e_2}^2}(T_2 - T_{e_2}) \tag{I.2b}$$

Assuming isentropic expansion along streamline from P_1 to P_b which are assumed to be constant through the boundary layer and shear layer respectively.

$$\frac{T_2}{T_1} = \frac{T_{e_2}}{T_{e_1}} = \left(\frac{P_b}{P_1}\right)^{\frac{\gamma-1}{\gamma}} \tag{I.3}$$

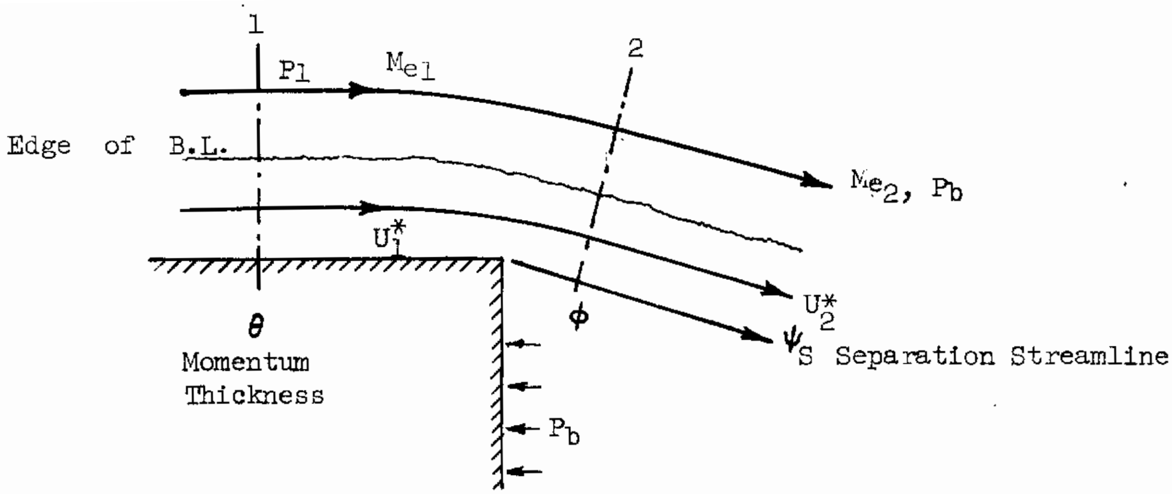

FIGURE 42 Viscous Separation Flow Model

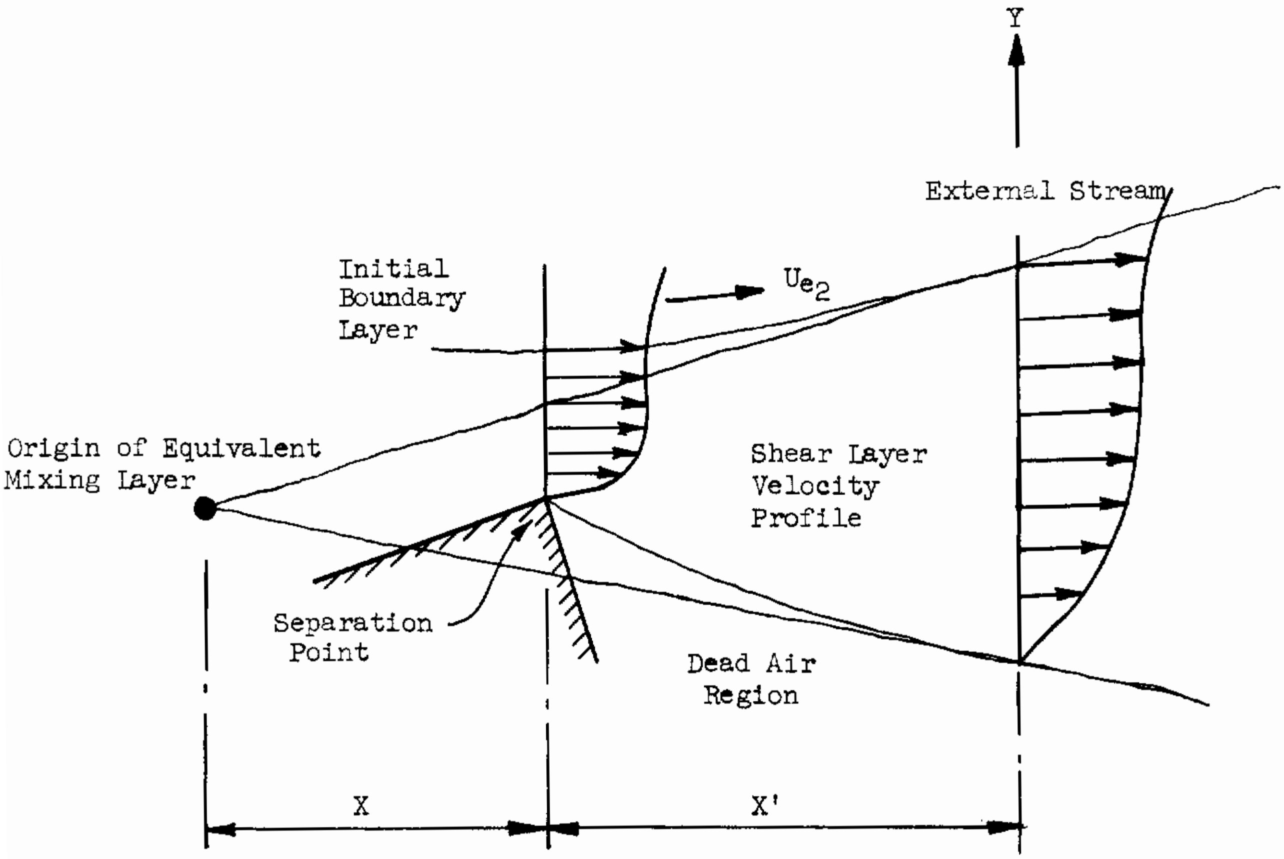

FIGURE 43 Equivalent Mixing Layer Flow Model

Combining(I.2a), (I.2b) and (I.3)

$$\frac{1 - u_2^{*2}}{1 - u_1^{*2}} = \frac{ue_1^2}{ue_2^2}\frac{Te_2}{Te_1} = \frac{Me_1^2}{Me_2^2} \qquad (I.4)$$

The development of the free shear layer from an initial boundary is defined if the momentum thickness, ϕ, at separation is specified. ϕ can be determined in terms of the momentum thickness, θ, at the corner using equation (I.4).

Using the stream function

$$\frac{\delta\psi}{\delta x} = \rho v \qquad \frac{\delta\psi}{\delta y} = \rho u \qquad (I.5)$$

the momentum thicknesses are defined by

$$\rho_{e1} ue_1 \theta = \int_{\psi_s}^{\infty} (1 - u_1^*)\, d\psi \qquad (I.6)$$

$$\rho e_2 ue_2 \phi = \int_{\psi_s}^{\infty} (1 - u_2^*)\, d\psi$$

where ψ_s represents the wall

In the turbulent boundary layer, the mean velocity is nearly equal to the velocity in the external stream.

$$1 - u_1^* = z$$

and

$$Me_2^2 = \frac{1}{r} Me_1^2$$

from equation (I.4)

$$1 - u_2^{*2} = r(1 - u_1^{*2})$$

$$u_2^{*2} = 1 - r(1 - u_1^{*2}) = 1 - r(1 + u_1^*)(1 - u_1^*) = 1 - r(2 - z)(z)$$

$$u_2^* = \left[1 - rz(2 - z)\right]^{1/2}$$

for $rz(2 - z) < 1$ using series expansion (binominal)

$$u_2^* = 1 - \frac{rz(2-z)}{2} + \frac{(1/2)(-1/2)\,r^2 z^2 (2-z)^2}{2} + \cdots\cdots$$

$$1 - u_2^* = \frac{rz\,(2-z)}{2} - \frac{r^2 z^2}{8}(2-z)^2 + \cdots\cdots$$

$$= rz - z^2 \frac{r}{2} \;(1 - r/4) + \cdots\cdots$$

$$1 - u_2^* = r\,(1 - u_1^*) - \frac{r}{2}\,(1 - r/4)(1 - u_1^*)^2 \qquad (I.7)$$

Substituting into equation (I.6)

$$\rho_{e_2}\; u_{e_2}\, \phi = \int_{\psi_s}^{\infty} \left[r(1 - u_1^*) - \frac{r}{2}\,(1 - \frac{r}{4})(1 - u_1^*)^2 \right] d\psi \qquad (I.8)$$

$$= r \int_{\psi_s}^{\infty} (1 - u_1^*)\,d\psi - \frac{r}{2}\,(1 - \frac{r}{4}) \int_{\psi_s}^{\infty} (1 - u_1^*)^2 d\psi$$

$$= r \int_{\psi_s}^{\infty} (1 - u_1^*)\,d\psi - \frac{r}{2}\,(1 - \frac{r}{4}) \int_{\psi_s}^{\infty} (2 - 2u_1^*) + (-1 + u_1^{*2})\,d\psi$$

$$\rho_{e_2}\; u_{e_2}\, \phi = r\int_{\psi_s}^{\infty} (1 - u_1^*)\,d\psi - \frac{r}{2}(1 - \frac{r}{4})\left[2\int_{\psi_s}^{\infty} (1 - u_1^*)\,d\psi - \int_{\psi_s}^{\infty} (1 - u_1^{*2})\,d\psi \right]$$

by definition

$$\int_{\psi_s}^{\infty} (1 - u_1^*)\,d\psi = \rho_{e_1} u_{e_1} \theta \qquad \int_{\psi_s}^{\infty} (1 - u_1^{*2})\,d\psi = \rho_{e_1} u_{e_1}\, \delta^{**}$$

Equation (I.8) becomes

$$\rho_{e_2}\, u_{e_2}\, \phi = r(\rho_{e_1} u_{e_1} \theta) - \frac{r}{2}(1 - \frac{r}{4}) \left\{ 2\rho_{e_1} u_{e_1} \theta - \rho_{e_1} u_{e_1} \delta^{**} \right\} \qquad (I.9)$$

$$= r\,\rho_{e_1} u_{e_1} \left\{ \theta - (\frac{4-r}{8})(2\theta - \delta^{**}) \right\}$$

Assuming terms $(2\theta - \delta^{**})$ and higher $\longrightarrow 0$

$$\frac{\rho_{e_2}\; u_{e_2}\; \phi}{\rho_{e_1}\; u_{e_1}\; \theta} = r = \frac{M_{e_1}^{\,2}}{M_{e_2}^{\,2}} \qquad (I.10)$$

the variation of r with P_b/P_1 is evaluated by

$$\frac{P_b}{P_1} = \left(\frac{1 + \frac{\gamma-1}{2} \; M_{e_1}^2}{1 + \frac{\gamma-1}{2} \; M_{e_2}^2} \right)^{\frac{\gamma}{\gamma-1}} \qquad (I.11)$$

2/ THE FREE SHEAR LAYER

Referring to Figure 43, the velocity profile can be approximated by

$$u^* = \frac{1}{2} \left(1 + \operatorname{erf} \frac{\sigma y}{X} \right) \qquad (I.12)$$

where σ can be estimated by the empirical relation

$$\sigma = 12 \, (1 + .23 \; M_{e_2})$$

The effect of the initial boundary layer is accounted for in equation (I.12) by replacing X by X + X' where X' is assumed to be proportional to θ.

The momentum thickness, Θ (X), (Θ = θ @ sep. pt) of a free mixing layer is defined by

$$\rho_{e_2} \; u_{e_2} \; \Theta = \int_{\psi_B}^{\infty} (1 - u^*) \, d\psi \qquad (I.13)$$

where

$$\psi_B (X) = \psi_{REF} - \int_{-\infty}^{Y_{REF}} \rho u \; dy \qquad (I.14)$$

and ψ_{REF} is any reference streamline

Assuming the total momentum of the equivalent shear layer is equal to the total momentum of the boundary layer at the separation point:

$$\left[\int_{\psi_{BO}}^{\psi_h} u^* \, d\psi \right]_{\substack{\text{EQUIV}\\ \text{SHEAR}\\ \text{LAYER}}} = \left[\int_{\psi_{BO}}^{\psi_h} u^* \, d\psi \right]_{\substack{\text{BOUNDARY}\\ \text{LAYER}}} = \Psi \qquad (I.15)$$

where ψ_h = streamline in the external source

$u_e \; \Psi$ = total momentum in shear layer

$$\rho_{e_2} u_{e_2} \phi = \int_{\psi_s}^{\psi_h} (1 - u^*) d\psi = \psi_h - \psi_s - \Psi \tag{I.16}$$

and at X = 0

$$\rho_{e_2} u_{e_2} \Theta = \int_{\psi_{BO}}^{\psi_h} (1 - u^*) d\psi = \psi_h - \psi_{BO} - \Psi \tag{I.17}$$

Since $\Theta = \phi$ at $X = 0$

$$\psi_{BO} = \psi_S \tag{I.18}$$

defining "median streamline"

$$\psi_M = \psi_h - \Psi \tag{I.19}$$

$$\psi_M - \psi_S = \psi_M - \psi_{BO} = \rho_{e_2} u_{e_2} \phi \tag{I.19a}$$

For the equivalent mixing layer the local velocity u^* in terms of ψ and X is given by

$$\psi_M - \psi = \rho_{e_2} u_{e_2} (x + x') f(u^*) \tag{I.20}$$

where the form of $f(u^*)$ depends on the shape of the velocity profile. The lower boundary of the flow field where $u^* = 0$ is represented by ψ_B (X) defined by

$$\psi_M - \psi_B = \rho_{e_2} u_{e_2} (x + x') f(0) \tag{I.21}$$

and at X = 0

$$\psi_M - \psi_{B_0} = \rho_{e_2} u_{e_2} x' f(0)$$

Hence X' is given by

$$x' = \frac{\psi_M \quad \psi_{B_0}}{\rho_{e_2} u_{e_2} f(0)} = \frac{\phi}{f(0)} \qquad (I.22)$$

eliminating X' in equations (I.20) and (I.22)

$$\frac{\psi_M - \psi}{\rho_{e_2} u_{e_2}} = x f(u^*) + \phi \frac{f(u^*)}{f(0)} \qquad (I.23)$$

finally, since $\psi_M - \psi_S = \rho_{e_2} u_{e_2} \phi$

$$\frac{\psi_S - \psi}{\rho_{e_2} u_{e_2}} = x f(u^*) - \phi \left\{ 1 - \frac{f(u^*)}{f(0)} \right\} \qquad (I.24)$$

Hence the mass flux between the separation streamline and any adjacent streamline can be expressed in terms of functions which relate to the velocity profile of the asymptotic turbulent mixing layer and the momentum thickness of the initial boundary layer, ϕ.

The function $f(u^*)$ uses the median streamline as a datum.. In the asymptotic free shear layer, the velocity on the median streamline is constant, u_c^*.

expressing the velocity profile by its similarity form

$$u^* = u^*(\zeta)$$

where $\zeta = \frac{\sigma y}{\overline{x}}$ and $\overline{X}$ is the distance from origin of asymptotic layer

The location ζ_M of the median streamline is

$$\int_{\zeta_M}^{\zeta_h} \rho^* u^* d\zeta = \int_{-\infty}^{\zeta_h} \rho^* u^{*2} d\zeta \qquad (I.25)$$

where ζ_h is a station in the stream outside the shear layer.

With the density and velocity related by

$$\rho^* = \left[1 + \frac{\gamma - 1}{2} M_e^2 (1 - u^{*2})\right]^{-1} \tag{I.26}$$

the position of ψ_M and the velocity u_c^* are known as functions of the Mach number, M_{e_2} and the shape of the velocity profile.

For subsonic flow u^*_c will be taken as equal to 0.58 .

After identifying ψ_M and u_c^*, the function $f(u^*)$ is given by

$$f(u^*) = \frac{1}{\sigma} \int_{\zeta}^{\zeta_M} \rho^* u^* d\zeta \tag{I.27}$$

the error function velocity profile is assumed

$$u^* = \frac{1}{2}(1 + \operatorname{erf} \zeta) \tag{I.28}$$

making a change of variable in equation (I.16)

$$f = \frac{1}{\sigma} \int_{u^*}^{u_c^*} \rho^* u^* \frac{d\zeta}{du^*} du^*$$

and by use of equation (I.28) becomes

$$f = \frac{\sqrt{\pi}}{\sigma} \int_{u^*}^{u_c^*} \rho^* u^* e^{\zeta^2} du^*$$

which for small values of ζ becomes

$$f = \frac{\sqrt{\pi}}{\sigma} \int_{u^*}^{u_c^*} \rho^* u^* du^* \tag{I.29}$$

from equation (I.26)

$$u^* du^* = \frac{d\rho^*}{(\gamma - 1) M_{e_2}^2 \rho^{*2}}$$

hence a further change of variables from u^* to ρ^*

$$f = \frac{\sqrt{\pi}}{(\gamma - 1)\sigma M_{e_2}^2} \int_{\rho^*}^{\rho_c^*} \frac{d\rho^*}{\rho^*} = \frac{\sqrt{\pi}}{(\gamma - 1)\sigma M_{e_2}^2} \log_e \lambda \qquad (I.30)$$

where

$$\lambda = \frac{\rho_c^*}{\rho^*} = \frac{1 + \frac{\gamma - 1}{2} M_{e_2}^2 (1 - u^{*2})}{1 + \frac{\gamma - 1}{2} M_{e_2}^2 (1 - u_c^*)} \qquad (I.31)$$

3/ THE RE-ATTACHMENT REGION

The base flow solution is closed by the re-attachment condition

$$\frac{P_r - P_b}{P_1 - P_b} = N \qquad (I.32)$$

where N remains to be found

Along ψ_R , (reattachment streamline)

$$\frac{\rho_r}{\rho_R} = \left(\frac{P_r}{P_b}\right)^{1/\gamma} \qquad (I.33)$$

Assuming the recovery temperature is constant through the cavity

$$\frac{\rho_b}{\rho_r} = \frac{P_b}{P_r}$$

$$\frac{\rho_b}{\rho_R} \left(\frac{P_b}{P_r}\right)^{\frac{\gamma - 1}{\gamma}} \qquad (I.34)$$

if
$$\lambda_R = \frac{\rho_c}{\rho_R} \quad \text{and} \quad \lambda_b = \frac{\rho_c}{\rho_b}$$

$$\lambda_R = \lambda_b \left(\frac{P_b}{P_r}\right)^{\frac{\gamma-1}{\gamma}} \tag{I.35}$$

where

$$\lambda_b = \frac{1 + \frac{\gamma-1}{2} M e_2^2}{1 + \frac{\gamma-1}{2}(1 - u_c^{*2})} \tag{I.36}$$

λ_R is a measure of the pressure rise to re-attachment

from equations (I.30) and (I.35)

$$f(u_R^*) = \frac{\sqrt{\pi}}{(\gamma-1)\sigma M e_2^2} \log_e \left\{ \lambda_b \left(\frac{P_b}{P_r}\right)^{\frac{\gamma-1}{\gamma}} \right\} \tag{I.37}$$

and also

$$\frac{f(u_R^*)}{f(0)} = 1 - \frac{\log_e \left(\frac{P_r}{P_b}\right)^{\frac{\gamma-1}{\gamma}}}{\log_e \lambda_b} \tag{I.38}$$

It now remains to apply the re-attachment condition to the known development of the shear layer at a distance ℓ from separation. Assuming a bleed mass flux q into the cavity, the streamline ψ_R is specified by

$$\psi_S - \psi_R = q \tag{I.39}$$

from equations (I.24), (I.39), with the values of $f(u_R^*)$ and $f(u_R^*)/f(0)$ from equations (I.37) and (I.38) the base flow solution is:

$$q = \rho_{e_2} u_{e_2} \left[\ell \cdot f(u_R^*) - \theta \left\{ 1 - \frac{f(u_R^*)}{f(0)} \right\} \right] \tag{I.40}$$

$$q = \rho_{e_2} u_{e_2} \left[\frac{\sqrt{\pi}\,\ell}{(\gamma-1)\sigma M e^2} \left\{ \log_e \lambda_b - \log_e \left(\frac{P_r}{P_b}\right)^{\frac{\gamma-1}{\gamma}} \right\} - \theta \frac{\log_e \left(\frac{P_r}{P_b}\right)^{\frac{\gamma-1}{\gamma}}}{\log_e \lambda_b} \right] \tag{I.41}$$

APPENDIX II

DERIVATION OF EQUATIONS FOR INVISCID FREE-STREAMLINE SOLUTIONS

1/ FREE-STREAMLINE SOLUTION FOR FLOW OVER BASE WITH ZERO FLOW INCLINATION

The free-streamline theory of Kirchoff-Helmholtz is applied to flow over a blunt base having zero flow inclination, shown in Figure 44a. The free-streamline separates from the corner B and impinges on the fence at C, recompressing to stagnation at point D. The pressure is known along boundary BC, being equal to the base pressure. Along the boundaries AB and CD, the flow angles are known. The stream function ψ is arbitrarily assigned the value zero along the boundary ABCDA.

Having the boundary conditions clearly defined, the solution proceeds with a conformal mapping technique involving the three planes shown in Figure 44.

The complex velocity along the boundary maps into the logarithmic complex velocity plane, $Q = \ln(\frac{U_0}{q}) + i\theta$, ($q,\theta$ identifies the velocity vector in polar coordinates) as a semi-infinite strip. The mapping of the vertices of the semi-infinite strip on to the points -1, $-k^2$, 0, 0 in the w plane using the transformation theorem of Schwarz-Christoffel closes the solution and allows the geometry to be determined completely.

The following paragraphs develop the mathematical procedure of the solution and the resulting integral equations defining the geometrical relationships for the free-streamline and the fence.

1.1 SCHWARZ-CHRISTOFFEL TRANSFORMATION

Referring to Figures 44b and 44c, the Schwarz-Christoffel transformation which maps the semi-infinite strip in the Q plane onto the real axis in the w plane is given by:

$$Q = K_1 \int (w+1)^{-1/2} (w+k^2)^{-1/2} (w)^{-1/2} (w)^{-1/2} dw + K_2 \qquad \text{(II.1)}$$

where $-1, -k^2, 0, 0$) correspond to the locations of the vertices of polygon ABCDD'A' on the real axis of the w plane. The expression is integrated as follows:

$$Q = K_1 \int^{o} \frac{dw}{w\sqrt{(w+1)(w+k^2)}} + K_2 = K_1 \int^{o} \frac{dw}{w\sqrt{w^2 + (k^2+1)w + k^2}} + K_2$$

$$= K_1 \left(-\frac{1}{k} \ln \left(\frac{\sqrt{w^2 + (k^2+1)w + k^2} + k}{w} + \frac{k+1}{2k} \right) \right) + K_2$$

$$= K_1 \left(-\frac{1}{k} \ln \left(\frac{2k\sqrt{w^2 + (k^2+1)w + k^2} + 2k^2 + (k^2+1)w}{2kw} \right) \right) + K_2$$

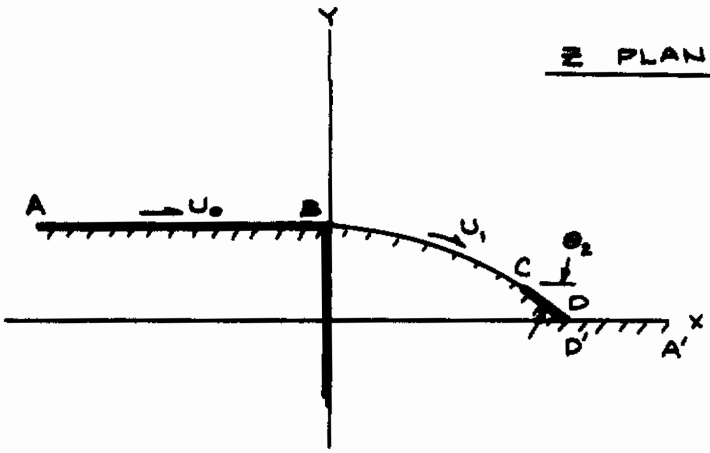

Figure 44 a

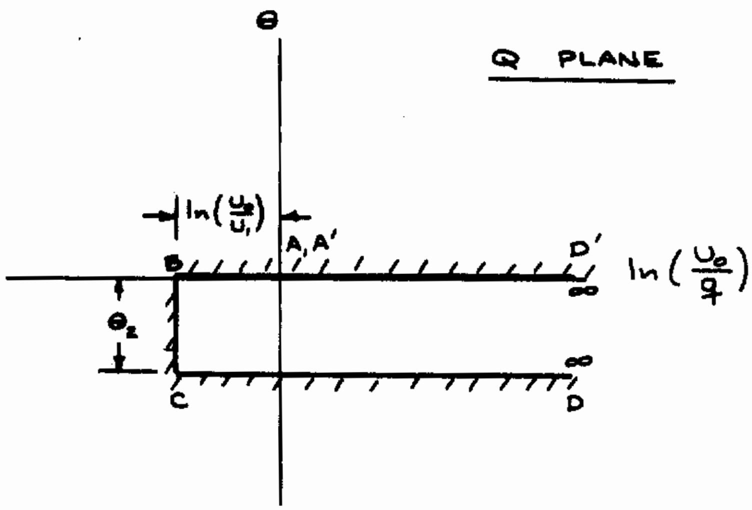

Figure 44b

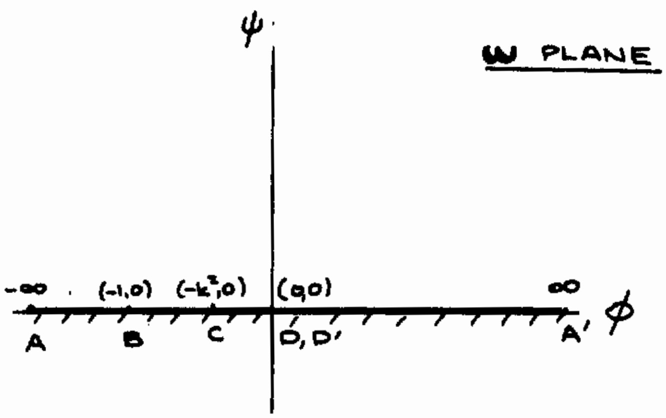

Figure 44c

Figure 44 Mapping planes $\theta_1 = 0$

$$= K_1 \left[\frac{1}{k} \ \text{ln} \left(\frac{2kw}{2k\sqrt{w^2+(k^2+1)w+k^2}+2k^2+(k^2+1)w} \right) \right] + K_2$$

let $k_2 = \frac{K_1}{K} \ \text{ln} \ \frac{L}{2k}$

$$Q = \frac{K_1}{K} \ \text{ln} \left[L \left(\frac{w}{2k\sqrt{w^2+(k^2+1)w+k^2}+2k^2+(k^2+1)w} \right) \right] \qquad \text{(II.2)}$$

1.2 EVALUATION OF CONSTANTS

1.2.1 AT POINT B.

$$W = \phi = 1 \qquad Q = \ln\left(\frac{U_0}{U_1}\right)$$

Equation (II.2) reduces to:

$$\ln\left(\frac{U_0}{U_1}\right) = \frac{K_1}{k} \ln\left[L \frac{1}{1-k^2}\right] \tag{II.3}$$

1.2.2 AT POINT C

$$\ln\left(\frac{U_0}{U_1}\right) - i\theta_2 = \frac{K_1}{k} \ln\left[L\left(\frac{-k^2}{2k\sqrt{k^4-(k^2+1)k^2+k^2+2k^2-(k^2+1)k^2}}\right)\right]$$

$$= \frac{K_1}{k} \ln\left[L\left(\frac{-k^2}{2k^2-k^4-k^2}\right)\right]$$

$$= \frac{K_1}{k} \ln\left[L\left(\frac{-1}{1-k^2}\right)\right]$$

$$\ln\left(\frac{U_0}{U_1}\right) + i\theta_2 = \frac{K_1}{k} \ln\left[L\left(\frac{1}{1-k^2}\right)\right] + \frac{K_1}{k}\ln(-1)$$

$$= \frac{K_1}{k} \ln\left[L\left(\frac{1}{1-k^2}\right)\right] + \frac{K_1}{k} i\pi$$

$$\therefore \quad \frac{K_1}{k} = \frac{\theta_2}{\pi} \tag{II.4}$$

$$\ln\left(\frac{U_0}{U_1}\right) = \frac{\theta_2}{\pi}\ln\left[L\left(\frac{1}{1-k^2}\right)\right]$$

$$\ln\left[\left(\frac{U_0}{U_1}\right)^{\frac{\pi}{\theta_2}}\right] = \ln\left[L\left(\frac{1}{1-k^2}\right)\right]$$

$$\left(\frac{U_0}{U_1}\right)^{\frac{\pi}{\theta_2}} = L\left(\frac{1}{1-k^2}\right)$$

$$L = \left(\frac{U_0}{U_1}\right)^{\frac{\pi}{\theta_2}}(1-k^2) \qquad \text{(II.5)}$$

∴ the transformation equation becomes:

$$Q = \frac{\theta_2}{\pi}\ln\left[\left(\frac{U_0}{U_1}\right)^{\frac{\pi}{\theta_2}}(1-k^2)\left(\frac{w}{2k\sqrt{w^2+(k^2+1)w+k^2}+2k^2+(k^2+1)w}\right)\right]$$

$$Q = \ln\left(\frac{U_0}{U_1}\right) + \frac{\theta_2}{\pi}\ln\left[(1-k^2)\left(\frac{w}{2k\sqrt{w^2+(k^2+1)w+k^2}+2k^2+(k^2+1)w}\right)\right] \qquad \text{(II.6)}$$

1.2.3 CHECK

at pt. B $\phi = -1$ $\theta = 0$ $q = U_1$

$$\ln\left(\frac{U_0}{U_1}\right) = \ln\left(\frac{U_0}{U_1}\right) + \frac{\theta_2}{\pi}\ln\left[(1-k^2)\left(\frac{-1}{2k^2-k^2-1}\right)\right]$$

$$\ln\left(\frac{U_0}{U_1}\right) = \ln\left(\frac{U_0}{U_1}\right)$$

at pt. C $\phi = -k^2$ $\theta = \theta_2$ $q = U_1$

$$\ln\left(\frac{U_0}{U_1}\right) + i\theta_2 = \ln\left(\frac{U_0}{U_1}\right) + \frac{\theta_2}{\pi}\ln\left[(1-k^2)\left(\frac{-k^2}{2k\sqrt{k^4-(k^2+1)k^2+k^2}+2k^2-(k^2+1)k^2}\right)\right]$$

$$= \ln\left(\frac{U_0}{U_1}\right) + \frac{\theta_2}{\pi}\ln\left[(1-k^2)\left(\frac{-k^2}{2k^2-k^2-k^4}\right)\right]$$

$$= \ln\left(\frac{U_0}{U_1}\right) + \frac{\theta_2}{\pi}\ln\left[(1-k^2)\left(\frac{-1}{(1-k^2)}\right)\right]$$

$$= \ln\left(\frac{U_0}{U_1}\right) + \theta_2 i + \frac{\theta_2}{\pi}\ln\left[\frac{1-k^2}{1-k^2}\right]$$

$$= \ln\left(\frac{U_0}{U_1}\right) + \theta_2 i$$

at pt. D $\quad \phi = 0 \quad \theta = \theta_2 \quad q = 0$

$$\ln\left(\frac{U_0}{0}\right) + i\theta_2 = \ln\left(\frac{U_0}{U_1}\right) + \frac{\theta_2}{\pi}\ln\left[(1-k^2)\left(\frac{-0}{4k^2}\right)\right]$$

$$= \ln\left(\frac{U_0}{U_1}\right) + \frac{\theta_2}{\pi}\ln\left[(1-k^2)\left(\frac{+0}{4k^2}\right)\right] + \theta_2 i$$

at pt. D' $\quad \phi = 0 \quad \theta = 0 \quad q = 0$

$$\ln\left(\frac{U_0}{0}\right) = \ln\left(\frac{U_0}{U_1}\right) + \frac{\theta_2}{\pi}\ln\left[\frac{+0}{4k^2}\right]$$

since $\theta_2 < 0$ and $\ln(0) = -\infty$

equations are satisfied

1.3 EVALUATION OF CONSTANT k

At point A' $\quad w = \infty \quad \frac{U_0}{q} = \frac{U}{U_0} = 1 \quad \theta = 0$

$$0 = \ln\left(\frac{U_0}{U_1}\right) - \frac{\theta_2}{\pi}\ln\left[\frac{1}{(1-k^2)}\;\frac{2k\sqrt{w^2+(k^2+1)w+k^2}+2k^2+(k^2+1)w}{w}\right]$$

$$= \ln\left(\frac{U_0}{U_1}\right) - \frac{\theta_2}{\pi}\ln\left[\frac{1}{(1-k^2)}\;2k+k^2+1\right]$$

$$= \ln\left(\frac{U_0}{U_1}\right) - \frac{\theta_2}{\pi}\ln\left(\frac{1+k}{1-k}\right)$$

$$\ln\left(\frac{1+k}{1-k}\right) = \ln\left[\left(\frac{U_0}{U_1}\right)^{\pi/\theta_2}\right]$$

$$\frac{1+k}{1-k} = \left(\frac{U_0}{U_1}\right)^{\pi/\theta_2} \qquad \text{(II.7)}$$

1.4 DETERMINATION OF GEOMETRY IN REAL PLANE

$$d\phi = \frac{\partial\phi}{\partial x}dx + \frac{\partial\phi}{\partial y}dy \tag{II.8}$$

$$d\psi = \frac{\partial\psi}{\partial x}dx + \frac{\partial\psi}{\partial y}dy \tag{II.9}$$

$$\frac{\partial\psi}{\partial x} = -\frac{\partial\phi}{\partial y} \qquad \frac{\partial\psi}{\partial y} = \frac{\partial\phi}{\partial x} \tag{II.10}$$

since $d\psi = 0$

$$d\phi = \frac{\partial\phi}{\partial x}dx + \frac{\partial\phi}{\partial y}dy$$

$$0 = -\frac{\partial\phi}{\partial y}dx + \frac{\partial\phi}{\partial x}dy$$

$$\therefore\ dy = \frac{\frac{\partial\phi}{\partial y}}{\frac{\partial\phi}{\partial x}}\,dx \tag{II.11}$$

$$d\phi = \frac{\partial\phi}{\partial x}dx + \frac{\left(\frac{\partial\phi}{\partial y}\right)^2}{\left(\frac{\partial\phi}{\partial x}\right)}dx \doteq \frac{\left(\frac{\partial^2\phi}{\partial x^2}\right) + \left(\frac{\partial^2\phi}{\partial y^2}\right)}{\frac{\partial\phi}{\partial x}}\,dx \tag{II.12}$$

Using definition of complex velocity in polar form:

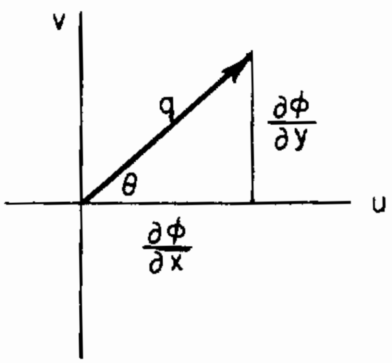

$$\frac{\partial\phi}{\partial y} = q\sin\theta \tag{II.13}$$

$$\frac{\partial\phi}{\partial x} = q\cos\theta \tag{II.14}$$

$$\therefore d\phi = \frac{q^2(\cos^2\theta + \sin^2\theta)}{q\cos\theta} dx$$

$$dx = \frac{\cos\theta}{q} d\phi$$

$$dy = \frac{\partial\phi}{\partial\phi}\frac{\partial y}{\partial x} dx = \frac{q\sin\theta}{q\cos\theta}\ \frac{\cos\theta}{q} d\phi = \frac{\sin\theta}{q} d\phi$$

$$\Delta x\Big|_{x_1}^{x_2} = \int_{\phi_1}^{\phi_2} \frac{\cos\theta}{q} d\phi \qquad \text{(II.16)}$$

$$\Delta y\Big|_{y_1}^{y_2} = \int_{\phi_1}^{\phi_2} \frac{\sin\theta}{q} d \qquad \text{(II.17)}$$

1.4.1 ALONG STREAMLINE BC

$$\ln\left(\frac{U_o}{U_1}\right) + i\,\theta_{BC} = \ln\left(\frac{U_o}{U_1}\right) + \frac{\theta_2}{\pi}\ln\left[(1-k^2)\left(\frac{\phi_{BC}}{2k\sqrt{\phi_{BC}^2+(k^2+1)\phi_{BC}+k^2}+2k^2+(k^2+1)\phi_{BC}}\right)\right]$$

$$i\,\theta_{BC} = \frac{\theta_2}{\pi}\ln\left[(1-k^2)\left(\frac{\phi_{BC}}{2k\sqrt{\phi_{BC}^2+(k^2+1)\phi_{BC}+k^2}+2k^2+(k^2+1)\phi_{BC}}\right)\right]$$

since $\phi_{BC}^2 + (k^2+1)\phi_{BC} + k^2 \lessgtr 0$ for $-1 < \phi_{BC} < -K^2$

$$i\,\theta_{BC} = \frac{\theta_2}{\pi}\ln\left[(1-k^2)\left(\frac{\phi_{BC}}{-2ki\sqrt{-\phi_{BC}^2-(k^2+1)\phi_{BC}-k^2}+2k^2+(k^2+1)\phi_{BC}}\right)\right]$$

$$i\,\theta_{BC} = -\frac{\theta_2}{\pi}\ln\left[\frac{1}{(1-k^2)}\left(\frac{-2ki\sqrt{-\phi_{BC}^2-(k^2+1)\phi_{BC}-k^2}+2k^2+(k^2+1)\phi_{BC}}{\phi_{BC}}\right)\right]$$

$$i\theta_{BC} = -\frac{\theta_2}{\pi}\left[\ln r + i\beta\right]$$

$$r^2 = x^2 + y^2$$

$$x^2 = \left(\frac{2k^2 + (k^2+1)\phi_{BC}}{\phi_{BC}(1-k^2)} \right)^2 = \frac{4k^4 + 4k^2(k^2+1)\phi_{BC} + (k^2+1)^2\phi_{BC}^2}{(1-k^2)^2\phi_{BC}^2}$$

$$y^2 = \frac{4k^2\left(-\phi_{BC}^2 - (k^2+1)\phi_{BC} - k^2\right)}{\phi_{BC}^2 (1-k^2)^2}$$

$$r^2 = \frac{4k^4 + 4k^4\phi_{BC} + 4k^2\phi_{BC} + k^4\phi_{BC}^2 + 2k^2\phi_{BC}^2 + \phi_{BC}^2 - 4k^2\phi_{BC}^2 - 4k^4\phi_{BC} - 4k^2\phi_{BC} - 4k^4}{(1-k^2)^2\phi_{BC}^2}$$

$$r^2 = \frac{k^4\phi_{BC}^2 - 2k^2\phi_{BC}^2 + \phi_{BC}^2}{(1-k^2)^2\phi_{BC}^2} = \frac{(k^2-1)^2\phi_{BC}^2}{(1-k^2)^2\phi_{BC}^2} = 1 \qquad \therefore \ln r = 0$$

$$\beta = \tan^{-1} \frac{y}{x}$$

$$= \tan^{-1} \frac{2k\sqrt{-\phi_{BC}^2 - (k^2+1)\phi_{BC} - k^2}}{2k^2 + (k^2+1)\phi_{BC}}$$

$$\therefore \theta_{BC} = -\frac{\theta_2}{\pi} \tan^{-1}\left(\frac{2k\sqrt{-\phi_{BC}^2 - (k^2+1)\phi_{BC} - k^2}}{2k^2 + (k^2+1)\phi_{BC}} \right) \qquad \text{(II.18)}$$

1.4.1.1 Check

$$@\ B\quad \phi = -1 \quad \theta = 0$$

$$\theta_{BC} = -\frac{\theta_2}{\pi}\tan^{-1}\left(\frac{2k\sqrt{-1+k^2+1-k^2}}{2k^2-k^2-1}\right) = -\frac{\theta_2}{\pi}\tan^{-1}(0)$$

$$= 0$$

$$@\ C\quad \phi = -k^2 \quad \theta = \theta_2$$

$$\theta_{BC} = -\frac{\theta_2}{\pi}\tan^{-1}\left(\frac{2k\sqrt{-k^4+(k^2+1)k^2-k^2}}{2k^2-(k^2+1)k^2}\right)$$

$$= -\frac{\theta_2}{\pi}\tan^{-1}(0) = -\frac{\theta_2}{\pi}(-\pi)$$

$$\theta_{BC} = \theta_2$$

substituting Θ_{BC} into equations (II.16) and (II.17)

$$x\Big/_0^{x_{BC}} = \int_{\phi_B}^{\phi_{BC}} \frac{\cos\theta}{q_{BC}}\, d\phi$$

$$x\Big/_0^{x} = \frac{1}{U_1}\int_{\phi_B}^{\phi_{BC}} \cos\left[-\frac{\theta_2}{\pi}\mathrm{Tan}^{-1}\left(\frac{2k\sqrt{-\phi_{BC}^2-(k^2+1)\phi_{BC}-k^2}}{2k^2+(k^2+1)\phi_{BC}}\right)\right] d\phi \qquad \text{(II.19)}$$

$$y \Big/_{h}^{y_{BC}} = \int_{\phi_B}^{\phi_{BC}} \frac{\sin\theta}{g_{BC}}\, d\phi$$

$$= \frac{1}{U_1} \int_{\phi_{BC}}^{\phi_{BC}} \sin\left[-\frac{\theta_2}{\pi}\tan^{-1}\left(\frac{2k\sqrt{-\phi_{BC}^2-(k^2+1)\phi_{BC}-k^2}}{2k^2+(k^2+1)\,\phi_{BC}}\right)\right] d\phi \qquad \text{(II.20)}$$

1.4.2 ALONG STREAMLINE CD

$$x \Big/_{x_C}^{x_D} = \int_{\phi_C}^{\phi_D} \frac{\cos\theta_2}{q_{CD}}\, d\phi = \cos\theta_2 \int_{\phi_C}^{\phi_D} \frac{d\phi}{g_{CD}}$$

$$y \Big/_{h_O}^{O} \quad \int_{\phi_C}^{\phi_D} \frac{\sin\theta_2}{q_{CD}}\, d\phi = \sin\theta_2 \int_{\phi_C}^{\phi_D} \frac{d\phi}{g_{CD}}$$

$$\ln\left(\frac{U_0}{q_{CD}}\right) + i\,\theta_2 = \ln\left(\frac{U_0}{U_1}\right) + \frac{\theta_2}{\pi}\ln\left[(1-k^2)\left(\frac{\phi_{CD}}{2k\sqrt{\phi^2+(k^2+1)\phi+k^2}+2k^2+(k^2+1)\phi}\right)\right]$$

$$\ln\left(\frac{U_0}{q_{CD}}\right) + i\,\theta_2 = \ln\left(\frac{U_0}{U_1}\right) + \frac{\theta_2}{\pi}\ln(-1) + \frac{\theta_2}{\pi}\ln\left[(1-k^2)\left(\frac{-\phi_{CD}}{2k\sqrt{\phi^2+(k^2+1)\phi+k^2}+2k^2+(k^2+1)\phi}\right)\right]$$

$$\ln\left(\frac{U_0}{q_{CD}}\right) = \ln\left(\frac{U_0}{v_1}\right) + \frac{\theta_2}{\pi}\ln\left[(1-k^2)\left(\frac{-\phi_{CD}}{2k\sqrt{\phi^2+(k^2+1)\phi+k^2}+2k^2+(k^2+1)\phi}\right)\right]$$

$$\frac{U_0}{q_{CD}} = \frac{U_0}{U_1}\left[(1-k^2)\left(\frac{-\phi_{CD}}{2k\sqrt{\phi_{CD}^2+(k^2+1)\phi_{CD}+k^2}+2k^2+(k^2+1)\phi_{CD}}\right)\right]^{\frac{\theta_2}{\pi}}$$

$$q_{CD} = U_1\left[(1-k^2)\left(\frac{-\phi_{CD}}{2k\sqrt{\phi_{CD}^2+(k^2+1)\phi_{CD}+k^2}+2k^2+(k^2+1)\phi_{CD}}\right)\right]^{-\frac{\theta_2}{\pi}} \qquad \text{(II.21)}$$

$$X\Big/_{X_C}^{X_D} = \frac{\cos\theta_2}{U_1}\int_{\phi_C}^{\phi_D}\left[(1-k^2)\left(\frac{-\phi_{CD}}{2k\sqrt{\phi_{CD}^2+(k^2+1)\phi_{CD}+k^2}+2k^2+(k^2+1)\phi_{CD}}\right)\right]^{\frac{\theta_2}{\pi}} d\phi$$

(II.22)

$$Y\Big/_{h_0}^{0} = \frac{\sin\theta_2}{U_1}\int_{\phi_C}^{\phi_D}\left[(1-k^2)\left(\frac{-\phi_{CD}}{2k\sqrt{\phi_{CD}^2+(k^2+1)\phi_{CD}+k^2}+2k^2+(k^2+1)\phi_{CD}}\right)\right]^{\frac{\theta_2}{\pi}} d\phi$$

(II.23)

1.4.2.1 Check

at pt. C $\quad \phi = -k^2$

$$q_{CD} = U_1\left[(1-k^2)\left(\frac{k^2}{2k\sqrt{k^4-(k^2+1)k^2+k^2}+2k^2-(k^2+1)k^2}\right)\right]^{-\frac{\theta_2}{\pi}}$$

$$= U_1\left[(1-k^2)\left(\frac{k^2}{k^2-k^4}\right)\right]^{-\frac{\theta_2}{\pi}} = U_1$$

at pt. D $\quad \phi = 0$

$$q_{CD} = U_1\left[(1-k^2)\left(\frac{0}{0+2k^2+0}\right)\right]^{-\frac{\theta_2}{\pi}}$$

$$q_{CD} = 0$$

1.4.2.2 Evaluation of Improper Integral

$$F(\phi) = \int_{-k^2}^{0} \left[\frac{2k\sqrt{\phi^2+(k^2+1)\phi+k^2}+2k^2+(k^2+1)\phi}{-\phi} \right]^{-\frac{\theta_2}{\pi}} d\phi$$

$$\frac{-2k^2\sqrt{\phi^2+(k^2+1)\phi+k^2}-2k^2-(k^2+1)\phi}{\phi} \leq \frac{2k^2}{\phi}$$

$$F(\phi) = \int_{-k^2}^{0} \left(\frac{2k^2}{\phi} \right)^{-\frac{\theta_2}{\pi}} d\phi$$

$$= (2k^2)^{-\frac{\theta_2}{\pi}} \int_{-k^2}^{0} \frac{d\phi}{(\phi)^{-\frac{\theta_2}{\pi}}}$$

$$= (2k^2)^{-\frac{\theta_2}{\pi}} \left(\frac{1}{1-\frac{\theta_2}{\pi}} \right) \left(\phi^{1-\frac{\theta_2}{\pi}} \right) \Big/_{-k^2}^{0} \qquad \text{(II.24)}$$

∴ expression converges and has a limit
integral can be evaluated

1.5 DETERMINATION OF k IN TERMS OF C_{P_b}

$$\frac{1+k}{1-k} = \left(\frac{U_0}{U_1} \right)^{\frac{\pi}{\theta_2}}$$

$$k = \frac{\left(\frac{U_0}{U_1} \right)^{\frac{\pi}{\theta_2}} - 1}{\left(\frac{U_0}{U_1} \right)^{\frac{\pi}{\theta_2}} + 1} \qquad \text{(II.25)}$$

from Bernoulli's equation:

$$\frac{U_0^2}{2} + \frac{P_0}{\rho_0} = \frac{U_1^2}{2} + \frac{P_b}{\rho_b} \qquad \text{(II.26)}$$

$$\rho_0 = \rho_b$$

$$\frac{P_b - P_0}{\rho_0} = \frac{U_0^2 - U_1^2}{2}$$

$$\frac{P_b - P_0}{\rho_0 \frac{U_0^2}{2}} = 1 - \left(\frac{U_1}{U_0}\right)^2$$

$$C_{P_b} = 1 - \left(\frac{U_1}{U_0}\right)^2$$

$$\left(\frac{U_1}{U_0}\right)^2 = 1 - C_{P_b}$$

$$\left(\frac{U_0}{U_1}\right)^2 = \frac{1}{1 - C_{P_b}}$$

$$k = \frac{\left(\frac{1}{1-C_{P_b}}\right)^{\frac{\pi}{2\theta_2}} - 1}{\left(\frac{1}{1-C_{P_b}}\right)^{\frac{\pi}{2\theta_2}} + 1} \qquad \text{(II.27)}$$

1.6 DETERMINATION OF GEOMETRICAL RELATIONSHIPS

The height of the base is determined from equations (II.20) and (II.23)

$$h = \Delta y_{BC} + \Delta y_{CD}$$

$$\text{where} \quad \phi_B = -1 \qquad \phi_C = -k^2 \qquad \phi_D = 0$$

summarizing:

$$x\Big/_{o}^{x_{BC}} = \frac{1}{U_1}\int_{\phi_B}^{\phi_{BC}} \cos\left[-\frac{\theta_2}{\pi}\tan^{-1}\left(\frac{2k\sqrt{-\phi_{BC}^2-(k^2+1)\phi_{BC}-k^2}}{2k^2+(k^2+1)\phi_{BC}}\right)\right] d\phi \qquad \text{(II.19)}$$

$$y\Big/_{h}^{y_{BC}} = \frac{1}{U_1}\int_{\phi_B}^{\phi_{BC}} \sin\left[-\frac{\theta_2}{\pi}\tan^{-1}\left(\frac{2k\sqrt{-\phi_{BC}^2-(k^2+1)\phi_{BC}-k^2}}{2k^2+(k^2+1)\phi_{BC}}\right)\right] d\phi \qquad \text{(II.20)}$$

$$x\Big/_{x_C}^{x_D} = \frac{\cos\theta_2}{U_1}\int_{\phi_C}^{\phi_D}\left[(1-k^2)\left(\frac{-\phi_{CD}}{2k\sqrt{\phi_{CD}+(k^2+1)\phi_{CD}+k^2}+2k^2+(k^2+1)\phi_{CD}}\right)\right]^{\frac{\theta_2}{\pi}} d\phi \qquad \text{(II.22)}$$

$$y\Big/_{ho}^{o} = \frac{\sin\theta_2}{U_1}\int_{\phi_C}^{\phi_D}\left[(1-k^2)\left(\frac{-\phi_{CD}}{2k\sqrt{\phi_{CD}^2+(k^2+1)\phi_{CD}+k^2}+2k^2+(k^2+1)\phi_{CD}}\right)\right]^{\frac{\theta_2}{\pi}} d\phi \qquad \text{(II.23)}$$

Evaluating equation (II.27) for k in terms of a known C_{pb}, the integrals of equations (II.19), (II.20), (II.22) and (II.23) can be evaluated. Non-dimensional values of the coordinates of the streamline between B and C can be obtained by integrating equations (II.19) and (II.20) by the value determined for h.

2/ FREE-STREAMLINE SOLUTION FOR FLOW OVER BASE WITH POSITIVE ANGLE

2.1 SCHWARZ-CHRISTOFFEL TRANSFORMATION

As before, the Schwarz-Christoffel transformation which maps the semi-infinite strip shown in Figure 45 is given by:

$$Q = K_1 \int (w'+C_1)^{-\frac{1}{2}} (w'+1)^{-1} (w')(w'-1)^{-1} (w'-C_2)^{-\frac{1}{2}} dw' + K_2 \qquad \text{(II.28)}$$

$$Q = K_1 \int \frac{w'\,dw'}{(w'+1)(w'-1)\sqrt{w'^2+(C_1-C_2)w'-C_1C_2}} + K_2$$

$$Q = \frac{K_1}{2}\left\{ \int \frac{w'\,dw'}{(w'-1)\sqrt{w'^2+(C_1-C_2)w'-C_1C_2}} - \int \frac{w'\,dw'}{(w'+1)\sqrt{w'^2+(C_1-C_2)w'-C_1C_2}} \right\} + K_2$$

$$\int \frac{x\,dx}{(mx+n)\sqrt{\phi}} = \frac{1}{m}\int \frac{dx}{\sqrt{\phi}} - \frac{n}{m}\int \frac{dx}{(mx+n)\sqrt{\phi}}$$

$$\therefore \int \frac{w'\,dw'}{(w'-1)\sqrt{\phi}} - \int \frac{w'\,dw'}{(w'+1)\sqrt{\phi}} = \int \frac{dw'}{\sqrt{\phi}} + \int \frac{dw'}{(w'-1)\sqrt{\phi}} - \int \frac{dw'}{\sqrt{\phi}} + \int \frac{dw'}{(w'+1)\sqrt{\phi}}$$

$$= \int \frac{dw'}{(w'-1)\sqrt{\phi}} + \int \frac{dw'}{(w'+1)\sqrt{\phi}}$$

$$\therefore Q = \frac{K_1}{2}\left\{ \int \frac{dw'}{(w'-1)\sqrt{w'^2+(C_1-C_2)w'-C_1C_2}} + \int \frac{dw'}{(w'+1)\sqrt{w'^2+(C_1-C_2)w'-C_1C_2}} \right\} + K_2$$

let $w'-1 = t \qquad w'+1 = s$

$\qquad dw' = dt \qquad dw' = ds$

$$Q = \frac{K_1}{2}\left\{ \int \frac{dt}{t\sqrt{t^2+(2+C_1-C_2)t+(1+C_1-C_2-C_1C_2)}} + \int \frac{ds}{s\sqrt{s^2-(2+C_2-C_1)s+(1+C_2-C_1-C_1C_2)}} \right\} + K_2$$

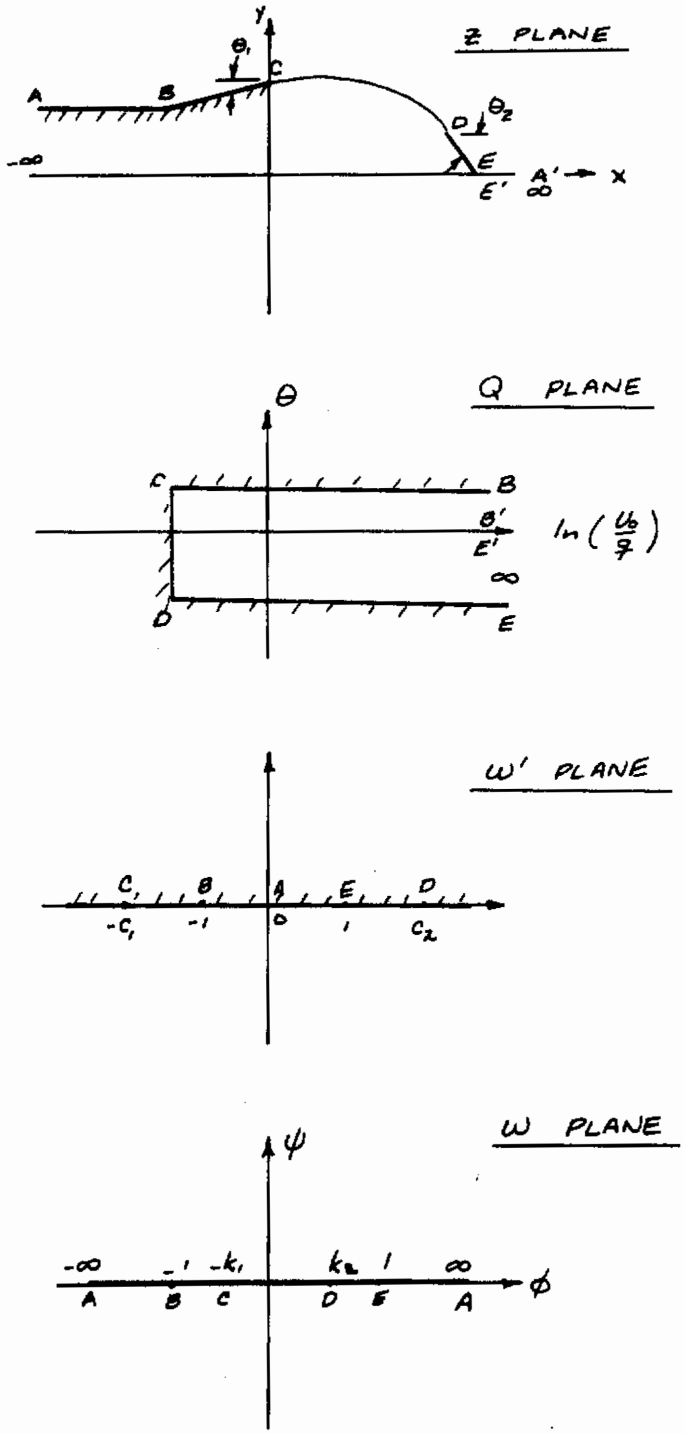

Figure 45 Mapping Planes θ>0

since $1+C_1-C_2-C_1C_2<0$, $1+C_2-C_1-C_1C_2<0$

$$Q = \frac{K_1}{2}\left\{\frac{1}{\sqrt{C_2-C_1+C_1C_2-1}}\,\sin^{-1}\left[\frac{(2+C_1-C_2)(w'-1)+2(1+C_1-C_2-C_1C_2)}{(w'-1)(C_1+C_2)}\right]\right.$$

$$\left.-\frac{1}{\sqrt{C_1-C_2+C_1C_2-1}}\,\sin^{-1}\left[\frac{(2+C_2-C_1)(w'+1)-2(1+C_2-C_1-C_1C_2)}{(w'+1)(C_1+C_2)}\right]\right\}+K_2$$

$$Q = \frac{K_1}{2}\left\{\frac{1}{\sqrt{C_2-C_1+C_1C_2-1}}\,\sin^{-1}\left[\frac{(2+C_1-C_2)w'+(C_1-C_2-2C_1C_2)}{(w'-1)(C_1+C_2)}\right]\right.$$

$$\left.-\frac{1}{\sqrt{C_1-C_2+C_1C_2-1}}\,\sin^{-1}\left[\frac{(2+C_2-C_1)w'+(C_1-C_2+2C_1C_2)}{(w'+1)(C_1+C_2)}\right]\right\}+K_2$$

transforming to upper-half of w plane using:

$$w' = \frac{1}{w} \qquad C_1 = \frac{1}{k_1} \qquad C_2 = \frac{1}{k_2}$$

$$Q = \frac{K_1}{2}\left\{\frac{1}{\sqrt{\frac{1}{k_2}-\frac{1}{k_1}+\frac{1}{k_1k_2}-1}}\,\sin^{-1}\left[\frac{\left(2+\frac{1}{k_1}-\frac{1}{k_2}\right)\frac{1}{w}+\left(\frac{1}{k_1}-\frac{1}{k_2}-2\frac{1}{k_1k_2}\right)}{\left(\frac{1}{w}-1\right)\left(\frac{1}{k_1}+\frac{1}{k_2}\right)}\right]\right.$$

$$\left.-\frac{1}{\sqrt{\frac{1}{k_1}-\frac{1}{k_2}+\frac{1}{k_1k_2}-1}}\,\sin^{-1}\left[\frac{\left(2+\frac{1}{k_2}-\frac{1}{k_1}\right)\frac{1}{w}+\left(\frac{1}{k_1}-\frac{1}{k_2}+2\frac{1}{k_1k_2}\right)}{\left(\frac{1}{w}+1\right)\left(\frac{1}{k_1}+\frac{1}{k_2}\right)}\right]\right\}+K_2$$

$$Q = \frac{K_1}{2}\left\{\frac{\sqrt{k_1k_2}}{\sqrt{k_1-k_2+1-k_1k_2}}\,\sin^{-1}\left[\frac{(2k_1k_2+k_2-k_1)+(k_2-k_1-2)w}{(1-w)(k_2+k_1)}\right]\right.$$

$$\left.-\frac{\sqrt{k_1k_2}}{\sqrt{k_2-k_1+1-k_1k_2}}\,\sin^{-1}\left[\frac{(2k_1k_2+k_1-k_2)+(k_2-k_1+2)w}{(1+w)(k_2+k_1)}\right]\right\} \quad K_2 \qquad \text{(II.29)}$$

2.2 EVALUATION OF CONSTANTS

2.2.1 AT POINT C $\phi = -k_1$ $Q = \ln\left(\frac{U_0}{U_1}\right) + i\,\theta_1$
Equation (II.29) reduces to:

$$\ln\left(\frac{U_0}{U_1}\right) + i\theta_1 = \frac{K_1\sqrt{k_1 k_2}}{2}\left\{\frac{1}{\sqrt{1+k_1-k_2-k_1k_2}}\sin^{-1}\left[\frac{(2k_1k_2+k_2-k_1)+(k_2-k_1-2)(-k_1)}{(1+k_1)(k_2+k_1)}\right.\right.$$

$$\left.\left. - \frac{1}{\sqrt{1+k_2-k_1-k_1k_2}}\sin^{-1}\left[\frac{(2k_1k_2+k_1-k_2)+(k_2-k_1+2)(-k_1)}{(1-k_1)(k_2+k_1)}\right]\right\} + K_2$$

$$\ln\left(\frac{U_0}{U_1}\right) + i\theta_1 = \frac{K_1\sqrt{k_1 k_2}}{2}\left\{\frac{1}{\sqrt{1+k_1-k_2-k_1k_2}}\sin^{-1}(1) - \frac{1}{\sqrt{1+k_2-k_1-k_1k_2}}\sin^{-1}(-1)\right\} + K_2$$

$$\ln\left(\frac{U_0}{U_1}\right) + i\theta_1 = \frac{K\sqrt{k_1 k_2}}{2}\left\{\frac{\pi}{2\sqrt{1+k_1-k_2-k_1k_2}} + \frac{\pi}{2\sqrt{1+k_2-k_1-k_1k_2}}\right\} + K_2 \qquad \text{(II.30)}$$

2.2.2 AT POINT D $\phi = k_2$ $\quad Q = \ln\left(\frac{U_0}{U_1}\right) + i\,\theta_2$

$$\ln\left(\frac{U_0}{U_1}\right) + i\theta_2 = \frac{K_1\sqrt{k_1 k_2}}{2}\left\{\frac{1}{\sqrt{k_1-k_2+1-k_1k_2}}\sin^{-1}\left[\frac{(2k_1k_2+k_2-k_1)+(k_2-k_1-2)(k_2)}{(1-k_2)(k_2+k_1)}\right]\right.$$

$$\left. - \frac{1}{\sqrt{k_2-k_1+1-k_1k_2}}\sin^{-1}\left[\frac{(2k_1k_2+k_1-k_2)+(k_2-k_1+2)(k_2)}{(1+k_2)(k_2+k_1)}\right]\right\} + K_2$$

$$\ln\left(\frac{U_0}{U_1}\right) + i\theta_2 = \frac{K_1\sqrt{k_1 k_2}}{2}\left\{\frac{1}{\sqrt{k_1-k_2+1-k_1k_2}}\sin^{-1}(-1) - \frac{1}{\sqrt{k_2-k_1+1-k_1k_2}}\sin^{-1}(1)\right\} + K_2$$

$$\ln\left(\frac{U_0}{U_1}\right) + i\theta_2 = \frac{K_1\sqrt{k_1 k_2}}{2}\left\{-\frac{\pi}{2\sqrt{k_1-k_2+1-k_1k_2}} - \frac{\pi}{2\sqrt{k_2-k_1+1-k_1k_2}}\right\} + K_2 \qquad \text{(II.31)}$$

Subtracting equation (II.31) from equation (II.30):

$$i\,(\theta_1 - \theta_2) = \frac{K_1\sqrt{k_1 k_2}}{2}\left\{\frac{\pi}{\sqrt{1+k_1-k_2-k_1k_2}} + \frac{\pi}{\sqrt{1+k_2-k_1-k_1k_2}}\right\}$$

$$\frac{K_1\sqrt{k_1 k_2}}{2} = i\left(\frac{\theta_1\ \theta_2}{\pi}\right)\left(\frac{\sqrt{1-(k_1^2+k_2^2)+k_1^2k_2^2}}{\sqrt{1+k_1-k_2-k_1k_2}+\sqrt{1+k_2-k_1-k_1k_2}}\right)$$

$$K_2 = \ln\left(\frac{U_0}{U_1}\right) + i\,\theta_1 - i\left(\frac{\theta_1-\theta_2}{\pi}\right)\left\{\frac{\sqrt{1-(k_1^2+k_2^2)+k_1^2k_2^2}}{\sqrt{1+k_1-k_2-k_1k_2}+\sqrt{1+k_2-k_1-k_1k_2}}\right\}\left[\frac{\pi}{2\sqrt{1+k_1-k_2-k_1k_2}} + \frac{\pi}{2\sqrt{1+k_2-k_1-k_2k_1}}\right]$$

$$K_2 = \ln\left(\frac{U_0}{U_1}\right) + i\left(\frac{\theta_1+\theta_2}{2}\right)$$

$$\therefore\ Q = i\left(\frac{\theta_1-\theta_2}{\pi}\right)\left(\frac{\sqrt{1-(k_1^2+k_2^2)+k_1^2k_2^2}}{\sqrt{1+k_1-k_2-k_1k_2}+\sqrt{1+k_2-k_1-k_2k_1}}\right)\left\{\frac{1}{\sqrt{1+k_1-k_2-k_1k_2}}\sin^{-1}\left[\frac{(2k_1k_2+k_2-k_1)+(k_2-k_1-2)w}{(1-w)(k_2+k_1)}\right]\right.$$

$$\left. - \frac{1}{\sqrt{1+k_2-k_1-k_1k_2}}\sin^{-1}\left[\frac{(2k_1k_2+k_1-k_2)+(k_2-k_1+2)w}{(1+w)(k_2+k_1)}\right]\right\} + \ln\left(\frac{U_0}{U_1}\right) + i\left(\frac{\theta_1+\theta_2}{2}\right) \qquad \text{(II.32)}$$

let $A = \sqrt{1+k_1-k_2-k_1k_2}$ $\qquad B = \sqrt{1+k_2-k_1-k_1k_2}$

$$Q = i\left(\frac{\theta_1-\theta_2}{\pi}\right)\left(\frac{AB}{A+B}\right)\left\{\frac{1}{A}\sin^{-1}\left[\frac{(2k_1k_2+k_2-k_1)+(k_2-k_1-2)w}{(1-w)(k_2+k_1)}\right]\right.$$

$$\left. - \frac{1}{B}\sin^{-1}\left[\frac{(2k_1k_2+k_1-k_2)+(k_2-k_1+2)w}{(1+w)(k_2+k_1)}\right]\right\} + \ln\left(\frac{U_0}{U_1}\right) + i\left(\frac{\theta_1+\theta_2}{2}\right) \qquad \text{(II.33)}$$

2.3 DETERMINATION OF GEOMETRY IN REAL PLANE:

As before:

$$X\Big/_{X_1}^{X_2} = \int_{\phi_1}^{\phi_2} \frac{\cos\theta}{q}\,d\phi \qquad \text{(II.16)}$$

$$Y\Big/_{Y_1}^{Y_2} = \int_{\phi_1}^{\phi_2} \frac{\sin\theta}{q}\,d\phi \qquad \text{(II.17)}$$

2.3.1 ALONG STREAMLINE CD

$$Q = \ln\left(\frac{U_1}{U_0}\right) + i\,\theta_{CD}$$

Evaluating equation (II.33) along CD:

$$\ln\left(\frac{U_1}{U_0}\right) + i\theta_{CD} = i\left(\frac{\theta_1-\theta_2}{\pi}\right)\left(\frac{AB}{A+B}\right)\left\{\frac{1}{A}\sin^{-1}\left[\frac{(2k_1k_2+k_2-k_1)+(k_2-k_1-2)\phi_{CD}}{(1-\phi_{CD})(k_2+k_1)}\right]\right.$$

$$\left.-\frac{1}{B}\sin^{-1}\left[\frac{(2k_1k_2+k_1-k_2)+(k_2-k_1+2)\phi_{CD}}{(1+\phi_{CD})(k_2+k_1)}\right]\right\} + \ln\left(\frac{V_0}{V_1}\right) + i\left(\frac{\theta_1+\theta_2}{2}\right) \qquad \text{(II.34)}$$

$$\theta_{CD} = \left(\frac{\theta_1-\theta_2}{\pi}\right)\left(\frac{AB}{A+B}\right)\left\{\frac{1}{A}\sin^{-1}\left[\frac{(2k_1k_2+k_2-k_1)+(k_2-k_1-2)\phi_{CD}}{(1-\phi_{CD})(k_2+k_1)}\right]\right.$$

$$\left.-\frac{1}{B}\sin^{-1}\left[\frac{(2k_1k_2+k_1-k_2)+(k_2-k_1+2)\phi_{CD}}{(1+\phi_{CD})(k_2+k_1)}\right]\right\} + \left(\frac{\theta_1+\theta_2}{2}\right) \qquad \text{(II.35)}$$

2.3.1.1 Check

At C $\theta_{CD} = \theta_1$ $\phi = -k_1$

Substituting into equation (II.33):

$$\theta_1 = \left(\frac{\theta_1 - \theta_2}{\pi}\right)\left(\frac{AB}{A+B}\right)\left\{\frac{1}{A}\sin^{-1}\left[\frac{(2k_1k_2+k_2-k_1)+(k_2-k_1-2)(-k_1)}{(1+k_1)(k_2+k_1)}\right]\right.$$

$$\left.-\frac{1}{B}\sin^{-1}\left[\frac{(2k_1k_2+k_1-k_2)+(k_2-k_1+2)(-k_1)}{(1-k_1)(k_2+k_1)}\right]\right\} + \left(\frac{\theta_1+\theta_2}{2}\right)$$

$$\theta_1 = \left(\frac{\theta_1 - \theta_2}{\pi}\right)\left(\frac{AB}{A+B}\right)\left\{\frac{1}{A}\sin^{-1}(1) - \frac{1}{B}\sin^{-1}(-1)\right\} + \left(\frac{\theta_1+\theta_2}{2}\right)$$

$$= \left(\frac{\theta_1 - \theta_2}{\pi}\right)\left(\frac{AB}{A+B}\right)\left(\frac{\pi}{2A}+\frac{\pi}{2B}\right) + \left(\frac{\theta_1+\theta_2}{2}\right) = \left(\frac{\theta_1 - \theta_2}{\pi}\right)\left(\frac{\pi}{2}\right) + \left(\frac{\theta_1+\theta_2}{2}\right)$$

$$\theta_i = \theta_i$$

at D $\theta_{CD} = \theta_2$ $\phi = k_2$

$$\theta_2 = \left(\frac{\theta_1 - \theta_2}{\pi}\right)\left(\frac{AB}{A+B}\right)\left\{\frac{1}{A}\sin^{-1}\left[\frac{(2k_1k_2+k_2-k_1)+(k_2-k_1-2)(k_2)}{(1-k_2)(k_2+k_1)}\right]\right.$$

$$\left.-\frac{1}{B}\sin^{-1}\left[\frac{(2k_1k_2+k_1-k_2)+(k_2-k_1+2)(k_2)}{(1+k_2)(k_2+k_1)}\right]\right\} + \left(\frac{\theta_1+\theta_2}{2}\right)$$

$$\theta_2 = \left(\frac{\theta_1 - \theta_2}{\pi}\right)\left(\frac{AB}{A+B}\right)\left\{\frac{1}{A}\sin^{-1}(-1) - \frac{1}{B}\sin^{-1}(1)\right\} + \left(\frac{\theta_1+\theta_2}{2}\right)$$

$$\theta_2 = \left(\frac{\theta_1 - \theta_2}{\pi}\right)\left(\frac{AB}{A+B}\right)\left\{-\frac{\pi}{2A} - \frac{\pi}{2B}\right\} + \left(\frac{\theta_1+\theta_2}{2}\right)$$

$$= \left(\frac{\theta_2 - \theta_1}{2}\right) + \left(\frac{\theta_1+\theta_2}{2}\right) = \theta_2$$

2.3.2 ALONG STREAMLINE DE

Evaluating equation (II.33) along DE:

$$\ln\left(\frac{U_0}{g_{DE}}\right) + i\theta_2 = i\left(\frac{\theta_1-\theta_2}{\pi}\right)\left(\frac{AB}{A+B}\right)\left\{\frac{1}{A}\sin\left[\frac{(2k_1k_2+k_2-k_1)+(k_2-k_1-2)\phi_{DE}}{(1-\phi_{DE})(k_2+k_1)}\right]\right.$$

$$\left.-\frac{1}{B}\sin^{-1}\left[\frac{(2k_1k_2+k_1-k_2)+(k_2-k_1+2)\phi_{DE}}{(1+\phi_{DE})(k_2+k_1)}\right]\right\} + \ln\left(\frac{U_0}{U_1}\right) + i\left(\frac{\theta_1+\theta_2}{2}\right) \quad \text{(II.36)}$$

$$\ln\left(\frac{U_0}{g_{DE}}\right) + i\theta_2 = i\left(\frac{\theta_1-\theta_2}{\pi}\right)\left(\frac{AB}{A+B}\right)\left\{-\frac{1}{A}\sin^{-1}(-Z_1) - \frac{1}{B}\sin^{-1}Z_2\right\} + \ln\left(\frac{U_0}{U_1}\right) + i\left(\frac{\theta_1+\theta_2}{2}\right)$$

using relation $\sin^{-1}Z = \frac{\pi}{2} - \cos^{-1}Z$

$$\ln\left(\frac{U_0}{g_{DE}}\right) + i\theta_2 = i\left(\frac{\theta_1-\theta_2}{\pi}\right)\left(\frac{AB}{A+B}\right)\left\{-\frac{\pi}{2A} - \frac{\pi}{2B} + \frac{1}{A}\cos^{-1}(-Z_1) + \frac{1}{B}\cos^{-1}(Z_2)\right\} + \ln\left(\frac{U_0}{U_1}\right) + i\left(\frac{\theta_1+\theta_2}{2}\right)$$

$$\ln\left(\frac{U_0}{g_{DE}}\right) + i\theta_2 = i\left(\frac{\theta_2-\theta_1}{\pi}\right) + i\left(\frac{\theta_1-\theta_2}{\pi}\right)\left(\frac{AB}{A+B}\right)\left\{\frac{1}{A}\cos^{-1}(-Z_1) + \frac{1}{B}\cos^{-1}(Z_2)\right\} + \ln\left(\frac{U_0}{U_1}\right) + i\left(\frac{\theta_1+\theta_2}{2}\right)$$

$$\ln\left(\frac{U_1}{g_{DE}}\right) = i\left(\frac{\theta-\theta_2}{\pi}\right)\left(\frac{AB}{A+B}\right)\left\{\frac{1}{A}\cos^{-1}(-Z_1) + \frac{1}{B}\cos^{-1}(Z_2)\right\}$$

using relation $\cos^{-1}Z = -i\ln\left(Z+\sqrt{Z^2-1}\right)$ let $Z_3 = -Z_1$

$$\ln\left(\frac{U_1}{g_{DE}}\right) = i\left(\frac{\theta_1-\theta_2}{\pi}\right)\left(\frac{AB}{A+B}\right)\left\{-\frac{i}{A}\ln\left(Z_3+\sqrt{Z_3^2-1}\right) - \frac{i}{B}\ln\left(Z_2+\sqrt{Z_2^2-1}\right)\right\}$$

$$\ln\left(\frac{U_1}{g_{DE}}\right) = \left(\frac{\theta_1-\theta_2}{\pi}\right)\left(\frac{AB}{A+B}\right)\left\{\frac{1}{A}\ln\left(Z_3+\sqrt{Z_3^2-1}\right) + \frac{1}{B}\ln\left(Z_2+\sqrt{Z_2^2-1}\right)\right\}$$

$$\frac{U_{1_1}}{q_{DE}} = \left\{ \left(Z_3 + \sqrt{Z_3^2 - 1} \right)^{\frac{B}{A+B}} \left(Z_2 + \sqrt{Z_2^2 - 1} \right)^{\frac{A}{A+B}} \right\}^{\frac{\theta_1 - \theta_2}{\pi}} \qquad \text{(II.37)}$$

$$Z_3 = -Z_1 = \frac{(2 + k_1 - k_2)\phi_{DE} + (k_1 - k_2 - 2k_1 \ k_2)}{(1 - \phi_{DE})\ (k_2 + k_1} \qquad \text{(II.38)}$$

$$Z_2 = \frac{(2 + k_2 - k_1)\phi_{DE} + (k_1 - k_2 + 2k_1 \ k_2)}{(1 + \phi_{DE})(k_2 + k_1)} \qquad \text{(II.39)}$$

2.3.2.1 Check

At point D $\phi = k_2$

$$Z_3 = \frac{2k_2 + k_1 \ k_2 - k_2^2 + k_1 - k_2 - 2k_1 \ k_2}{k_2 + k_1 - k_2^2 - k_1 k_2} = 1$$

$$Z_2 = \frac{2\ k_2 + k_2^2 - k_1 k_2 + k_1 - k_2 + 2k_1 \ k_2}{k_2 + k_1 + k_2^2 + k_1 k_2} = 1$$

$$\frac{U_1}{q_{DE}} = 1 \qquad\qquad q_{DE} = U_1$$

At point E $\phi = 1$

$$Z_3 = \frac{2 + k_1 - k_2 + k_1 - k_2 - 2k_1k_2}{0} = \frac{2 - 2k_1k_2}{0} = \infty$$

$$Z_2 = \frac{2 + k_2 - k_1 + k_1 - k_2 - 2k_1k_2}{2k_2 + 2k_1} = \frac{2 - 2k_1k_2}{2k_1 + 2k_2} = \frac{1 + k_1k_2}{k_1 + k_2} = F$$

$$\frac{U}{q_{DE}} = (\infty) \quad \therefore \quad q_{DE} = 0$$

2.4 DETERMINATION OF GEOMETRICAL REALTIONSHIPS

$$h_0 = \frac{\sin\theta_2}{U_1}\int_1^{k_2}\left\{\left(Z_3 + \sqrt{Z_3^2 - 1}\right)^{\frac{B}{A+B}}\left(Z_2 + \sqrt{Z_2^2 - 1}\right)^{\frac{A}{A+B}}\right\}^{\frac{\theta_1 - \theta_2}{\pi}} d\phi \qquad \text{(II.40)}$$

$$x\Big/_0^{\ell} = \frac{1}{U_1}\int_{-k_1}^{k_2} \cos\ \theta_{CD}\ d\phi \qquad \text{(II.41)}$$

$$y\Big/_h^{h_0} = \frac{1}{U_1}\int_{\alpha k_1}^{k_2} \sin\ \theta_{CD}\ d\phi \qquad \text{(II.42)}$$

where

$$\theta_{CD} = \left(\frac{\theta_1 - \theta_2}{\pi}\right)\left(\frac{AB}{A+B}\right)\left\{\frac{1}{A}\sin^{-1}\left[\frac{(2k_1k_2 + k_2 - k_1) + (k_2 - k_1 - 2)\phi_{CD}}{(1 - \phi_{CD})(k_2 + k_1)}\right]\right.$$

$$\left. - \frac{1}{B}\sin^{-1}\left[\frac{(2k_1k_2 + k_1 - k_2) + (k_2 - k_1 + 2)\phi_{CD}}{(1 + \phi_{CD})(k_2 + k_1)}\right]\right\} + \left(\frac{\theta_1 + \theta_2}{2}\right) \qquad \text{(II.35)}$$

2.4 EVALUATION OF CONSTANT k

At point A' $W = \infty$ $Q = \ln\left(\frac{U_o}{U_o}\right) = 0$

$$-\ln\left(\frac{U_o}{U_1}\right) = i\left(\frac{\theta_1+\theta_2}{2}\right) + i\left(\frac{\theta_1-\theta_2}{\pi}\right)\left(\frac{AB}{A+B}\right)\left\{\frac{1}{A}\sin^{-1}\left(\frac{2+k_1-k_2}{k_2+k_1}\right) - \frac{1}{B}\sin^{-1}\left(\frac{2+k_2-k_1}{k_2+k_1}\right)\right\} \tag{II.43}$$

$$-\ln\left(\frac{U_o}{U_1}\right) = i\left(\frac{\theta_1+\theta_2}{2}\right) + i\left(\frac{\theta_1-\theta_2}{\pi}\right)\left(\frac{AB}{A+B}\right)\left\{\frac{\pi}{2A} - \frac{1}{A}\cos^{-1}\left(\frac{2+k_1-k_2}{k_2+k_1}\right) - \frac{\pi}{2B} + \frac{1}{B}\cos^{-1}\left(\frac{2+k_2-k_1}{k_1+k_2}\right)\right\}$$

$$-\ln\left(\frac{U_o}{U_1}\right) = i\left(\frac{\theta_1+\theta_2}{2}\right) + i\left(\frac{\theta_1-\theta_2}{2}\right)\left(\frac{B-A}{B+A}\right) + i\left(\frac{\theta_1-\theta_2}{\pi}\right)\left(\frac{AB}{A+B}\right)\left\{\frac{1}{B}\cos^{-1}\left(\frac{2+k_2-k_1}{k_1+k_2}\right) - \frac{1}{A}\cos^{-1}\left(\frac{2+k_1-k_2}{k_2+k_1}\right)\right\}$$

$$-\ln\left(\frac{U_o}{U_1}\right) = i\left(\frac{\theta_1+\theta_2}{2}\right) + i\left(\frac{\theta_1-\theta_2}{2}\right)\left(\frac{B-A}{B+A}\right) + i\left(\frac{\theta_1-\theta_2}{\pi}\right)\left(\frac{AB}{A-B}\right)\left\{-\frac{i}{B}\ln\left(Y_2+\sqrt{Y_2^2-1}\right) + \frac{i}{A}\ln\left(Y_1+\sqrt{Y_1^2-1}\right)\right\}$$

$$Y_1 = \frac{2+k_1-k_2}{k_1+k_2} \qquad \sqrt{Y_1^2-1} = \frac{2}{k_1+k_2}\sqrt{1+k_1-k_2-k_1k_2}$$

$$Y_2 = \frac{2+k_2-k_1}{k_1+k_2} \qquad \sqrt{Y_2^2-1} = \frac{2}{k_1+k_2}\sqrt{1+k_2-k_1-k_1k_2}$$

$$-\ln\left(\frac{U_0}{U_1}\right) + \ln\left(e^{i\left(\frac{\theta_1-\theta_2}{2}\;\frac{B-A}{B+A}\right)}\right) = -\ln\left(e^{i\left(\frac{-\theta_2-\theta_1}{2}\right)}\right) - \left\{\frac{1}{A}\ln\left(\frac{2+k_1-k_2+2\sqrt{1+k_1-k_2-k_1k_2}}{k_1+k_2}\right)\right.$$

$$\left. -\frac{1}{B}\ln\left(\frac{2+k_2-k_1+2\sqrt{1+k_2-k_1-k_1k_2}}{k_1+k_2}\right)\right\}\left(\frac{\theta_1-\theta_2}{\pi}\right)\left(\frac{AB}{A+B}\right)$$

$$\ln\left(\frac{U_0}{U_1}\right) + \ln\left(e^{i\left(\frac{\theta_1-\theta_2}{2}\right)\left(\frac{B-A}{B+A}\right)}\right) = \ln\left(e^{i\left(\frac{-\theta_2-\theta_1}{2}\right)}\right) + \ln\left\{\frac{X_1^{1/A}}{X_2^{1/B}}\right\}^{\left(\frac{\theta_1-\theta_2}{\pi}\right)\left(\frac{AB}{A+B}\right)}$$

$$\frac{U_0}{U_1}\, e^{i\left(\frac{\theta_1-\theta_2}{2}\right)\left(\frac{B-A}{B+A}\right)} = e^{i\left(\frac{-\theta_2-\theta_1}{2}\right)}\left\{\frac{X_1^{1/A}}{X_2^{1/B}}\right\}^{\left(\frac{\theta_1-\theta_2}{\pi}\right)\left(\frac{AB}{A+B}\right)}$$

$$\frac{U_0}{U_1}\left\{\cos\left[\left(\frac{\theta_1-\theta_2}{2}\right)\left(\frac{B-A}{B+A}\right)\right] + i\sin\left[\left(\frac{\theta_1-\theta_2}{2}\right)\left(\frac{B-A}{B+A}\right)\right]\right\} = \left\{\frac{X_1^{1/A}}{X_2^{1/B}}\right\}^{\left(\frac{\theta_1-\theta_2}{\pi}\right)\left(\frac{AB}{A+B}\right)}$$

$$\left\{\cos\left(\frac{-\theta_2-\theta_1}{2}\right) + i\sin\left(\frac{-\theta_2-\theta_1}{2}\right)\right\}$$

equating real parts:

$$\frac{U_0}{U_1}\cos\left\{\left(\frac{\theta_1-\theta_2}{2}\right)\left(\frac{B-A}{B+A}\right)\right\} = \left\{\frac{X_1^{1/A}}{X_2^{1/B}}\right\}^{\left(\frac{\theta_1-\theta_2}{\pi}\right)\left(\frac{AB}{A+B}\right)}\cos\left(\frac{-\theta_2-\theta_1}{2}\right)$$

$$\frac{U_0}{U_1} = \left\{\frac{X_1^{1/A}}{X_2^{1/B}}\right\}^{\left(\frac{\theta_1-\theta_2}{\pi}\right)\left(\frac{AB}{A+B}\right)} \frac{\cos\left(\frac{-\theta_2-\theta_1}{2}\right)}{\cos\left\{\left(\frac{\theta_1-\theta_2}{\pi}\right)\left(\frac{B-A}{B+A}\right)\right\}}$$

$$\frac{U_o}{U_1} = \left\{ \frac{X_1^{1/A}}{X_2^{1/B}} \right\}^{\left(\frac{\theta_1-\theta_2}{\pi}\right)\left(\frac{AB}{A+B}\right)} \frac{\cos\left(\frac{-\theta_2-\theta_1}{2}\right)}{\cos\left\{\left(\frac{\theta_1-\theta_2}{\pi}\right)\left(\frac{B-A}{B+A}\right)\right\}} \qquad \text{(II.44)}$$

where $B = \sqrt{1+k_2-k_1-k_1k_2}$

$A = \sqrt{1+k_1-k_2-k_1k_2}$

$$X_1 = \frac{2+k_1-k_2+2\sqrt{1+k_1-k_2-k_1k_2}}{k_1+k_2}$$

$$X_2 = \frac{2+k_2-k_1+2\sqrt{1+k_2-k_1-k_1k_2}}{k_1+k_2}$$

3/ FREE-STREAMLINE SOLUTION FOR FLOW OVER BASE WITH NEGATIVE ANGULARITY

3.1 SCHWARZ-CHRISTOFFEL TRANSFORMATION

The infinite strip (ABB'CDEE'A') shown in Figure 46 is mapped onto the real axis of the w plane by the Schwarz-Christoffel transformation:

$$dQ = (w+1)^{-1}(w+k_1)^{\frac{1}{2}}(w-k_2)^{-\frac{1}{2}}(w-1)^{-1}\,dw \qquad \text{(II.45)}$$

$$Q = K_1 \int \frac{\sqrt{w+k_1}}{(w+1)(w-1)\sqrt{w-k_2}}\,dw + K_2$$

$$= \frac{K_1}{2}\left\{ \int \frac{\sqrt{w+k_1}\,dw}{(w-1)\sqrt{w-k_2}} - \int \frac{\sqrt{w+k_1}\,dw}{(w+1)\sqrt{w-k_2}} \right\} + K_2$$

let $w - 1 = s$ $\qquad w + 1 = t$

$w = s + 1$ $\qquad w = t - 1$

$$Q = \frac{K_1}{2}\left\{ \int \frac{\sqrt{s+1+k_1}\,ds}{s\sqrt{s+1-k_2}} - \int \frac{\sqrt{t+1-k_1}\,dt}{t\sqrt{t-1-k_2}} \right\} + K_2$$

$$Q = \frac{K_1}{2}\left\{ \ln\left(\frac{\sqrt{s+1+k_1}+\sqrt{s+1-k_2}}{\sqrt{s+1+k_1}-\sqrt{s+1-k_2}}\right) - \sqrt{\frac{1+k_1}{1-k_2}}\,\ln\left(\frac{\sqrt{1-k_2}\sqrt{s+1+k_1}+\sqrt{1+k_1}\sqrt{s+1-k_2}}{\sqrt{1-k_2}\sqrt{s+1+k_1}-\sqrt{1+k_1}\sqrt{s+1-k_2}}\right)\right.$$

$$\left. -\ln\left(\frac{\sqrt{t+k_1-1}+\sqrt{t-1-k_2}}{\sqrt{t+k_1-1}-\sqrt{t-1-k_2}}\right) + \sqrt{\frac{1-k_1}{1+k_2}}\,\ln\left(\frac{\sqrt{-1-k_2}\sqrt{t+k_1-1}+\sqrt{k_1-1}\sqrt{t-1-k_2}}{\sqrt{-1-k_2}\sqrt{t+k_1-1}-\sqrt{k_1-1}\sqrt{t-1-k_2}}\right)\right\} + K_2$$

$$Q = \frac{K_1}{2}\left\{ \ln\left(\frac{\sqrt{w+k_1}+\sqrt{w-k_2}}{\sqrt{w+k_1}-\sqrt{w-k_2}}\right) - \sqrt{\frac{1+k_1}{1-k_2}}\,\ln\left(\frac{\sqrt{1-k_2}\sqrt{w+k_1}+\sqrt{1+k_1}\sqrt{w-k_2}}{\sqrt{1-k_2}\sqrt{w+k_1}-\sqrt{1+k_1}\sqrt{w-k_2}}\right)\right.$$

$$\left. -\ln\left(\frac{\sqrt{w+k_1}+\sqrt{w-k_2}}{\sqrt{w+k_1}-\sqrt{w-k_2}}\right) + \sqrt{\frac{1-k_1}{1+k_2}}\,\ln\left(\frac{\sqrt{1+k_2}\sqrt{w+k_1}+\sqrt{1-k_1}\sqrt{w-k_2}}{\sqrt{1+k_2}\sqrt{w+k_1}-\sqrt{1-k_1}\sqrt{w-k_2}}\right)\right\} + K_2$$

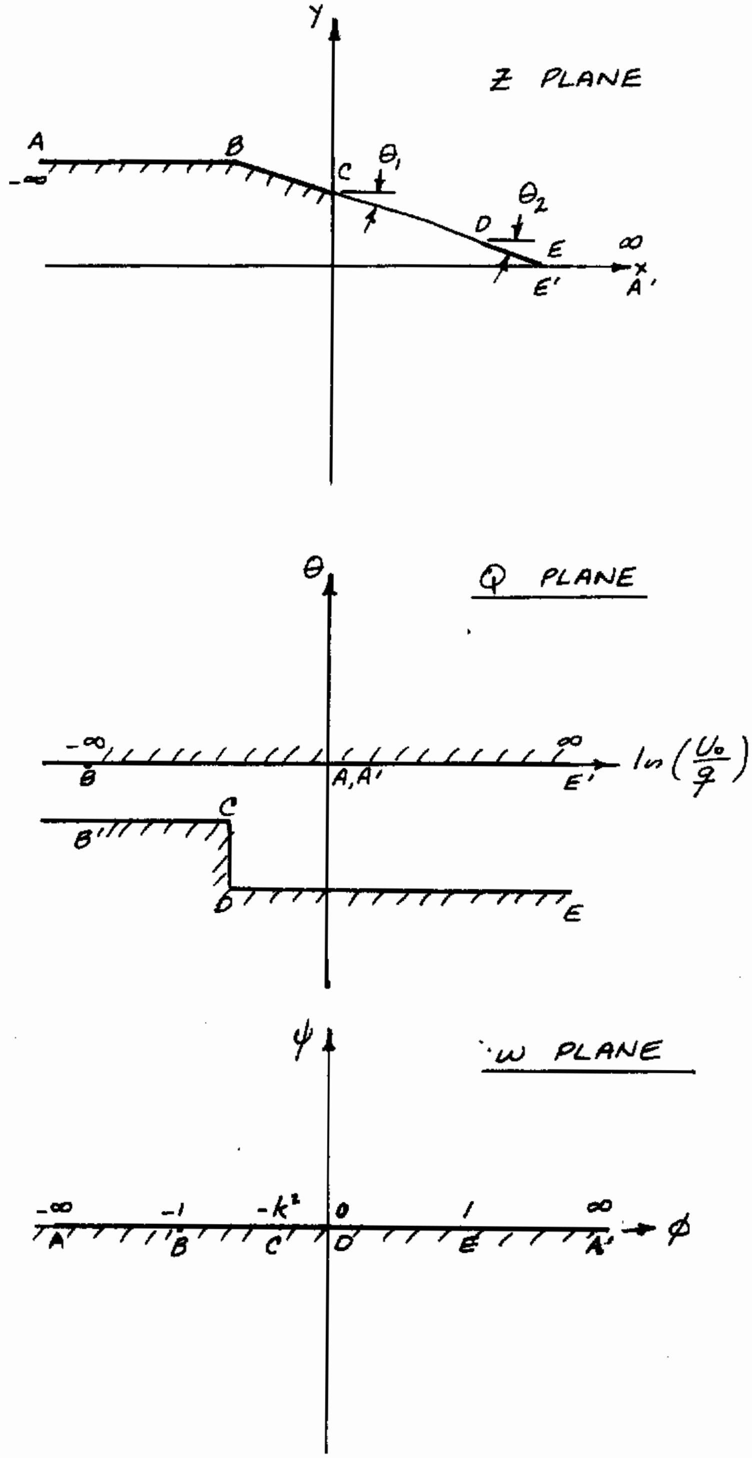

Figure 46. Mapping Planes θ<0

$$Q = \frac{K_1}{2}\left\{\sqrt{\frac{1-k_1}{1+k_2}}\ln\left[L\left(\frac{\sqrt{1+k_2}\sqrt{w+k_1}+\sqrt{1-k_1}\sqrt{w-k_2}}{\sqrt{1+k_2}\sqrt{w+k_1}-\sqrt{1-k_1}\sqrt{w-k_2}}\right)\right]\right.$$

$$\left.-\sqrt{\frac{1+k_1}{1-k_2}}\ln\left[L\left(\frac{\sqrt{1-k_2}\sqrt{w+k_1}+\sqrt{1+k_1}\sqrt{w-k_2}}{\sqrt{1-k_2}\sqrt{w+k_1}-\sqrt{1+k_1}\sqrt{w-k_2}}\right)\right]\right\} \qquad \text{(II.46)}$$

3.2 EVALUATION OF CONSTANTS

3.2.1 At C $W = -k_1$ $\qquad Q = \ln\left(\frac{U_0}{U_1}\right) + i\theta_1$

Equation (II.46) reduces to:

$$\ln\left(\frac{U_0}{U_1}\right)+i\theta_1 = \frac{K_1}{2}\left\{\sqrt{\frac{1-k_1}{1+k_2}}\ln\left[L(-1)\right] - \sqrt{\frac{1+k_1}{1-k_2}}\ln\left[L(-1)\right]\right\}$$

$$= \frac{K_1}{2}\left\{\sqrt{\frac{1-k_1}{1+k_2}}\ln\left[L+i\pi\right] - \sqrt{\frac{1+k_1}{1-k_2}}\ln\left[L+i\pi\right]\right\} \qquad \text{(II.47)}$$

3.2.2 At D $W = k_2$ $\qquad Q = \ln\left(\frac{U_0}{U_1}\right) + i\theta_2$

Equation (II.46) reduces to:

$$\ln\left(\frac{U_0}{U_1}\right)+i\theta_2 = \frac{K_1}{2}\left\{\sqrt{\frac{1-k_1}{1+k_2}}\ln\left[L(1)\right] - \sqrt{\frac{1+k_1}{1-k_2}}\ln\left[L(1)\right]\right\} \qquad \text{(II.48)}$$

subtracting equation (II.48) from equation (II.47):

$$i(\theta_1-\theta_2) = \frac{K_1}{2}\left\{\sqrt{\frac{1-k_1}{1+k_2}} - \sqrt{\frac{1+k_1}{1-k_2}}\right\} i\pi$$

$$\frac{K_1}{2} = \frac{\theta_1-\theta_2}{\pi}\left\{\frac{1}{\sqrt{\frac{1-k_1}{1+k_2}} - \sqrt{\frac{1+k_1}{1-k_2}}}\right\}$$

$$\ln\left(\frac{U_0}{U_1}\right)+i\theta_2 = \frac{\theta_1-\theta_2}{\pi}\ln(L)$$

$$L = \left(\frac{U_0}{U_1}e^{i\theta_2}\right)^{\frac{\pi}{\theta_1-\theta_2}}$$

$$\therefore\ Q = \frac{\theta_1-\theta_2}{\pi}\left\{\frac{1}{K_1-K_2}\right\}\left[K_1 \ \ln\left\{\left(\frac{U_0}{U_1}e^{i\theta_2}\right)^{\frac{\pi}{\theta_1-\theta_2}}\left(\frac{\sqrt{1+k_2}\ \sqrt{w+k_1}+\sqrt{1-k_1}\ \sqrt{w-k_2}}{\sqrt{1+k_2}\ \sqrt{w+k_1}-\sqrt{1-k_2}\ \sqrt{w-k_1}}\right)\right\}\right.$$

$$\left. - K_2\ \ln\left\{\left(\frac{U_0}{U_1}e^{i\theta_2}\right)^{\frac{\pi}{\theta_1-\theta_2}}\left(\frac{\sqrt{1-k_2}\ \sqrt{w+k_1}+\sqrt{1+k_1}\ \sqrt{w-k_2}}{\sqrt{1-k_2}\ \sqrt{w+k_1}-\sqrt{1+k_1}\ \sqrt{w-k_2}}\right)\right\}\right] \qquad \text{(II.49)}$$

where $K_1 = \sqrt{\dfrac{1-k_1}{1+k_2}}$ $\qquad K_2 = \sqrt{\dfrac{1-k_1}{1+k_2}}$

3.3 DETERMINATION OF GEOMETRY IN REAL PLANE

As before:

$$x\Big/_{x_1}^{x_2} = \int_{\phi_1}^{\phi_2}\frac{\cos\theta}{q}\,d\phi \qquad \text{(II.16)}$$

$$y\Big/_{y_1}^{y_2} = \int_{\phi_1}^{\phi_2}\frac{\sin\theta}{q}\,d\phi \qquad \text{(II.17)}$$

3.3.1 ALONG STREAMLINE CD

Evaluating equation (II.49) along CD: $\quad Q = \ln\left(\frac{U_0}{U_1}\right) + i\ \theta_{CD}$

$$\ln\left(\frac{U_0}{U_1}\right) + i\theta_{CD} = \ln\left(\frac{U_0}{U_1}\right) + i\theta_2 + \frac{\theta_1-\theta_2}{\pi}\left(\frac{1}{K_1-K_2}\right)\left(K_1\ \ln\left(\frac{\sqrt{1-k_2}\sqrt{\phi+k_1}+\sqrt{1-k_1}\ \sqrt{\phi-k_2}}{\sqrt{1+k_2}\ \sqrt{\phi+k_1}-\sqrt{1-k_1}\ \sqrt{\phi-k_2}}\right)\right.$$

$$\left. - K_2\ \ln\left(\frac{\sqrt{1-k_2}\ \sqrt{\phi+k_1}+\sqrt{1+k_1}\sqrt{\phi-k_2}}{\sqrt{1-k_2}\ \sqrt{\phi+k_1}-\sqrt{1+k_1}\sqrt{\phi-k_2}}\right)\right) \qquad \text{(II.50)}$$

$$i\theta_{CD} = i\theta_2 + \left(\frac{\theta_1\ \theta_2}{\pi}\right)\left(\frac{1}{K_1-K_2}\right)\left\{K_1\left[\ln\left(\sqrt{1+k_2}\ \sqrt{\phi+k_1}+i\sqrt{1-k_1}\ \sqrt{\overset{-\phi}{\phi+k_2}}\right)\right.\right.$$

$$\left. - \ln\left(\sqrt{1+k_2}\ \sqrt{\phi+k_1}-i\sqrt{1-k_1}\ \sqrt{\overset{-\phi}{\phi+k_2}}\right)\right] - K_2\left[\ln\left(\sqrt{1-k_2}\sqrt{\phi+k_1}+i\sqrt{1+k_1}\ \sqrt{\overset{-\phi}{\phi+k_2}}\right)\right.$$

$$\left.\left. - \ln\left(\sqrt{1-k_2}\ \sqrt{\phi+k_1}-i\ \sqrt{1+k_1}\ \sqrt{\phi+k_2}\right)\right]\right\}$$

$$i\,\theta_{CD} = i\theta_2 + \frac{\theta_1\ \ \theta_2}{\pi}\left(\frac{1}{K_1+K_2}\right)\left\{K_1\left[\ln R_1 + i\tan^{-1}K_1\frac{\sqrt{-\phi+k_2}}{\sqrt{\phi+k_1}} - \ln R_1 + \tan^{-1}K_1\frac{\sqrt{\phi+k_2}}{\sqrt{\phi+k_1}}\right.\right.$$

$$\left.\left. - K_2\left[\ln R_2 + i\tan^{-1}K_2\frac{\sqrt{-\phi+k_2}}{\sqrt{\phi+k_1}} - \ln R_2 + i\tan^{-1}K_2\frac{\sqrt{-\phi+k_2}}{\sqrt{\phi+k_1}}\right]\right\}$$

$$\theta_{CD} = \theta_2 + \left(\frac{\theta_1-\theta_2}{\pi}\right)\left(\frac{2}{K_1-K_2}\right)\left(K_1\tan^{-1}K_1\frac{\sqrt{-\phi+k_2}}{\sqrt{\phi+k_1}} - K_2\tan^{-1}K_2\frac{\sqrt{-\phi+k_2}}{\sqrt{\phi+k_1}}\right) \quad \text{(II.51)}$$

3.3.2 ALONG STREAMLINE DE:

Evaluating equation (II.49) along DE:

$$\ln\left(\frac{U_0}{q_{DE}}\right) + i\theta_2 = \ln\left(\frac{U_0}{U_1}\right) + i\theta_2 + \frac{\theta_1-\theta_2}{\pi}\left(\frac{1}{K_1-K_2}\right)\left(K_1\ln\left(\frac{\sqrt{1+k_2}\sqrt{\phi+k_1}+\sqrt{1-k_1}\sqrt{\phi-k_2}}{\sqrt{1+k_2}\sqrt{\phi+k_1}-\sqrt{1-k_1}\sqrt{\phi-k_2}}\right)\right.$$

$$\left. - K_2\ln\left(\frac{\sqrt{1-k_2}\ \sqrt{\phi+k_1}+\sqrt{1+k_1}\ \sqrt{\phi-k_2}}{\sqrt{1-k_2}\ \sqrt{\phi+k_1}-\sqrt{1+k_1}\ \sqrt{\phi-k_2}}\right)\right) \quad \text{(II.52)}$$

$$\frac{U_1}{q_{DE}} = \left[\left(\frac{\sqrt{1+k_2}\ \sqrt{\phi+k_1}+\sqrt{1-k_1}\ \sqrt{\phi-k_2}}{\sqrt{1+k_2}\ \sqrt{\phi+k_1}-\sqrt{1-k_1}\ \sqrt{\phi-k_2}}\right)^{K_1}\left(\frac{\sqrt{1-k_2}\ \sqrt{\phi+k_1}-\sqrt{1+k_1}\ \sqrt{\phi-k_2}}{\sqrt{1-k_2}\ \sqrt{\phi+k_1}+\sqrt{1+k_1}\ \sqrt{\phi-k_2}}\right)^{K_2}\right]^{\frac{\theta_1-\theta_2}{\pi}\left(\frac{1}{K_1-K_2}\right)}$$

(II.53)

3.4 DETERMINATION OF GEOMETRICAL RELATIONSHIPS

Evaluating equations (II.16) and (II.17) using equations (II.53) and (II.51) yields:

$$h_0 = \frac{\sin\theta_2}{U_1}\int_0^{\infty}\left[\left(\frac{\sqrt{1+k_2}\sqrt{\phi+k_1}+\sqrt{1-k_1}\sqrt{\phi-k_2}}{\sqrt{1+k_2}\sqrt{\phi+k_1}-\sqrt{1-k_1}\sqrt{\phi-k_2}}\right)^{K_1}\left(\frac{\sqrt{1-k_2}\sqrt{\phi+k_1}-\sqrt{1+k_1}\sqrt{\phi-k_2}}{\sqrt{1-k_2}\sqrt{\phi+k_1}+\sqrt{1+k_1}\sqrt{\phi-k_2}}\right)^{K_2}\right]^{\frac{\theta_1-\theta_2}{\pi}\left(\frac{1}{K_1-K_2}\right)} d\phi \tag{II.54}$$

$$x\Big/_0^{\ell} = \frac{1}{U_1}\int_{-k^2}^{0}\cos\theta_{CD}\,d\phi \tag{II.55}$$

$$Y\Big/_h^{h_0} = \frac{1}{U_1}\int_{-k^2}^{0}\sin\theta_{CD}\,d\phi \tag{II.56}$$

where

$$\theta_{CD} = \theta_2 + \frac{\theta_1-\theta_2}{\pi}\left(\frac{2}{K_1-K_2}\right)\left(K_1\tan^{-1}K_1\frac{\sqrt{-\phi+k_2}}{\sqrt{\phi+k_1}} - K_2\tan^{-1}K_2\frac{\sqrt{-\phi+k_2}}{\sqrt{\phi+k_1}}\right) \tag{II.51}$$

3.5 EVALUATION OF CONSTANTS k_1 & k_2

Evaluating equation (II.49):

$$0 = \ln\left(\frac{U_0}{U_1}\right) + i\theta_2 + \frac{\theta_1-\theta_2}{\pi}\left(\frac{1}{K_1-K_2}\right)\left(K_1\ln\left(\frac{\sqrt{1+k_2}+\sqrt{1-k_1}}{\sqrt{1+k_2}-\sqrt{1-k_1}}\right) - K_2\ln\left(\frac{\sqrt{1-k_2}+\sqrt{1+k_1}}{\sqrt{1-k_2}-\sqrt{1+k_1}}\right)\right)$$

$$\left(\frac{U_0}{U_1}e^{i\theta_2}\right)^{\frac{\pi}{\theta_1-\theta_2}} = \left[\left(\frac{\sqrt{1+k_2}+\sqrt{1-k_1}}{\sqrt{1+k_2}-\sqrt{1-k_1}}\right)^{K_1}\left(\frac{\sqrt{1-k_2}-\sqrt{1+k_1}}{\sqrt{1-k_2}+\sqrt{1+k_1}}\right)^{K_2}\right]^{\frac{1}{K_2-K_1}}$$

$$\text{since } \sqrt{1-k_2}-\sqrt{1+k_1} < 0$$

$$\left(\sqrt{1-k_2}-\sqrt{1+k_1}\right)^{\frac{K_2}{K_2-K_1}} = \left(\sqrt{1+k_1}-\sqrt{1-k_2}\right)^{\frac{K_2}{K_2-K_1}}\left\{\cos\frac{\pi K_2}{K_2-K_1} + i\sin\frac{\pi K_2}{K_2-K_1}\right\}$$

equating real parts

$$\left(\frac{U_0}{U_1}\right)^{\frac{\pi}{\theta_1-\theta_2}}\cos\left(\frac{\pi\theta_2}{\theta_1-\theta_2}\right) = \left[\left(\frac{\sqrt{1+k_2}+\sqrt{1-k_1}}{\sqrt{1+k_2}-\sqrt{1-k_1}}\right)^{K_1}\left(\frac{\sqrt{1+k_1}-\sqrt{1-k_2}}{\sqrt{1+k_1}+\sqrt{1-k_2}}\right)^{K_2}\right]^{\frac{1}{K_2-K_1}}\cos\frac{\pi K_2}{K_2-K_1}$$

(II.57)

APPENDIX III - GENERALIZED PREDICTION DIGITAL COMPUTER PROGRAM

III. 1. Flow Diagram. A simplified flow diagram is presented in Figure 47. This diagram shows the major steps in computing the predicted base pressure coefficients and the program options.

III. 2. Program Listing. Table III shows the complete listing of the digital program for prediction of base pressures. The program is written in Fortran II.

III. 3. Input Format. Table IV presents the input nomenclature required for program operation. Input format for each program option is presented in Figure 48.

III. 4. Sample Output. Figures 49 and 50 present a sample output for each of the program options.

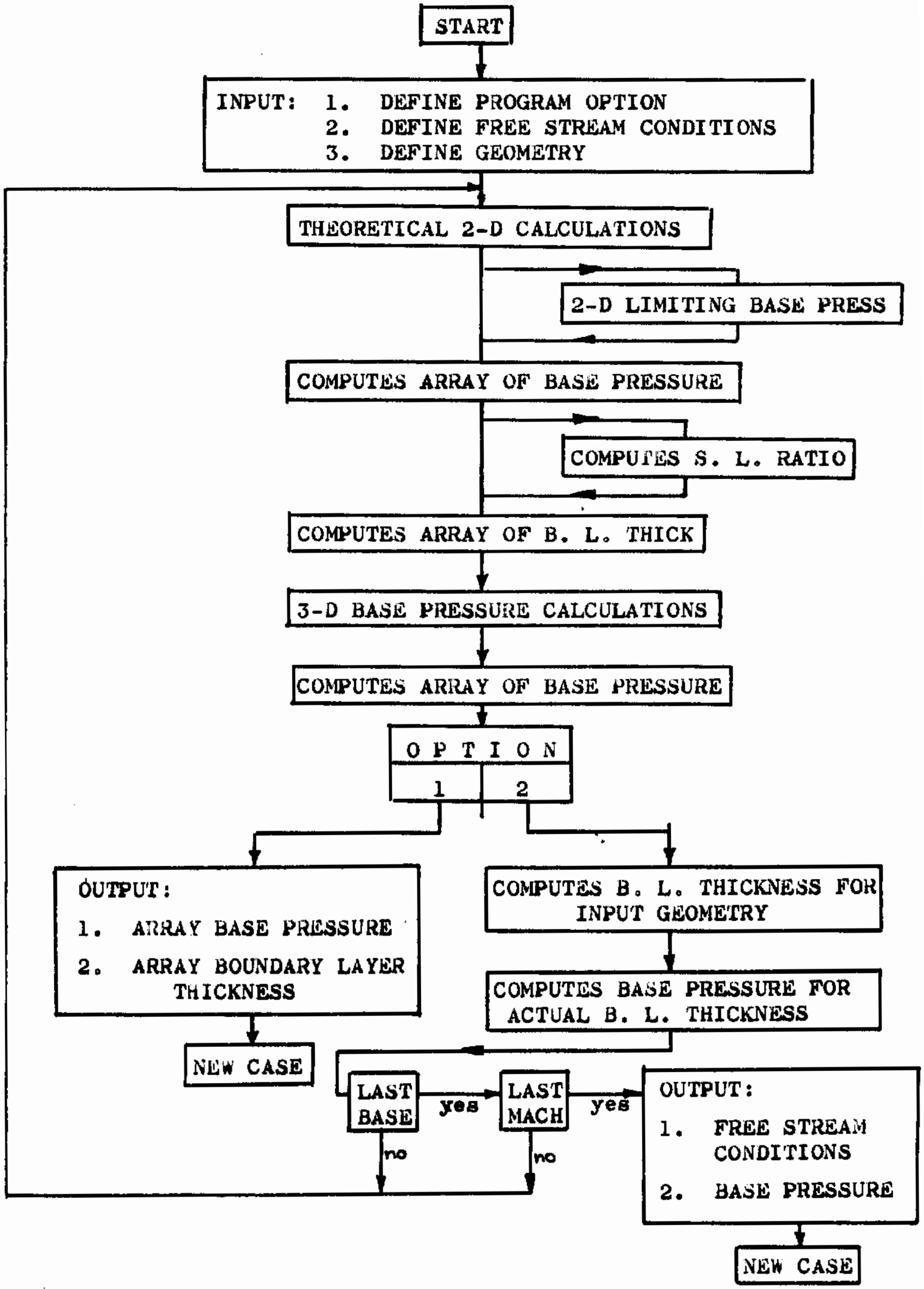

FIGURE 47 Flow Diagram for Generalized Prediction Computer Program.

TABLE III

Generalized Prediction Digital Computer Program Listing

```
*       FORTRAN

C       NOPP=1  COMPUTES ARRAY OF BASE PRESSURE AND BOUNDARY LAYER THICK
C       COMPLETE INPUT MUST BE READ IN FOR EACH CASE CONSIDERED
C       WHEN USING NOPP=1  NBASE AND NATMOS MUST BE = 1
C       NOPP=2  COMPUTES BASE PRESSURE FOR A PARTICULAR CONFIGURATION
C       AT ANY FREE STREAM CONDITION
C       NBASE IS NUMBER OF PARTS OF BASE
C       NATMOS IS NUMBER OF FREE STREAM CONDITIONS CONSIDERED
        DIMENSION AMACH(25),PRES(25),GEPRAM(25),THETD(25),AMU(25),RHO(25)
        DIMENSION CPRAT2(25),BLTHK(25),CPB(25),MCNT(25),XMAC(25)
        DIMENSION EFFHI(25),CPBA(25),SBASE(25),CONFIG(12)
   10   READ INPUT TAPE 5 (160) CONFIG
        READ INPUT TAPE 5 (170) NOPP,NBASE,NATMOS
        GO TO (20,30), NOPP
   20   I=1
        K=1
        READ INPUT TAPE 5 (180) AMACH(I),PRES(I),GEPRAM(K),THETD(K)
        GO TO 60
   30   DO 40 I=1,NATMOS
   40   READ INPUT TAPE 5 (180) AMACH(I),PRES(I),AMU(I),RHO(I)
        DO 50 K=1,NBASE
   50   READ INPUT TAPE 5 (180) GEPRAM(K),THETD(K),XMAC(K),EFFHI(K),SBASE(
       1K)
   60   DO 100 I=1,NATMOS
        CPBA(I)=0.0
        DO 90 K=1,NBASE
        THETR=.0174533*THETD(K)
        CALL THCPB2(AMACH(I),PRES(I),THETD(K),CPRAT2,BLTHK,CPBL2,MCNT)
        CPRAT=-.22024/(GEPRAM(K)-.8038)+1.4286+.10415*GEPRAM(K)
        CPBLZ=CPRAT*CPBL2
        CPBLE=CPBLZ-THETR
        CPB(1)=CPBLE
        BLTHK(1)=0.0
        CPRAT2(1)=1.0
        DO 70 J=2,11
        CPB(J)=CPBLE*CPRAT2(J)
   70   CONTINUE
        GO TO (90,80), NOPP
   80   CALL BLTHKA(AMACH(I),XMAC(K),AMU(I),RHO(I),PRES(I),EFFHI(K),ABLTHK
       1)
        CALL INTPOL(BLTHK,CPB,ABLTHK,CPBDEL,MCHK)
        CPBPAR=CPBDEL*SBASE(K)
        CPBA(I)=CPBA(I)+CPBPAR
   90   CONTINUE
  100   CONTINUE
        GO TO (110,130), NOPP
  110   WRITE OUTPUT TAPE 6 (190)
        WRITE OUTPUT TAPE 6 (200) CONFIG
        WRITE OUTPUT TAPE 6 (210) AMACK(1),PRES(1)
        WRITE OUTPUT TAPE 6 (220) THETD(1),GEPRAM(1)
        WRITE OUTPUT TAPE 6 (230)
        DO 120 J=1,11
  120   WRITE OUTPUT TAPE 6 (240) BLTHK(J),CPB(J)
        GO TO 10
  130   WRITE OUTPUT TAPE 6 (190)
        WRITE OUTPUT TAPE 6 (200) CONFIG
        DO 140 K=1,NBASE
        WRITE OUTPUT TAPE 6 (250)K,SBASE(K)
        WRITE OUTPUT TAPE 6 (260) THETD(K),GEPRAM(K)
        WRITE OUTPUT TAPE 6 (270) EFFHI(K),XMAC(K)
```

```
  140 CONTINUE
      WRITE OUTPUT TAPE 6 (280)
      DO 150 I=1,NATMOS
      WRITE OUTPUT TAPE 6 (290) AMACH(I),PRES(I),RHO(I),AMU(I),CPBA(I)
  150 CONTINUE
      GO TO 10
  160 FORMAT(12A6)
  170 FORMAT(3I4)
  180 FORMAT(5E14.8)
  190 FORMAT(1H1,26X,33HSUBSONIC BASE PRESSURE PREDICTION)
  200 FORMAT(1H0,12A6)
  210 FORMAT(//10X,21HFREE STREAM MACH NO.=,F7.4,6X,26HFREE STREAM PRESS
     1URE(PSF)=,F8.2)
  220 FORMAT(//10X,16HTHETA EFF.(DEG)=,F7.4,11X,21HBASE GEOM. PARAMETER=
     1,F7.4)
  230 FORMAT(///20X,24HMOM. B.L. THICK/HITE EFF,5X,20HBASE PRESSURE COEF
     1F.)
  240 FORMAT(//25X,F9.6,23X,F7.4)
  250 FORMAT(//10X,11HSUBREGION  ,I2,22X,15H(PERCENT BASE =,F4.2,1H))
  260 FORMAT(//16X,16HTHETA EFF.(DEG)=,F8.4,11X,21HBASE GEOM. PARAMETER=
     1,F7.4)
  270 FORMAT(//16X,14HHITE EFF.(FT)=,F7.4,14X,16HMEAN LENGTH(FT)=,F7.4)
  280 FORMAT(///10X,8HMACH NO.,4X,10HPRESS(PSF),4X,17HDENSITY(SLUG/FT3),
     13X,22HVISCOSITY(SLUG/FT'SEC),3X,7HBASE CP)
  290 FORMAT(//10X,F7.4,5X,F9.2,9X,F9.6,11X,F12.9,9X,F9.6)
      END
```

```
*       FORTRAN
        SUBROUTINE THCPB2(XMIN,PIN,T1DEG,CPRAT2,BLTHK,CPBL,MCNT)
C       2-D THEORETICAL BASE PRESSURE
        DIMENSION XCPB(25),CPRAT2(25),BLTHK(25),MCNT(25)
        CP1=0.0
        XMSB1=XMIN
        XNRAT=1.0
        IF (T1DEG) 10,20,20
   10   T2DEG=-27.5+2.5*T1DEG
        GO TO 30
   20   T2DEG=-90.
   30   CALL LIMCPB(XMIN ,PIN ,CP1,XMSB1,XNRAT,CPBL)
        NUM=CPBL/.025
        XNUM=NUM
        CPTEMP=XNUM*.025
        DO 40 J=2,11
        XCPB(J)=CPTEMP
        CPRAT2(J)=XCPB(J)/CPBL
        CPTEMP=CPTEMP+.025
   40   CONTINUE
        DO 80 J=2,11
        CPB=XCPB(J)
        PSUB1=PIN *(.7*CP1*XMIN **2+1.)
        PSUBB=PIN *(.7*CPB*XMIN **2+1.)
        PRAT=PSUBB/PSUB1
        FPR1=PRAT**(-.286)
        FM1=1.+.2*XMSB1**2
        FM2=5.*(FM1*FPR1-1.)
        XMSB2=SQRTF(ABSF(FM2))
        SIGMA=12.*(1.+.23*XMSB2)
        UCAST=.578
        FM3=1.+.2*XMSB2**2*(1.-UCAST**2)
        FM4=1.+.2*XMSB2**2
        XLMDB=FM4/FM3
        PSUBR=XNRAT*(PSUB1-PSUBB)+PSUBB
        PRAT2=PSUBB/PSUBR
        FP1=XLMDB*PRAT2**.286
        FP2=LOGF(ABSF(FP1))
        FURAST=(4.425*FP2)/(SIGMA*XMSB2**2)
        FP3=LOGF(ABSF(PRAT2**(-.286)))
        FP4=LOGF(ABSF(XLMDB))
        FRAT=1.-(FP3/FP4)
        BLRAT=FURAST/(1.-FRAT)
        CALL GEOM(CPB,T1DEG,T2DEG,XLNRAT,SLRAT,LCNT)
        IF (LCNT-25) 60,60,50
   50   MCNT(J)=J
        GO TO 80
   60   MCNT(J)=0
   70   BLTHK(J)=BLRAT*SLRAT
   80   CONTINUE
        RETURN
        END
```

```
*     FORTRAN
      SUBROUTINE LIMCPB (XMIN ,PIN ,CP1,XMSB1,XNRAT,CPBL)
C     LIMITING BASE PRESSURE SUBROUTINE
      JSWA=1
      CPB=-.80
      PSUB1=PIN *(.7*CP1*XMIN **2+1.)
      PSUBB=PIN *(.7*CPB*XMIN **2+1.)
      PRAT=PSUBB/PSUB1
   10 FPR1=PRAT**(-.286)
      FM1=1.+.2*XMSB1**2
      FM2=5.*(FM1*FPR1-1.)
      XMSB2=SQRTF(ABSF(FM2))
      UCAST=.578
      FM3=1.+.2*XMSB2**2*(1.-UCAST**2)
      FM4=1.+.2*XMSB2**2
      XLMDB=FM4/FM3
      FLD1=XLMDB**3.5-1.0
      FLD2=FLD1/XNRAT
      PRC=1./(1.+FLD2)
      ERR=(PRAT-PRC)/PRC
      IF (ABSF(ERR)-.00005) 50,50,20
   20 GO TO (30,40), JSWA
   30 PRAT1=PRAT
      ERR1=ERR
      PRAT=PRAT-.0001
      JSWA=2
      GO TO 10
   40 PRAT2=PRAT
      ERR2=ERR
      SLP=(ERR2-ERR1)/(PRAT2-PRAT1)
      B=ERR1-SLP*PRAT1
      PRAT=-B/SLP
      PRAT1=PRAT2
      ERR1=ERR2
      GO TO 10
   50 CPBL=(PRAT-1.)/(.7*XMIN **2)
      RETURN
      END
```

```
*     FORTRAN
      SUBROUTINE GEOM(CPB,T1DEG,T2DEG,XLNRAT,SLRAT,LCNT)
C     FREE LAYER GEOMETRY SUBROUTINE
      DIMENSION PHIBC(50),FPHIBC(50),XFBC(50),YFBC(50),XDIM(50),YDIM(50)
      DIMENSION FPHICD(50),PHICD(50),XFCD(50),YFCD(50)
      DIMENSION FPHIDE(50),PHIDE(50)
      DIMENSION DL(50),XRAT(50),YRAT(50),DELT(25)
      THETA1=.0174533*T1DEG
      THETA2=.0174533*T2DEG
      VRAT=1.0/SQRTF(1.0-CPB)
      IF (THETA1) 70,10,170
   10 PWR1=3.141593/THETA2
      LCNT=0
      FVR1=VRAT**PWR1-1.0
      FVR2=VRAT**PWR1+1.0
      CONK=FVR1/FVR2
      CKSQ=CONK**2
      RNGBC=1.0-CKSQ
      DEL1=RNGBC/25.
      PHIBC(1)=-1.0
      DO 50 J=1,25
      FBC=PHIBC(J)
      FP1=-(FBC**2)-(CKSQ+1.0)*FBC-CKSQ
      FP2=2.0*CONK*SQRTF(FP1)
      FP3=2.0*CKSQ+(CKSQ+1.0)*FBC
      FP4=FP2/FP3
      IF (FP4) 20,20,30
   20 FPHIBC(J)=(-THETA2/3.141593)*ATANF(FP4)
      GO TO 40
   30 FPHIBC(J)=(-THETA2/3.141593)*(ATANF(FP4)-3.141593)
   40 PHIBC(J+1)=PHIBC(J)+DEL1
      XFBC(J)=COSF(FPHIBC(J))
      YFBC(J)=SINF(FPHIBC(J))
   50 CONTINUE
      XFBC(26)=COSF(THETA2)
      YFBC(26)=SINF(THETA2)
      NO=25
      XLIM=0.
      CALL  INTGRT(XLIM,XDIM,XFBC,DEL1,NO)
      YLIM=0.
      CALL  INTGRT(YLIM,YDIM,YFBC,DEL1,NO)
      DEL2=(.995*CKSQ)/25.
      PHICD(1)=-CKSQ
      DO 60 J=1,26
      FCD=PHICD(J)
      FP5=FCD**2+(CKSQ+1.0)*FCD+CKSQ
      FP6=2.0*CONK*SQRTF(FP5)
      FP7=2.0*CKSQ+(CKSQ+1.0)*FCD
      FP8=FP6+FP7
      FP9=-(1.0-CKSQ)*FCD
      FP10=FP9/FP8
      FP11=THETA2/3.141593
      FPHICD(J)=FP10**FP11
      PHICD(J+1)=PHICD(J)+DEL2
   60 CONTINUE
      CALL  INTGRT(XLIM,DL,FPHICD,DEL2,NO)
      GO TO 410
   70 CK2=.825+.005*T1DEG
      CK1=.4
      J=1
      FT1=(T1DEG-T2DEG)/180.
```

```
      VFK=(VRAT**(1.0/FT1))*COSF(THETA2/FT1)
   80 CALL FKMIN(CK1,CK2,FKM)
      ERR=FKM/VFK-1.0
      IF (ABSF(ERR)-.001) 140,140,90
   90 GO TO (100,110), J
  100 F1=FKM
      C1=CK1
      CK1=CK1+.005
      LCNT=1
      J=2
      GO TO 80
  110 F2=FKM
      C2=CK1
      LCNT=LCNT+1
      IF (LCNT-25) 120,120,130
  120 DELFK=F2-F1
      SLP=DELFK/(C2-C1)
      FINT=F1-SLP*C1
      CK1=(VFK-FINT)/SLP
      C1=C2
      F1=F2
      GO TO 80
  130 RETURN
  140 FC1=SQRTF(1.0-CK1)
      FC2=SQRTF(1.0+CK1)
      FC3=SQRTF(1.0-CK2)
      FC4=SQRTF(1.0+CK2)
      FK1=FC1/FC4
      FK2=FC2/FC3
      FK3=1.0/(FK1-FK2)
      DEL1=(CK1+CK2)/25.
      PHICD(1)=-CK1
      DO 150 J=1,26
      FCD=PHICD(J)
      FM1=SQRTF(-FCD+CK2)
      FM2=SQRTF(FCD+CK1)
      FM3=FK1*FM1/FM2
      FM4=FK1*ATANF(FM3)
      FM5=FK2*FM1/FM2
      FM6=FK2*ATANF(FM5)
      FM7=FM4-FM6
      FPHICD(J)=THETA2+2.0*FT1*FK3*FM7
      PHICD(J+1)=PHICD(J)+DEL1
      XFCD(J)=COSF(FPHICD(J))
      YFCD(J)=SINF(FPHICD(J))
  150 CONTINUE
      NO=25
      XLIM=0.
      CALL INTGRT(XLIM,XDIM,XFCD,DEL1,NO)
      YLIM=0.
      CALL INTGRT(YLIM,YDIM,YFCD,DEL1,NO)
      DEL2=(.995*(1.0-CK2))/25.
      PHIDE(1)=CK2
      DO 160 J=1,26
      FDE=PHIDE(J)
      FN1=SQRTF(FDE+CK1)
      FN2=SQRTF(FDE-CK2)
      FN3=FC4*FN1+FC1*FN2
      FN4=FC4*FN1-FC1*FN2
      FN5=(FN3/FN4)**FK1
      FN6=FC3*FN1-FC2*FN2
```

```
      FN7=FC3*FN1+FC2*FN2                                              GEOM1220
      FN8=(FN6/FN7)**FK2                                               GEOM1230
      FPHIDE(J)=(FN5*FN8)**(FT1*FK3)                                   GEOM1240
      PHIDE(J+1)=PHIDE(J)+DEL2                                         GEOM1250
  160 CONTINUE                                                         GEOM1260
      CALL  INTGRT(XLIM,DL,FPHIDE,DEL2,NO)                             GEOM1270
      GO  TO  410                                                      GEOM1280
  170 CK2=1.9393/(T1DEG-66.6668)+1.00289+.0003333*T1DEG                GEOM1290
      CK1=CK2-.04                                                      GEOM1300
      J=1                                                              GEOM1310
  180 CALL  FKPLUS(T1DEG,T2DEG,CK1,CK2,FKP)                            GEOM1320
      ERR=FKP/VRAT-1.0                                                 GEOM1330
      IF  (ABSF(ERR)-.001)  240,240,190                                GEOM1340
  190 GO  TO  (200,210),  J                                            GEOM1350
  200 F1=FKP                                                           GEOM1360
      C1=CK1                                                           GEOM1370
      CK1=CK1-.005                                                     GEOM1380
      LCNT=1                                                           GEOM1390
      J=2                                                              GEOM1400
      GO  TO  180                                                      GEOM1410
  210 F2=FKP                                                           GEOM1420
      C2=CK1                                                           GEOM1430
      LCNT=LCNT+1                                                      GEOM1440
      IF  (LCNT-25)  220,220,230                                       GEOM1450
  220 DELFK=F2-F1                                                      GEOM1460
      SLP=DELFK/(C2-C1)                                                GEOM1470
      FINT=F1-SLP*C1                                                   GEOM1480
      CK1=(VRAT-FINT)/SLP                                              GEOM1490
      C1=C2                                                            GEOM1500
      F1=F2                                                            GEOM1510
      GO  TO  180                                                      GEOM1520
  230 RETURN                                                           GEOM1530
  240 XFA=SQRTF(1.0+CK1-CK2-(CK1*CK2))                                 GEOM1540
      XFB=SQRTF(1.0+CK2-CK1-(CK1*CK2))                                 GEOM1550
      XT1=(T1DEG-T2DEG)/180.                                           GEOM1560
      DEL1=(CK1+CK2)/25.                                               GEOM1570
      PHICD(1)=-CK1                                                    GEOM1580
      DO  390  J=1,26                                                  GEOM1590
      FCD=PHICD(J)                                                     GEOM1600
      FM1=(CK2-CK1-2.0)*FCD                                            GEOM1610
      FM2=((2.0*CK1*CK2)+CK2-CK1)+FM1                                  GEOM1620
      FM3=(CK2+CK1)*(1.0-FCD)                                          GEOM1630
      FM4=FM2/FM3                                                      GEOM1640
      IF  (FM4)  250,310,280                                           GEOM1650
  250 IF  (FM4+1.0)  260,310,310                                       GEOM1660
  260 IF  (FM4+1.1)  310,310,270                                       GEOM1670
  270 FM4=-1.0                                                         GEOM1680
      GO  TO  310                                                      GEOM1690
  280 IF  (FM4-1.0)  310,310,290                                       GEOM1700
  290 IF  (FM4-1.1)  300,310,310                                       GEOM1710
  300 FM4=1.0                                                          GEOM1720
  310 CONTINUE                                                         GEOM1730
      FC1=(1.0/XFA)*ASINF(FM4)                                         GEOM1740
      FM5=(CK2-CK1+2.0)*FCD                                            GEOM1750
      FM6=((2.0*CK1*CK2)+CK1-CK2)+FM5                                  GEOM1760
      FM7=(CK1+CK2)*(1.0+FCD)                                          GEOM1770
      FM8=FM6/FM7                                                      GEOM1780
      IF  (FM8)  320,380,350                                           GEOM1790
  320 IF  (FM8+1.0)  330,380,380                                       GEOM1800
  330 IF  (FM8+1.1)  380,380,340                                       GEOM1810
  340 FM8=-1.0                                                         GEOM1820
```

```
      GO TO 380
  350 IF (FM8-1.0) 380,380,360
  360 IF (FM8-1.1) 370,380,380
  370 FM8=1.0
  380 CONTINUE
      FC2=(1.0/XFB)*ASINF(FM8)
      FC3=FC1-FC2
      FM9=(XFA*XFB)/(XFA+XFB)
      FM10=(THETA1+THETA2)/2.0
      FPHICD(J)=(XT1*FM9*FC3)+FM10
      PHICD(J+1)=PHICD(J)+DEL1
      XFCD(J)=COSF(FPHICD(J))
      YFCD(J)=SINF(FPHICD(J))
  390 CONTINUE
      NO=25
      XLIM=0.
      CALL INTGRT(XLIM,XDIM,XFCD,DEL1,NO)
      YLIM=0.
      CALL INTGRT(YLIM,YDIM,YFCD,DEL1,NO)
      DEL2=(.995*(1.0-CK2))/25.
      PHIDE(1)=CK2
      DO 400 J=1,26
      FDE=PHIDE(J)
      FN1=(2.0+CK1-CK2)*FDE
      FN2=(CK1-CK2-(2.0*CK1*CK2))+FN1
      FN3=(CK1+CK2)*(1.0-FDE)
      Z3=FN2/FN3
      FZ1=Z3+SQRTF((Z3**2)-1.0)
      FN4=XFA/(XFA+XFB)
      FZ2=FZ1**FN4
      FN5=(2.0+CK2-CK1)*FDE
      FN6=(CK1-CK2+(2.0*CK1*CK2))+FN5
      FN7=(CK1+CK2)*(1.0+FDE)
      Z2=FN6/FN7
      FN8=XFB/(XFA+XFB)
      FZ3=Z2+SQRTF((Z2**2)-1.0)
      FZ4=FZ3**FN8
      FPHIDE(J)=(FZ2*FZ4)**XT1
      PHIDE(J+1)=PHIDE(J)+DEL2
  400 CONTINUE
      CALL INTGRT(XLIM,DL,FPHIDE,DEL2,NO)
      GO TO 410
  410 DLX0=DL(26)*COSF(THETA2)
      DLY0=-DL(26)*SINF(THETA2)
      HITE=ABSF(YDIM(26))+DLY0
      DO 420 J=1,26
      YRAT(J)=(HITE-ABSF(YDIM(J)))/HITE
      XRAT(J)=XDIM(J)/HITE
  420 CONTINUE
      TEMPLN=0.
      DO 430 J=1,25
      XSIDE=XRAT(J+1)-XRAT(J)
      YSIDE=YRAT(J)-YRAT(J+1)
      HYPSQ=XSIDE**2+YSIDE**2
      DELT(J)=SQRTF(HYPSQ)
      SLN=TEMPLN+DELT(J)
      TEMPLN=SLN
  430 CONTINUE
      XORAT=DLX0/HITE
      YORAT=DLY0/HITE
      XLN=XDIM(26)+DLX0
```

```
      XLNRAT=XLN/HITE                                              GEOM2440
      SLRAT=SLN+(DL(26)/HITE)                                      GEOM2450
      RETURN                                                       GEOM2460
      END                                                          GEOM2470
```

```
*      FORTRAN
       SUBROUTINE FKPLUS (T1DEG,T2DEG,CONK,CK2,FKP)
C      SUBROUTINE F(K) PLUS
       XFB=SQRTF(1.0+CK2-CONK-(CK2*CONK))
       XFA=SQRTF(1.0+CONK-CK2-(CONK*CK2))
       XSUB1=(2.0+CONK-CK2+2.0*XFA)/(CONK+CK2)
       XSUB2=(2.0+CK2-CONK+2.0*XFB)/(CONK+CK2)
       THETA1=T1DEG*.0174533
       THETA2=T2DEG*.0174533
       F1=(XSUB1**(1.0/XFA))/(XSUB2**(1.0/XFB))
       PWR1=(AT1-AT2)*((XFA*XFB)/(XFB+XFA))
       F2=F1**PWR1
       F3=COSF((-THETA1-THETA2)/2.0)
       F4=(THETA1-THETA2)/2.0
       F5=(XFB-XFA)/(XFB+XFA)
       F6=F4*F5
       F7=COSF(F6)
       FKP=(F2*F3)/F7
       RETURN
       END
```

```
*     FORTRAN
      SUBROUTINE FKMIN (CK1,CK2,FKM)
      FC1=SQRTF(1.0+CK2)
      FC2=SQRTF(1.0-CK2)
      FC3=SQRTF(1.0+CK1)
      FC4=SQRTF(1.0-CK1)
      FK1=FC4/FC1
      FK2=FC3/FC2
      FC5=(FC1+FC4)/(FC1-FC4)
      FC6=FC5**FK1
      FC7=(FC3-FC2)/(FC3+FC2)
      FC8=FC7**FK2
      FC9=FC6*FC8
      FC10=1.0/(FK2-FK1)
      FC11=FC9**FC10
      FC12=(3.141593*FK2)/(FK2-FK1)
      FKM=FC11*COSF(FC12)
      RETURN
      END
```

```
*     FORTRAN
      SUBROUTINE INTGRT (BLIM,X,F,DELF,N)
C     SUBROUTINE INTEGRATE
      DIMENSION X(100),F(100)
      X(1)=BLIM
      TEMP=X(1)
      DO 10 J=1,N
      AREA=.5*DELF*(F(J)+F(J+1))
      X(J+1)=TEMP+AREA
      TEMP=X(J+1)
   10 CONTINUE
      RETURN
      END
```

```
*     FORTRAN
      SUBROUTINE BLTHKA (XMIN,XMAC,VISC,RHO,PIN,EFFHI,BLTHK)
C     SUBROUTINE FOR BOUNDARY LAYER THICKNESS
      FB1=XMIN/VISC
      FB2=FB1**(-.20)
      FB3=1.405*PIN*RHO
      FB4=FB3**(-.10)
      BLMOM=.036*(XMAC**.8)*FB2*FB4
      BLTHK=BLMOM/EFFHI
      RETURN
      END
```

```
*       FORTRAN
        SUBROUTINE INTPOL(X,Y,XA,YA,MCHK)
C       INTERPOLATION SUBROUTINE
        DIMENSION X(25),Y(25)
        J=1
        MCHK=0
   10   IF (XA-X(J)) 90,80,20
   20   J=J+1
        IF (J-11) 30,30,90
   30   IF (XA-X(J)) 40,80,20
   40   IF (J-10) 50,50,60
   50   J=J-1
        GO TO 70
   60   J=J-2
   70   A=XA-X(J)
        B=XA-X(J+1)
        C=XA-X(J+2)
        D=X(J)-X(J+1)
        E=X(J)-X(J+2)
        F=X(J+1)-X(J+2)
        YA=B*C*Y(J)/(D*E)+A*C*Y(J+1)/(-D*F)+A*B*Y(J+2)/(-F*(-E))
        RETURN
   80   YA=Y(J)
        RETURN
   90   MCHK=1
        RETURN
        END
```

OPTION 1

CARD 1

COL	1 … 72
	CONFIG

CARD 2

COL	1 – 4	5 – 8	9 – 12
	NOPP	NBASE	NATMOS

CARD 3

COL	1 – 14	15 – 28	29 – 42	43 – 56
	AMACH	PRES	GEPRAM	THETD

OPTION 2

CARD 1

COL	1 … 72
	CONFIG

CARD 2

COL	1 – 4	5 – 8	9 – 12
	NOPP	NBASE	NATMOS

CARD 3 *

COL	1 – 14	15 – 28	29 – 42	43 – 56	57
	AMACH	PRES	AMU	RHO	

CARD 4 **

COL	1 – 14	15 – 28	29 – 42	43 – 56	57 – 68
	GEPRAM	THETD	XMAC	EFFHI	SBASE

* Card 3 repeated the NATMOS times

** Card 4 repeated n = NBASE times

FIGURE. 48 Generalized Prediction Digital Computer Program Input Format

TABLE IV

INPUT NOMENCLATURE FOR GENERALIZED PREDICTION
DIGITAL COMPUTER PROGRAM

AMACH	-	Free Stream Mach Number
AMU	-	Free Stream Viscosity ~ Slug/Ft-Sec
CONFIG	-	Identification of Configuration
EFFHI	-	Effective semi-height of Base Area ~ Ft
GEPRAM	-	Geometry Parameter - Perimeter/ $2\sqrt{\pi \text{ Base Area}}$
NATMOS	-	Number of Different Free Stream Conditions to be Considered for Option 2
NBASE	-	Number of Segments the Base is Divided into for a Composite Geometry
NOPP	-	Program Options 1. Computes array of base pressures and boundary layer thickness, NATMOS and NBASE must = 1 2. Computes actual base pressure for configuration
PRES	-	Free stream pressure ~ PSF
RHO	-	Free Stream Density ~ Slug/Ft^3
SBASE	-	Percentage of Total Base Area of Each Segment
THETD	-	Average Angle of Base Geometry ~ Degrees
XMAC	-	Length of Configuration ~ Ft.

SUBSONIC BASE PRESSURE PREDICTION

FREE STREAM MACH NO.= 0.2000 FREE STREAM PRESSURE(PSF)= 2112.00

THETA EFF.(DEG)= 0. BASE GEOM. PARAMETER= 1.0000

MOM. B.L. THICK/HITE EFF	BASE PRESSURE COEFF.
0.	-0.2027
0.001743	-0.1949
0.004627	-0.1846
0.008141	-0.1743
0.012460	-0.1641
0.017827	-0.1538
0.024574	-0.1436
0.033168	-0.1333
0.044283	-0.1231
0.058929	-0.1128
0.078627	-0.1026

Figure 49 Generalized Prediction Digital Computer Program Sample Output-Option 1

SUBSONIC BASE PRESSURE PREDICTION

CONFIGURATION M1 + A1

SUBREGION 1 (PERCENT BASE =0.62)

THETA EFF.(DEG)= 0. BASE GEOM. PARAMETER= 1.0000

HITE EFF.(FT)= 0.2500 MEAN LENGTH(FT)= 2.6700

SUBREGION 2 (PERCENT BASE =0.38)

THETA EFF.(DEG)= 0. BASE GEOM. PARAMETER= 1.4200

HITE EFF.(FT)= 0.0420 MEAN LENGTH(FT)= 0.6500

MACH NO.	PRESS(PSF)	DENSITY(SLUG/FT3)	VISCOSITY(SLUG/FT'SEC)	BASE CP
0.1600	2116.00	0.002378	0.000000373	-0.242351

Figure 50 Generalized Prediction Digital Computer Program Sample Output-Option 2

Security Classification

DOCUMENT CONTROL DATA - R&D

(Security classification of title, body of abstract and indexing annotation must be entered when the overall report is classified)

1. ORIGINATING ACTIVITY *(Corporate author)* GD/Convair General Dynamics Corporation	2a. REPORT SECURITY CLASSIFICATION Unclassified 2b. GROUP

3. REPORT TITLE

Development of Subsonic Base Pressure Prediction Methods - Volume I

4. DESCRIPTIVE NOTES *(Type of report and inclusive dates)*

Final Report

5. AUTHOR(S) *(Last name, first name, initial)*

Butsko, J.E., Carter, W.V., Herman, W.

6. REPORT DATE	7a. TOTAL NO. OF PAGES	7b. NO. OF REFS
September 1965	168	28

8a. CONTRACT OR GRANT NO. AF 33(615)-1615 b. PROJECT NO. 1366 c. Task 136613 d.	9a. ORIGINATOR'S REPORT NUMBER(S) AFFDL-TR-65-157 - Vol. I 9b. OTHER REPORT NO(S) *(Any other numbers that may be assigned this report)*

10. AVAILABILITY/LIMITATION NOTICES

Qualified users may obtain copies of this report from DDC. Foreign announcement and dissemination of this report is not authorized. ~~DDC release to OTS is authorized.~~

11. SUPPLEMENTARY NOTES	12. SPONSORING MILITARY ACTIVITY AF Flight Dynamics Laboratory Research and Technology Division Air Force Systems Command WPAFB, Ohio 45433

13. ABSTRACT

A combined analytic-experimental investigation of the subsonic base pressure phenomenon, especially as applied to blunt bodies typical of hypersonic flight vehicles, results in the development of a generalized method to predict base pressure in three-dimensional flow at subsonic speeds. A mathematical description of the fluid mechanics of steady two-dimensional subsonic base flow is developed. Two and three-dimensional wind tunnel testing of blunt based configurations is used to verify the two-dimensional analytic solution and obtain empirical relations which extend the analysis to three-dimensional base flow.

Volume II contains the results of the experimental investigation.

DD FORM 1 JAN 64 1473

Unclassified

Security Classification

Security Classification

14. KEY WORDS	LINK A		LINK B		LINK C	
	ROLE	WT	ROLE	WT	ROLE	WT

INSTRUCTIONS

1. ORIGINATING ACTIVITY: Enter the name and address of the contractor, subcontractor, grantee, Department of Defense activity or other organization *(corporate author)* issuing the report.

2a. REPORT SECURITY CLASSIFICATION: Enter the overall security classification of the report. Indicate whether "Restricted Data" is included. Marking is to be in accordance with appropriate security regulations.

2b. GROUP: Automatic downgrading is specified in DoD Directive 5200.10 and Armed Forces Industrial Manual. Enter the group number. Also, when applicable, show that optional markings have been used for Group 3 and Group 4 as authorized.

3. REPORT TITLE: Enter the complete report title in all capital letters. Titles in all cases should be unclassified. If a meaningful title cannot be selected without classification, show title classification in all capitals in parenthesis immediately following the title.

4. DESCRIPTIVE NOTES: If appropriate, enter the type of report, e.g., interim, progress, summary, annual, or final. Give the inclusive dates when a specific reporting period is covered.

5. AUTHOR(S): Enter the name(s) of author(s) as shown on or in the report. Enter last name, first name, middle initial. If military, show rank and branch of service. The name of the principal author is an absolute minimum requirement.

6. REPORT DATE: Enter the date of the report as day, month, year; or month, year. If more than one date appears on the report, use date of publication.

7a. TOTAL NUMBER OF PAGES: The total page count should follow normal pagination procedures, i.e., enter the number of pages containing information.

7b. NUMBER OF REFERENCES: Enter the total number of references cited in the report.

8a. CONTRACT OR GRANT NUMBER: If appropriate, enter the applicable number of the contract or grant under which the report was written.

8b, 8c, & 8d. PROJECT NUMBER: Enter the appropriate military department identification, such as project number, subproject number, system numbers, task number, etc.

9a. ORIGINATOR'S REPORT NUMBER(S): Enter the official report number by which the document will be identified and controlled by the originating activity. This number must be unique to this report.

9b. OTHER REPORT NUMBER(S): If the report has been assigned any other report numbers *(either by the originator or by the sponsor)*, also enter this number(s).

10. AVAILABILITY/LIMITATION NOTICES: Enter any limitations on further dissemination of the report, other than those imposed by security classification, using standard statements such as:

(1) "Qualified requesters may obtain copies of this report from DDC."

(2) "Foreign announcement and dissemination of this report by DDC is not authorized."

(3) "U. S. Government agencies may obtain copies of this report directly from DDC. Other qualified DDC users shall request through ________________."

(4) "U. S. military agencies may obtain copies of this report directly from DDC. Other qualified users shall request through ________________."

(5) "All distribution of this report is controlled. Qualified DDC users shall request through ________________."

If the report has been furnished to the Office of Technical Services, Department of Commerce, for sale to the public, indicate this fact and enter the price, if known.

11. SUPPLEMENTARY NOTES: Use for additional explanatory notes.

12. SPONSORING MILITARY ACTIVITY: Enter the name of the departmental project office or laboratory sponsoring *(paying for)* the research and development. Include address.

13. ABSTRACT: Enter an abstract giving a brief and factual summary of the document indicative of the report, even though it may also appear elsewhere in the body of the technical report. If additional space is required, a continuation sheet shall be attached.

It is highly desirable that the abstract of classified reports be unclassified. Each paragraph of the abstract shall end with an indication of the military security classification of the information in the paragraph, represented as *(TS)*, *(S)*, *(C)*, or *(U)*.

There is no limitation on the length of the abstract. However, the suggested length is from 150 to 225 words.

14. KEY WORDS: Key words are technically meaningful terms or short phrases that characterize a report and may be used as index entries for cataloging the report. Key words must be selected so that no security classification is required. Identifiers, such as equipment model designation, trade name, military project code name, geographic location, may be used as key words but will be followed by an indication of technical context. The assignment of links, rules, and weights is optional.